MReadings: molecular MRI

Contributions from our Biograph mMR users

SIEMENS

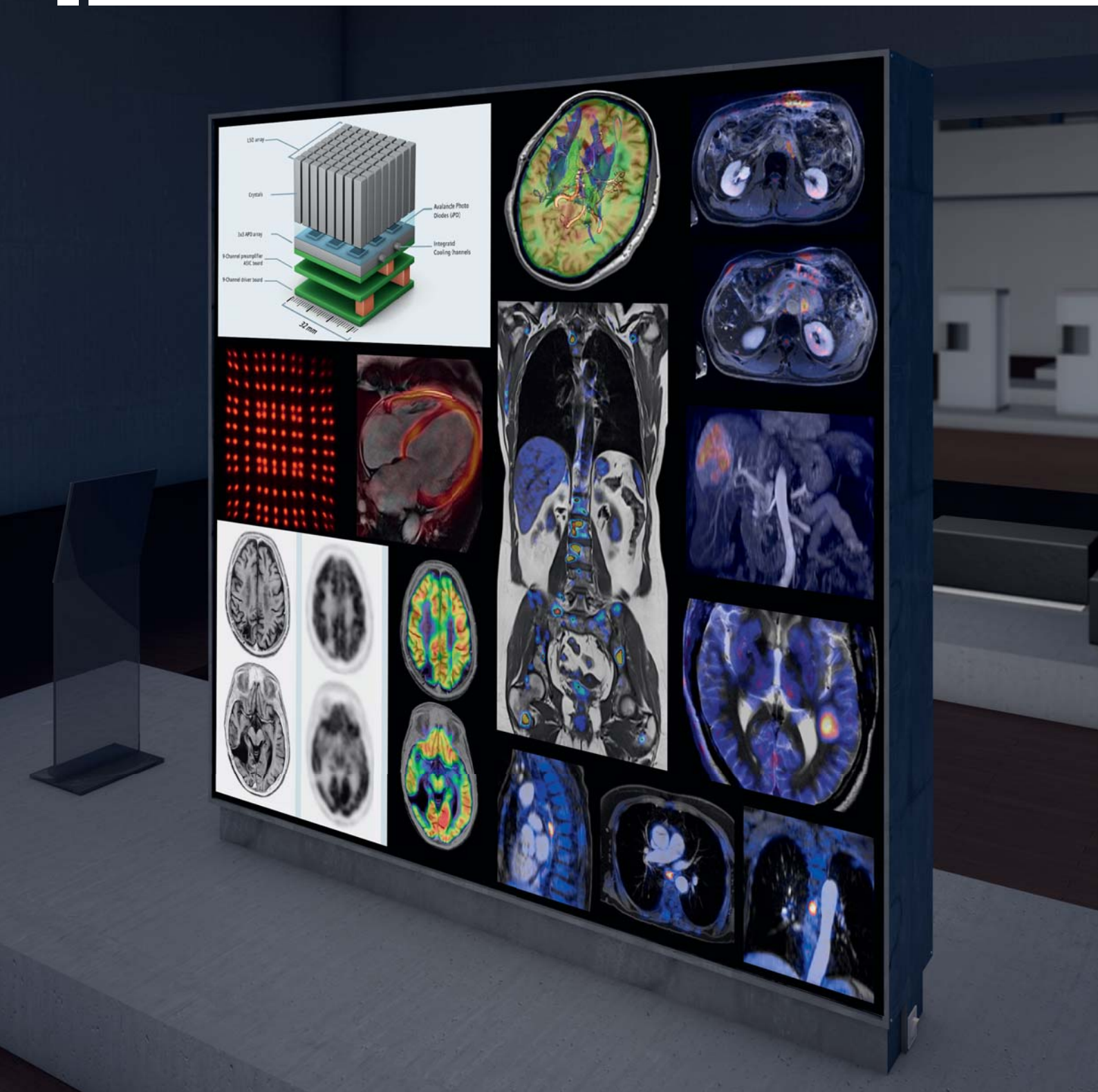

Content

Technical

Clinical

Further Reading

MR/PET – Hybrid Imaging for the Next Decade

Thomas Beyer, Ph.D.[1]; Nina Schwenzer, M.D.[2]; Sotirios Bisdas, M.D.[2]; Claus D. Claussen, M.D.[2]; Bernd J. Pichler, Ph.D.[3]

[1]*Imaging Science Institute (ISI) Tübingen, University Hospital Tübingen, Germany*
[2]*Department of Diagnostic and Interventional Radiology, University Hospital Tübingen, Germany*
[3]*Laboratory for Preclinical Imaging and Imaging Technology, University Hospital Tübingen, Germany*

Dual-modality imaging

Traditionally, medical imaging is dominated by anatomical imaging, such as X-ray, ultrasound (US), computed tomography (CT) and magnetic resonance imaging (MRI). Functional imaging plays a minor, albeit important role. Most functional imaging modalities, including positron emission tomography (PET), are operated in the realms of nuclear medicine, sometimes mockingly referred to as 'unclear' medicine, so as to point to the fact that nuclear medicine images are comparatively noisy and of lower spatial resolution than, for example, CT or MR images. Nonetheless, PET in particular has been demonstrated to be of particular value in a number of disease staging and follow-up regimens.
Despite the clinical usefulness of standalone nuclear medicine and radiology imaging, the desire to combine anatomical, functional (e.g. perfusion) and especially metabolic imaging has been pursued since the 1960's when physicians manually added body contours to planar scintigraphy images of the thyroid. Subsequent approaches to image fusion included side-by-side viewing of complementary image sets on film and on light boxes; image fusion was performed in the head of the physicians and mainly dominated by the personal experience and expertise. The first reliable approaches to computer-assisted image co-registration and fusion were presented in the mid 1980's in an attempt to align brain studies from MR and PET. While retrospective image alignment and fusion works usually well for the brain, similar approaches do not work as well for extra-cerebral studies that are affected by multiple degrees of patient motion.
The introduction of combined, dual-modality imaging systems in the late 1990's offered for the first time the acquisition of high quality anatomical and functional / metabolic image information within a single examination. This was a unique stimulus for non-invasive diagnosis, and has resulted in an extraordinary rapid growth and commercial adoption of imaging systems such as SPECT (single photon emission tomography)/CT and PET/CT. A decade after its prototype introduction, PET/CT, for example, has become the modality-of-choice for a variety of clinical indications in oncology. Today, over 5,000 PET/CT systems are installed worldwide and up to 90% of all PET-investigations are performed for oncology indications with ^{18}F-FDG (fluorodesoxyglucose) being the tracer-of-choice in most of these indications. As discussed in this article, an alternative combination of MR with PET, while technically challenging, has a number of advantages compared to existing dual-modality imaging systems. Prototype MR/PET systems were first proposed for small animal imaging in the 1990's. Recently first prototype MR/PET systems were proposed for imaging humans and case reports and initial pilot studies have promoted a rising interest in this combination of two well-established diagnostic modalities.

MR/PET: From a PET attached to a CT to a PET inside an MR

Tracer principle

The origins of positron emission tomography date back more than 30 years. PET is a functional / metabolic imaging technique based on the detection of coincident photons originating from the annihilation of emitted positrons with electrons from surrounding tissues. PET employs biomolecules that are labeled with neutron-deficient nuclei, i.e. positron emitters. As such, the whole-body distribution of positron-emitting biomarkers can be followed and imaged with high sensitivity using PET (Fig. 1).
Upon decay of a neutron-deficient radioisotope (e.g. ^{18}F) attached to the biomolecule being traced (e.g. glucose) a positron is emitted. After traveling a mean path of

less than a mm in tissue the positron annihilates with an electron, thus creating two 511 keV photons that are emitted in opposite direction. PET scintillation detectors arranged around the patient register the annihilation photons in coincidence and store the events in sinograms from which PET activity distributions are reconstructed following the emission acquisition.

PET detector

PET detector arrangements are based on Anger readout (Fig. 2) which is based in turn on light sharing and mapping many small scintillation crystals to few light detectors (in clinical PET/CT scanners usually photomultiplier tubes (PMT)). The annihilation photon (Fig. 1) is stopped in the scintillator (Fig. 2) and the energy is transformed into secondary scintillation light pulses, which produce photoelectrons at the first cathode level of the PMT, next to the entrance window. These photoelectrons are directed and amplified (multiplied) by an electric field applied to the PMT. For each annihilation photon stopped an electric pulse is generated from the scintillator-PMT detector and stored with respect to the location of the crystal depending on the Anger localization. In the 1990's, bismuth germanate (BGO) was the crystal material of choice for almost all PET systems. Today, BGO is replaced mainly by lutetium oxyorthosilicate (LSO), or variations thereof; a scintillator material that combines fast timing properties with high light output and good stopping power for 511 keV photons. Modern PET system designs include several detector rings that fully surround the patient providing an axial field-of-view (FOV) of 15–22 cm with a measured transverse FOV of up to 70 cm. Most whole-body PET systems yield an intrinsic spatial resolution of 4–6 mm. Sensitivity and spatial resolution are key parameters for PET systems and both depend directly on the properties of the scintillation crystals as part of the PET detector system.

PET/CT systems

Today, close to 70% of all installed PET units are combined PET/CT devices. All but 2 of 8 PET system vendors, who offer standalone PET systems designed for dedicated clinical tasks, offer PET systems for clinical use that are combined with a CT system. The main advantages of combined PET/CT are the intrinsic availability of co-registered functional and anatomical information from PET and CT, for local and whole-body examinations respectively alike. Second, the ability to use available CT transmission images to replace lengthy PET transmission images using 511 keV rod sources, thus reducing overall examination time significantly and limiting noise propagation from measured attenuation correction.

Dual-modality PET/CT systems combine a whole-body PET and a standard multi-slice CT within a single gantry. Various design concepts exist (Fig. 3), all aiming at reducing footprint and bringing the PET and CT components closer together. No fully-integrated, single-detector PET/CT exists today, however, because of the challenges to manufacture a detector system that is capable of CT (40–140 keV) and PET (511 keV) imaging. By using novel patient handling systems, patients are positioned accurately and reproducibly for co-axial imaging. Reports on residual displacements between CT and PET along the co-axial imaging range in combined PET CT indicate a maximum displacement of error of 0.5 mm. Thus, PET/CT yields the best possible alignment of extensive, complementary image volumes. With the benefits of intrinsically aligned PET and CT data, shorter overall scan times and the logistical advantages for patients and staff, combined PET/CT imaging has become a modality-of-choice for patient management in clinical oncology.

Challenges and drawbacks of PET/CT

There are a few challenges when designing a PET/CT imaging system and making it clinically viable. First, the axial displacement of the CT and PET components (Fig. 3) is unavoidable as long as no single PET and CT detectors are available, thus allowing for only sequential rather than simultaneous acquisition modes. Sequential imaging holds the risk of involuntary patient motion in between the two examinations and, therefore, may increase the chance of local misalignment of the two studies. Second, residual patient motion is unavoidable in combined PET/CT imaging. Involuntary patient motion from, for example, respiration, cardiac motion, or muscle relaxation leads to PET–CT misregistration that may translate into artifacts on PET images following CT-based attenuation correction. Optimized imaging protocols are required to minimize these types of artifacts and image distortions. Third, the overall exposure from a whole-body PET/CT examination performed with ^{18}F-FDG is rather high at 20–25 mSv per study and 370 MBq of ^{18}F-FDG injected. This dose is justified whenever a clinical indication for a combined contrast-enhanced PET/CT study exists, but at the same time it limits the use of PET/CT in selected patients that undergo repeat studies or in subjects for pharmaceutical trials.

Rise of MR/PET

The development of hybrid MR/PET systems started in the late 1990's. CT is not the only available anatomical complement to PET. In comparison to CT, MRI offers a multitude of endogenous contrasts and a superb capa-

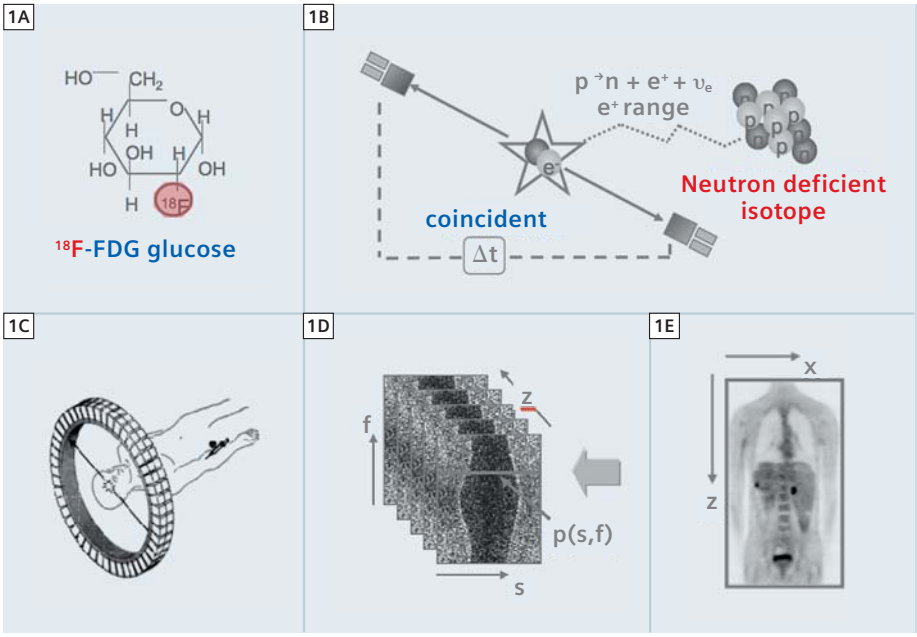

1 PET is based on the tracing of radioactively labeled metabolites. A radiotracer, e.g. ^{18}F-FDG **(A)**, is injected into the patient **(B)**: ^{18}F decays by emitting a positron, which annihilates with an electron, thus resulting in two annihilation photons along a straight line-of-response (LOR), **(C)** annihilation events are registered in coincidence and stored in raw sinogram space **(D)**. PET images are reconstructed following a number of physical and methodological corrections **(E)**. *(Figure adapted from DW Townsend, Singapore.)*

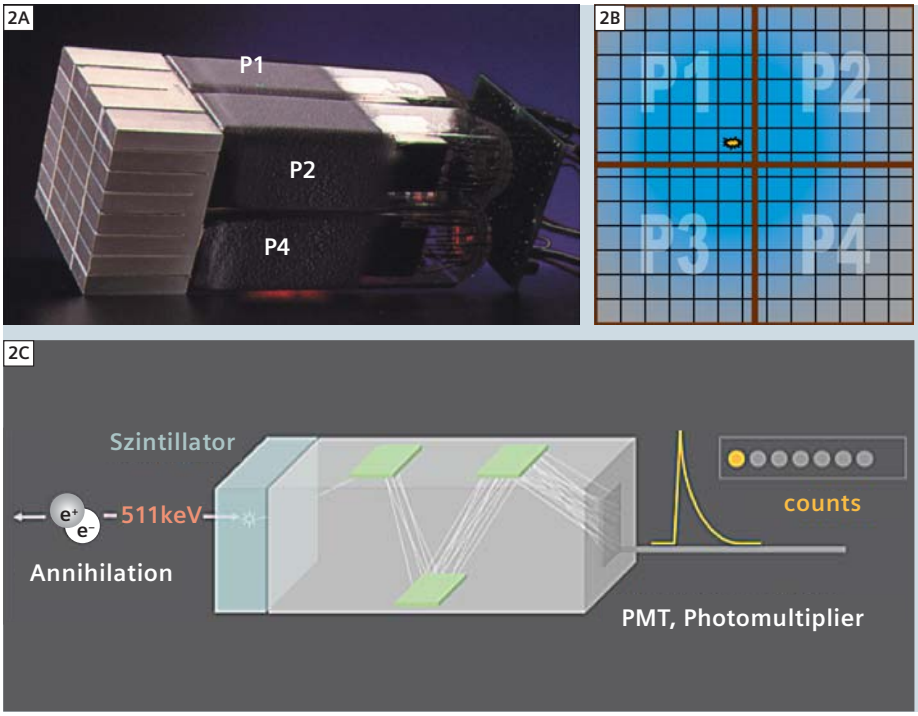

2 Block detector. **(A)** Example of PMT-bismuth germanate block detector from a clinical PET system (Fig. 1C). Readout is performed using only the 4 PMTs that are connected to pixilated scintillator block. Light sharing is used to distribute light originating from single pixel between the 4 readout PMTs (P1, P2, P3, P4). **(B)** Depending on crystal position, scintillation light will be uniquely distributed to readout PMTs. Using Anger weighting algorithm on measured signals, position of incident annihilation photon (i.e. the activated crystal) can be calculated. **(C)** Schematics of detection process from annihilation to stopping the annihilation photons in the crystal and signal transformation inside the photomultiplier.

bility of differentiating soft tissues. With a sensitivity in the picomolar range, PET is ideally suited for the visualization of specific molecules in living organisms. However, PET lacks the spatial resolution offered by MRI, which in turn lacks sensitivity compared to PET. Therefore, the combination of PET and MRI is highly complementary. MRI also offers anatomical image information with the advantage of causing no risk to the patient from ionizing radiation and by offering much higher soft tissue contrast than CT, even in the absence of MR contrast agents. But MRI goes beyond plain anatomical imaging. MR spectroscopy, for example, can be used to dissect the molecular composition of tissues by applying selective radiofrequency excitation pulses. The Fourier transformation of the acquired signal provides a spectrum that allows for discrimination between various metabolites.

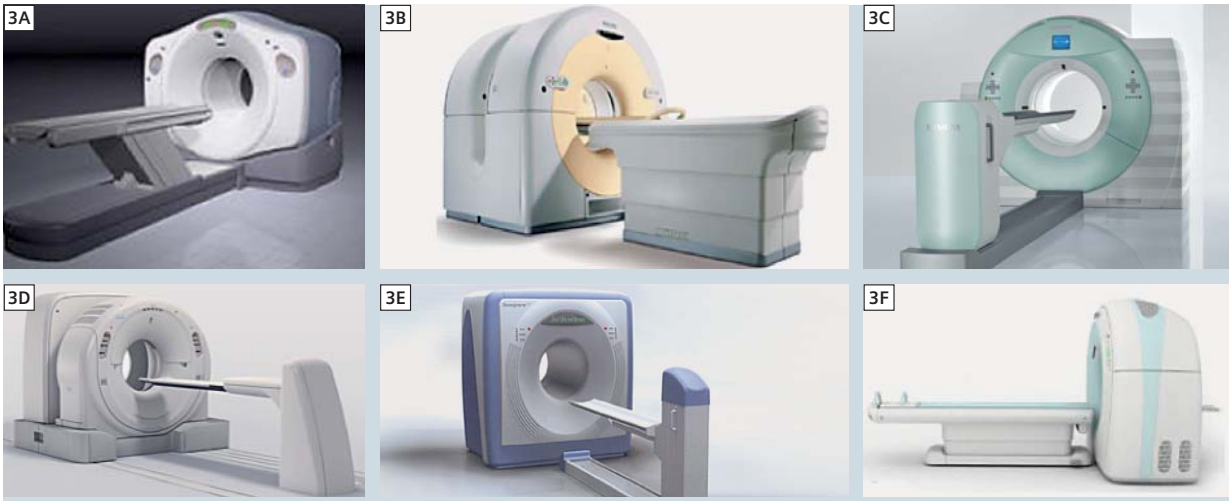

3A–F Current commercial PET/CT systems: **(A)** Discovery series from General Electrics Healthcare, **(B)** Gemini series from Philips Healthcare, **(C)** Biograph mCT from Siemens Healthcare, **(D)** Acquiduo series from Toshiba Medical Systems, **(E)** Sceptre series from Hitachi Medical Systems, **(F)** Anyscan from Mediso (this device can be combined with a SPECT to form a triple-modality imaging system). Variations apply to the individual performance parameters of PET and CT.

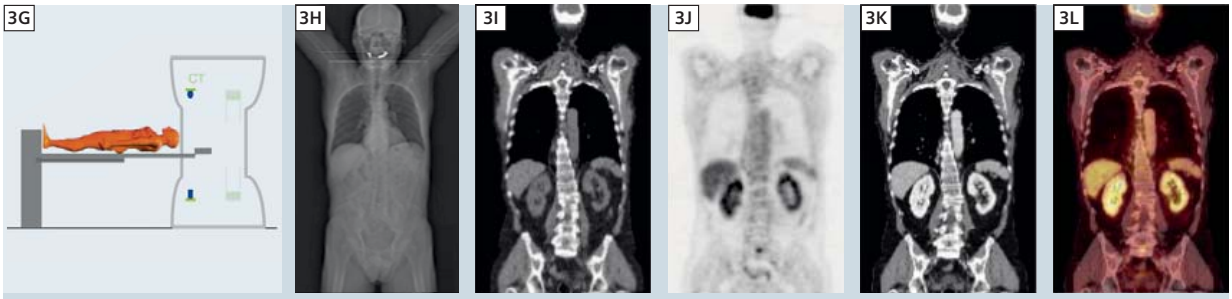

3G–L Schematic illustration of a standard PET/CT investigation: tracer injection, uptake time and patient positioning **(G)**, topogram and scan range definition **(H)**, CT acquisition for attenuation correction **(I)**, emission scan **(J)**, contrast-enhanced CT scan **(K)** and image reconstruction/fusion **(L)**.

Spectroscopic images of extended anatomical volumes can be generated for preoperative staging of gliomas, pH imaging, monitoring of temperature, or the evaluation of lactate changes during brain activation.
Functional processes in living subjects can also be studied via diffusion-weighted MRI. Here, the magnetic field, generated by different gradients, is used to map phase differences in the MRI signal that are caused by diffusing molecules. Many MRI sequences can be made sensitive to diffusion by using adequate gradient pulses. Diffusion MRI has various potential clinical applications ranging from diagnosing ischemia, cancer, multiple sclerosis, or Alzheimer's disease to general fiber tracking via diffusion tensor imaging. Diffusion imaging is not restricted to the brain; it has also been applied to other regions of the body (e.g., for oncologic diagnosis), where it provides qualitative and quantitative understanding of the tumor microenvironment and the integrity of cell membranes.
Functional MRI (fMRI) studies are frequently based on the BOLD (blood oxygen level dependent) effect. This technique is based on the fact that the magnetic properties of oxygenated and deoxygenated hemoglobin in the blood are different and, therefore, produce different signals when imaged with T2*-sensitive MRI sequences. Unlike contrast-enhanced MRI, BOLD effect is a non-invasive technique based on endogenous information. The BOLD effect also has certain applications in cancer imaging, such as the study of tumor angiogenesis, tumor oxygenation and brain activation in eloquent areas prior to surgical resection.
Lately, MRI has become a whole-body imaging modality

thanks to the advent of Tim (Total imaging matrix) and parallel imaging techniques. Image acquisition times have been shortened, thus allowing whole-body MRI examinations with high spatial resolution in less than one hour. Initial results show that whole-body MRI is a promising modality in oncology, especially for the detection of metastases and hematologic malignancies. In summary, MRI holds a great potential in replacing CT as the complementary modality to PET in dual-modality tomographs and in selected indications where MR already outperforms CT.

Challenges of combined MR/PET

Traditional PET systems use PMTs to detect the scintillation light. However, PMTs are sensitive to magnetic fields and are therefore not functional inside an MRI system. To overcome this problem, various approaches to the combination of PET and MRI have been established. For example, optical fibers can be used to lead the light from the scintillation crystals outside the fringe field of the magnet to the PMTs. Alternatively, split magnets with the PET detector positioned between the two magnet halves and connected via light fibers have been proposed. In either design, long optical fibers result in a loss of light and consequently in lower performance of such a PET system operated in the vicinity of an MR scanner.

This loss can be overcome by the use of magnetic field-compatible solid state light detectors, such as APDs (Fig. 4). This approach also permits easier expansion of the axial FOV of the PET system. The mutual interference between PET and MR is a critical problem; MR can affect PET performance because of the high static magnetic field, gradient fields, and radiofrequency field. MR image quality, however, can be impaired by either radiofrequency noise introduced by the PET electronics or magnetic field inhomogeneities caused by the presence of different materials in the PET insert and eddy currents induced from the gradient system in the conducting structures of the PET housing and circuit boards. Moreover, the operating temperature needs to be stabilized to ensure reliable PET and MR performance.

Finally, any combined MR/PET system must offer alternative approaches to deriving the necessary attenuation correction factors for the emission data. While in PET/CT attenuation data can be derived from transforming available CT transmission images into maps of attenuation coefficients at 511 keV, no such transmission data are available in MR/PET. This is due to the lack of physical space in general to host a transmission source. Secondly, a rotating metal-encased transmission

Conventional PET detectors

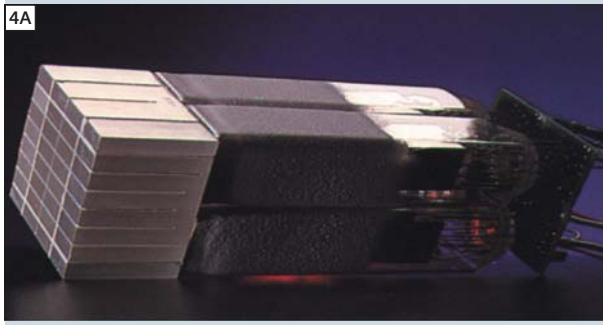

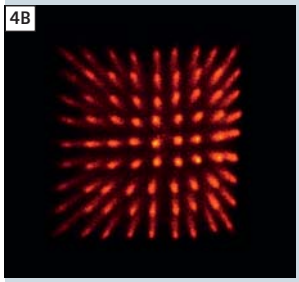

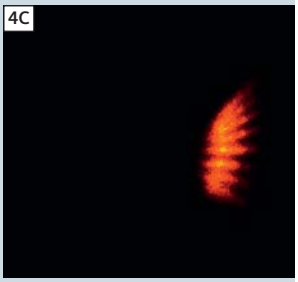

B = 0 B ≠ 0

APD-based PET detectors

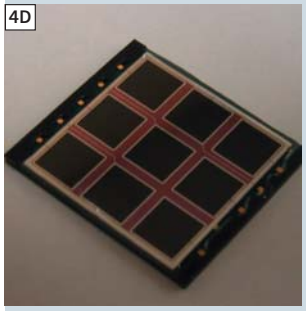

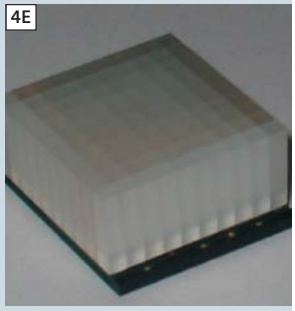

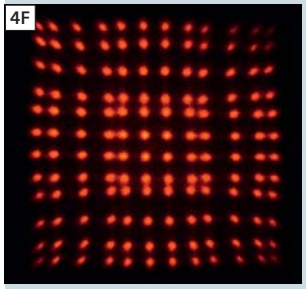

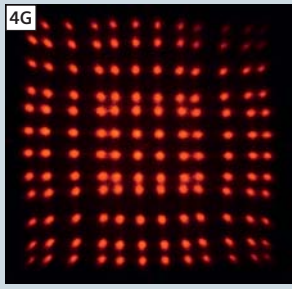

B = 0 B ≠ 0

4 Conventional PET detectors **(A)** are based on scintillation crystals and Anger-logics readout. They work only outside magnetic fields **(B)**. If a PMT is operated inside a magnetic field (B ≠ 0) then the multiplier step is construed and the readout map severely distorted **(C)**. Avalanche photodiodes (APD) based detectors **(D, E)** are semiconductors that can be operated in magnetic fields, even at ultra-high field strengths **(F, G)**. *(Image courtesy of Prof. B. Pichler, University of Tübingen, Germany.)*

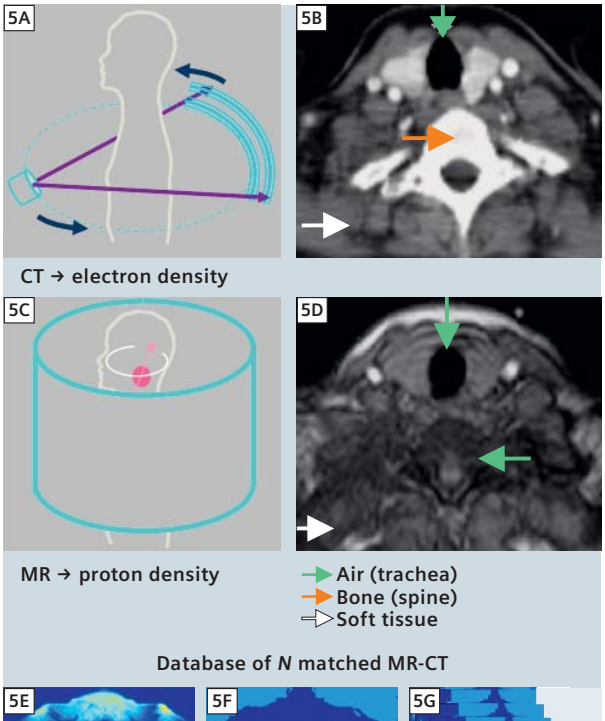

5 The challenges of MR-based attenuation correction: unlike CT images, that represent the attenuation of ionizing radiation (from an external source) by tissues in the field-of-view **(A)**, MR produces maps of proton densities **(C)**. Reconstructed images are different in the sense that highly attenuating tissues (e.g. bone) appear bright on CT and can be separated easily from low-attenuating tissues (e.g. air) **(B)**, which is not the case for MR images where air and bone have frequently similar appearances **(D)**. Therefore, segmentation-based algorithms for MR-based attenuation correction may fail to produce accurate PET attenuation maps. An alternative approach would be an atlas algorithm **(E–J)**: pairs of CT **(F)** and MR image volumes **(E)** are aligned and used to create a database of MR-CT data pairs **(G)**. The MR images **(H)** of a patient undergoing an MR/PET examination are compared voxel-by-voxel with the MR-database and a corresponding CT image is composed **(I)** and used to calculate the PET attenuation coefficients **(J)**.

source, whether X-ray tube, rod or point sources would lead to grave crosstalk effects with the MR magnetic field. And finally, the available MR images represent, in essence, proton densities that cannot be transformed to maps of electron densities as obtained from CT transmission measurements. Therefore, MR/PET requires novel approaches to MR-based attenuation correction. Segmentation-based approaches have been proposed and seem to work in brain imaging. However, MR-based attenuation correction in extracranial applications is much more demanding (Fig. 5).

Clinical prototype MR/PET

The development of combined MR/PET tomographs has been the reverse experience to that of PET/CT. The first PET/CT design emerged from industry-academia collaboration and was a prototype for human clinical use that stimulated a commercial response and later led to the development of PET/CT for imaging small animals. In contrast, MR/PET in the mid 1990's began with small animal designs.

Then, over a decade later, a prototype MR/PET was developed for human brain scanning that acquired the first images in November 2006. This prototype design is based on a PET insert for a 3T MR, and offers a transverse FOV limited to scanning the brain, or the extremities (Fig. 6). As of today four brain insert MR/PET systems have been installed worldwide; industrial backing for this human MR/PET prototype development is impressive and exceeds that of the early PET/CT developments.

This insert design is one of three general approaches to MR/PET being discussed today. An alternative design encompassing a co-axial arrangement of a 3T MRI and a TOF (time-of-flight) PET with a rotating patient handling system in between within one room was proposed in early 2010 (Fig. 6). A comparable system but with separate cabins for MRI and PET has been in existence for brain research since 2007. Again, several prototype systems were installed for clinical testing. A third, much simpler approach is also illustrated in figure 6. While the integrated MR/PET is the most sophisticated and perhaps ideal solution to combined imaging, the third design is that of a standalone PET and a standalone MR with a unified table docking station.

First experiences with MR/PET

First results of clinical simultaneous MR/PET

We received a prototype MR/PET system in 2008 and have evaluated the system since then. Our patient studies, as approved by the Ethic Committee, aim at demonstrating the feasibility of simultaneous MR/PET imaging of the human brain by using APD-based PET

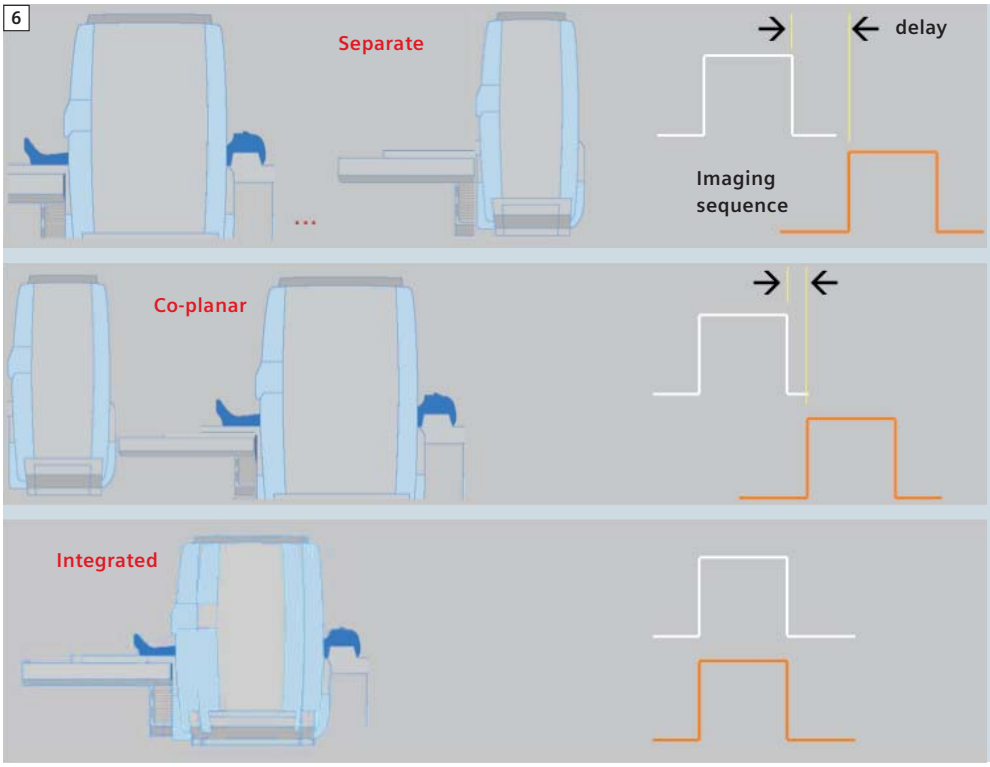

6 Different designs for combined MR/PET systems. Separate operations in different rooms is suggested as a low-budget approach to combined MR/PET; however, several practical challenges exist. An alternative approach to combine MR and PET information is to use a PET and an MR in tandem with a joined table platform. A third, and most challenging approach, is pursued by Siemens Healthcare and tested as a prototype at our institution with a PET insert that is slim fit into a whole-body 3T MR offering simultaneous MR/PET acquisitions.

detector technology integrated into a clinical 3T MAGNETOM Tim Trio system. The PET system consists of blocks of a 12 x 12 LSO matrix with an individual crystal size of 2.5 x 2.5 x 20 mm^3. The block is displayed on a 3 x 3 APD array with individual diodes that have an active surface of 5 x 5 mm. Six LSO-APD block detectors form a cassette; the cassettes are arranged along the z (main) axis of the tomograph, thus forming 72 crystal rings. The entire PET system consists of 32 radially arranged cassettes and has an axial FOV of 19.2 cm and an inner ring diameter of 35.5 cm. The system has a time resolution of 5.6 ms (full width at half maximum, FWHM) and a mean energy resolution at 511 keV of 22% (FWHM). All PET detector components such as amplifiers, resistors, shielding material and housing were selected to minimize interference with the MR imaging B field, gradients, and radio-frequency.

MR examinations are performed during PET data acquisition. Conventional MR imaging of the brain includes axial T2-weighted turbo spin-echo (TSE), fluid-attenuated inversion recovery sequence (FLAIR) and 3D T1-weighted fast low-angle shot sequence (FLASH) sequences. For diffusion-weighted imaging (DWI), a single-shot echo-planar imaging (SS-EPI) sequence is applied.

For PET imaging, the patients fast for at least 4 hours prior to the intravenous injection of ^{18}F-FDG. Body-weight adjusted, we inject in mean 370 mBq of ^{18}F-FDG. The distribution of the tracer is recorded during the entire MRI acquisition (time-range for simultaneous MR/PET from 20 to 40 minutes in most cases) at a steady state at 120 min post injection. The extended uptake time is due to the fact that all patients first undergo a clinically indicated PET/CT. PET data are acquired in 96-bit list mode containing complete information for each coincident event and stored on a disk, accumulating approximately 20 GB of raw data during a 40 min of PET acquisition. Emission data set is reconstructed iteratively (6 iterations and 16 subsets). The image volume consists of 153 transaxial image planes with a voxel size of 1.25 mm^3. Reconstructed resolution is 2.5 mm (FWHM) in the center and 4.5 mm at 10 cm off axis (for a line source in air reconstructed by using OPOSEM3D).

Our experience and studies indicate that – following system set-up and quality control - simultaneous MR/PET of intracranial tumors using ^{18}F-FDG, ^{11}C-methionine or ^{68}Ga-DOTATOC can be performed reliably. The image quality and quantitative data achieved using MR/PET is similar to that using PET/CT. An example MR/PET study is shown in Figure 7.

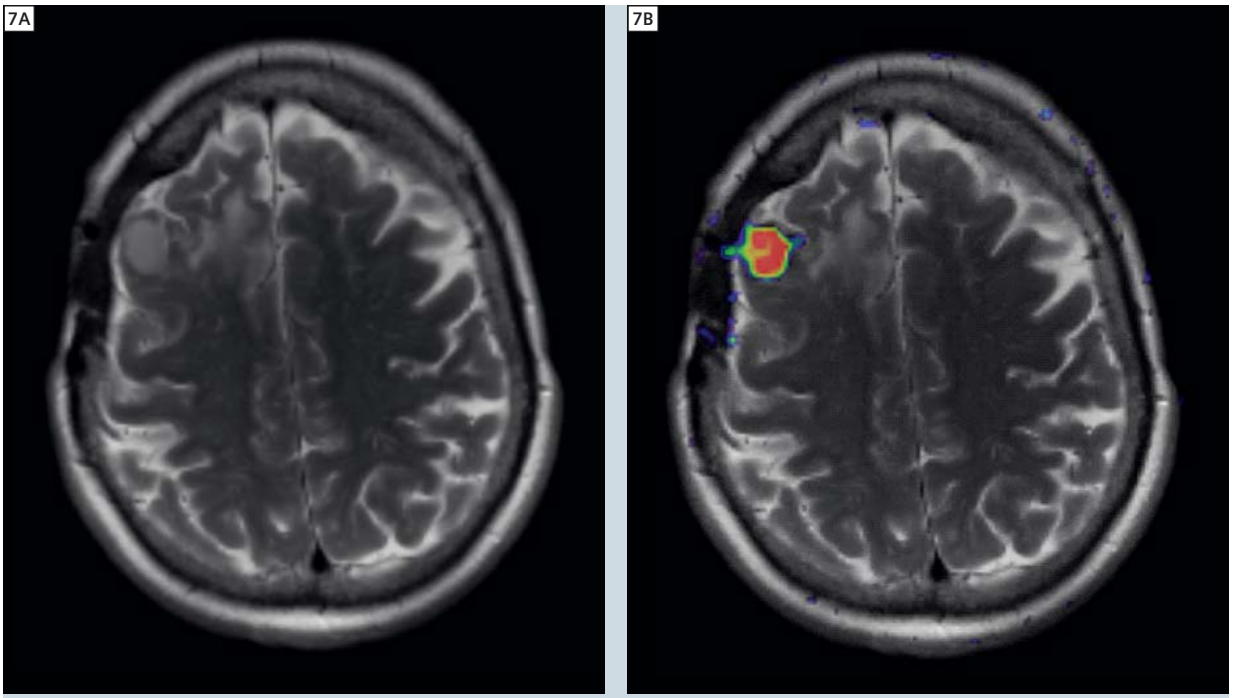

7 MR/PET imaging of a 65-year-old patient with a meningioma in the right frontal lobe. **(A)** Axial T2w MR images. **(B)** The intrinsic fusion of the simultaneously acquired MR and ^{68}Ga-DOTATOC PET images highlights the advantage of hybrid imaging regarding the accurate spatial coregistration without distorting artifacts. Data have been acquired using the integrated BrainPET MR/PET system (Siemens Healthcare, Erlangen, Germany).

The development of a prototype integrated MR/PET imaging system with no detrimental effect on the performance of PET and no degradation of MR images for a number of standard clinical MR images has put MR/PET imaging on the verge of being applied to clinical neurosciences. The combined system will certainly broaden the impact and possibilities of simultaneous imaging of morphologic, functional and metabolic information. First patient data are promising and highlight the scientific and clinical potential of the integrated system.

Challenges of (simultaneous) MR/PET: Quantification

Together with the clinical and performance evaluation of the prototype MR/PET at our hospital, we have initiated the development of versatile approaches to MR-based attenuation correction (AC) for clinical use. Performing PET attenuation correction with MR image information is challenging. Various approaches for predicting the attenuation maps from MR images have been proposed by several groups. MR image segmentation works well for the brain but can fail on extra-cerebral images, mainly due to the similar appearance of air and bony tissues as well as artifacts towards the edge of the FOV of MR images. If a separation of bone and air is required, torso MR/PET imaging in particluar requires more sophisticated methodologies. We focus on a combination of an atlas approach and machine-learning algorithm to estimate a PET attenuation map from the available MR images (Fig. 5), which was shown to work well in our hypothesized whole-body MR/PET data. In general, MR-AC must address adequate transformation of MRI pixel value information to appropriate PET attenuation values and account for additional pitfalls, such as truncation effects from patients extending beyond the transverse FOV of the MR system and the presence of MR surface coils typically not seen on MR imaging. In latter cases, dedicated MRI sequences using ultra-short echo times appear as promising adjuncts to MR imaging for the purpose of MR-AC.

Challenges of simultaneous MR/PET: workflow

In terms of workflow aspects and logistics, integrated imaging techniques – in theory – can outperform any separate or sequential imaging. This has direct implications on patient comfort and compliance. Nonetheless, a number of questions remain with respect to the overall integration of this new combined modality into clinical workflow, be it as an adjunct or as a

replacement method; this needs to be addressed by prospective studies. In the interim there are indications for numerous research applications that benefit from simultaneous MR/PET imaging, currently for brain application only, in the near future for larger imaging areas. Simultaneous imaging functionalities must comprise hardware and software tools. As hardware integration of the combined system progresses, so must the integration with respect to software and data processing. Current viewing tools need to be expanded to allow efficient screening, accurate analysis and quantification, where needed, of data sets that comprise 3D images, dynamic data and additional information, such as spectra, perfusion maps or multiple metabolic pathways.

Simultaneous versus sequential MR/PET imaging

It may be too early to predict a prevalence of one over another acquisition mode. The question of sequential over simultaneous imaging is the subject of an ongoing debate. From a technical perspective simultaneous imaging allows for a number of advanced data processing steps that are not straight forward in sequential MR/PET (and PET/CT imaging). This includes motion correction for involuntary patient motion and any subsequent quantification that may be biased from patient motion during the examination. MR-based motion correction is work-in-progress.

To correct for patient motion, special MRI sequences can be applied by either 1-dimensional navigator scans or in 2 to 3 dimensions to detect the motion of the subject. Ideally, these protocols can be combined with the MRI sequence already running to provide motion information about the subject in intervals of as short as 1 s. The motion vectors may be extracted from the motion-sensitive MRI scans and made available to the PET system, allowing either online or post acquisition motion correction of the PET images. General advantages of simultaneous data acquisition include temporal correlation of PET and MR imaging data, reduced imaging time compared with sequential imaging, and the option for cardiac and respiratory motion correction of PET data.

MR/PET – What can be expected in the near future?

With the success of PET/CT in mind, the expectations for any new combination, such as MR/PET are very high. Obviously, MRI provides excellent soft tissue contrast without using ionizing radiation. Thus, it seems a perfect anatomical complement to PET (Table 1). The main idea behind merging PET and MRI is to combine the functional / metabolic information provided by PET with the high soft-tissue contrast and the func-

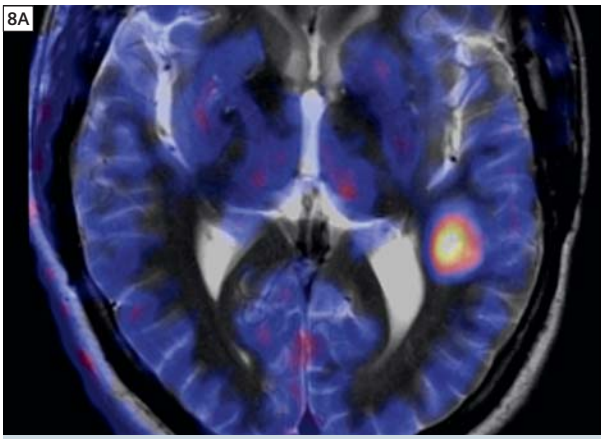

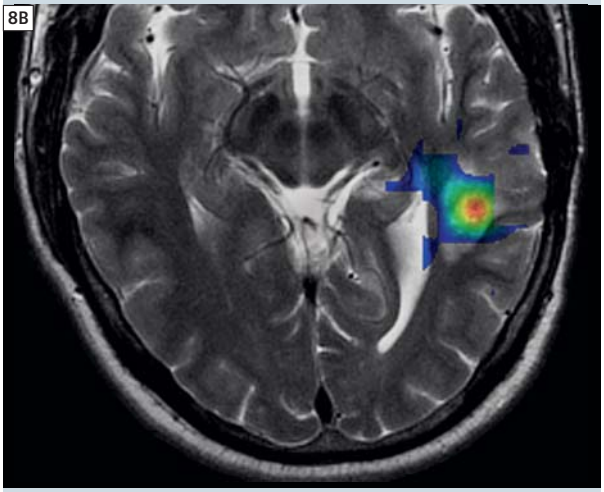

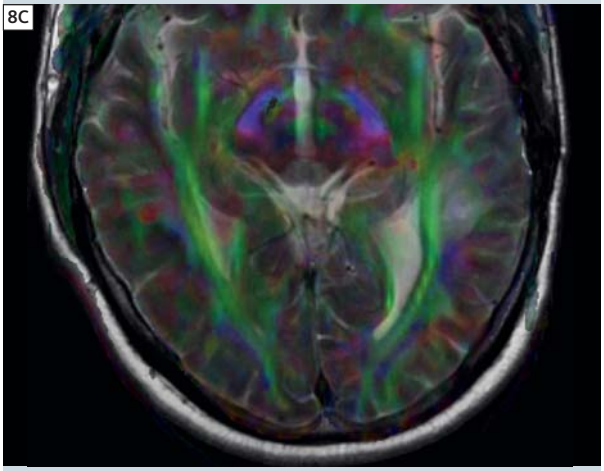

8 Simultaneously acquired and superimposed on ^{11}C-methionine-PET and MR imaging avid tracer uptake of the atypical neurocytoma on the left side in a 42-year-old patient **(A)**. Simultaneously acquired chemical shift imaging (CSI) MR spectroscopy provides a map of choline to N-acetyl-aspartate ratio **(B)** indicating the high proliferating index of the tumor, while simultaneous diffusion tensor imaging **(C)** shows the clear relationship to the adjacent optic radiation.

tional information offered by MRI. However, the potential areas of application of combined MR/PET extend far beyond high-contrast image fusion. This is supported by our in-house studies where the pre-clinical and clinical prototypes have convincingly demonstrated that the APD-based PET system can be operated simultaneously with the MRI without sacrificing the performance of either modality.

Brain studies, for example, benefit greatly from the additional morphologic information provided by MRI. Simultaneous data acquisition will allow the addition of kinetic, functional and metabolic information for real time multi-parametric functional imaging; to name just two applications:

- MRS can provide additional metabolic information to regional metabolic data from PET in stroke, gliomas, and degenerative disorders;
- MR-based perfusion-weighted imaging (PWI) can be correlated with hypoxic markers (^{18}F-MISO PET) for correcting PET results and also for further understanding of tumor microenvironment.

For complex studies of brain functions combinations of modalities or additional functional techniques will open new insights into the organization of the brain and the changes in disease. For example, diffusion tensor imaging can be added to activation studies and therefore, effects on transmitter release, receptor occupancy and metabolism in connected areas can be analyzed as substrates of connectivity in networks (Fig. 8).

The list of conceivable research topics and clinical applications of MR/PET is extensive. It could be particularly useful for early tumor detection and functional therapy monitoring in oncology. It will likely be used to investigate the effect of novel drugs, such as inhibitors of angiogenesis or modulators of the immune system. Integrated information on individual cell metabolism and microenvironment and their response to therapy will help elucidate the mechanism of action and optimize treatment schedules.

In the field of cardiology, the potential of MRI to assess cardiac function can be combined with the possibilities offered by cardiac PET; this combination would allow clinicians to assess the metabolic viability of the heart muscle, its perfusion and functional impairment. Initial studies combining MR spectroscopy with PET have already been performed on isolated perfused rat hearts, but may also elaborate cardiac MR/PET studies involving cardiac stress simultaneously assessed with PET and MRI. Dual functional studies correlating the same parameters (e.g. perfusion in PET via radioactive water or ammonia and in MRI using arterial spin labeling or MRI contrast agents) can help to cross correlate and validate different acquisition techniques. Using the strengths of each individual modality, one can simultaneously assess different molecular parameters. For instance, diffusion processes may be tracked simultaneously with PET tracer uptake, or PET perfusion can be correlated with the MRI BOLD effect. Because of the large number of existing PET probes and the various functional imaging capabilities of MRI, the number of possible combinations for molecular imaging readouts is virtually unlimited. The advantage of truly simultaneous MR/PET is that the same subject is scanned at the same time with identical environmental parameters and stimuli. It is

Table 1: Assessment of biological properties by MR and PET.

MR	PET
Morphology	Flow ($H_2{}^{15}O$)
Water diffusion capacity (DWI)	Metabolism (^{18}F-FDG)
Vascular anatomy (MRA)	Blood volume ($C^{15}O$)
Perfusion (PWI, DCE-MRI)	Oxygen consumption (^{15}O)
Tissue metabolites (MRS)	Hypoxia (^{18}F-MISO)
Functional activation (fMRI)	Vascular permeability (labeled AA)
Cerebral fiber tracts (DTI)	Nuclide acid synthesis (^{18}F-FLT)
Oxygen consumption (^{17}O)	Transmitters (e.g. ^{18}F-DOPA)
Migration of cells (Fe labeling)	Enzymatic activity (e.g., MP4A)
Angiogenesis (e.g. ^{18}F-RGD)	
Distribution and kinetics of tracers and drugs (labeled compounds)	
Enzymatic activity in transfected cells	

likely that such functional studies will further push the limits for basic biologic research and will open new realms for studying biology in vivo.
Finally, applications of MR/PET imaging in oncology are likely to expand. Recent clinical studies comparing whole-body MRI and PET/CT have indicated the potential advantages of a combination of MR and PET. The superior soft tissue contrast of MR is in general relevant for all types of soft tissue tumors regarding detection, delineation, characterization, and staging. Nonetheless, CT is still more sensitive than MR in revealing smallest lung nodules. On the other hand, dynamic MR studies that yield various parameters for quantification of perfusion without additional radiation exposure, and PET studies that may be performed simultaneously visualize in whole the tissue and the vascular components of the tumor.
One of the primary strengths of MRI is its ability to provide anatomical detail in addition to detect abnormalities within boney structures (e.g. marrow, joint spaces). ^{18}F-FDG PET is useful in the diagnosis of acute infections and is an accurate imaging modality to exclude the diagnosis of osteomyelitis. When combined and clinically available, MR/PET may provide a more accurate diagnosis of patients with osteomyelitis including those with complicated diabetic foot disease.
The complementary morphological and metabolic data can be relevant for defining biopsy targets, particularly by differentiating areas of active tumor involvement from inflammatory disease, fibrosis or necrosis. Combined morphological and metabolic imaging is also important for the evaluation of early treatment response. Metabolic information assessed e.g. by ^{18}F-FDG (marker for glucose consumption and therefore energy consumption) or ^{18}F-FLT (fluorothymidine; marker for nuclide acid synthesis and therefore proliferation) is more sensitive for detecting therapy-induced metabolic and necrotic tissue damage. Additional high-resolution morphologic information may be potentially helpful in the planning of subsequent surgery and radiotherapy.

A decade of hybrid imaging

A mere two years after the advent of commercial PET/CT, Johannes Czernin from UCLA commented: "PET/CT is a technical *evolution* that has led to a medical *revolution*". Today, at the dawn of MR/PET imaging, we may extend his phrase by "integrated MR/PET is a medical *evolution* based on a technical *revolution*". PET/CT appears to have replaced stand-alone PET for nearly all oncologic indications. Ongoing and future studies using first prototype and clinical systems will show how much MR/PET could supplement PET/CT imaging in the clinic. We believe that MR/PET is a required and valuable adjunct to modern healthcare and that there will be indications for which MR/PET may become a primary or secondary diagnostic test during work-up or follow-up of a variety of patients.
Nevertheless, MR/PET will not replace PET/CT as a molecular imaging modality in the near future. Both modalities are here to stay because both platforms incorporate the diagnostic power of PET. In fact, with PET/CT being a "*dual*-modality imaging" platform by virtue of combining functional (PET) and anatomical (CT) imaging only MR/PET offers true "*multi*-modality imaging" by virtue of combining function (PET) and anatomy and function (both MR). This will open, without a doubt, new avenues in non-invasive imaging as part of clinical patient management and clinical research.

Contact
Thomas Beyer, Ph.D.
Imaging Science Institute (ISI) Tübingen
University Hospital Tübingen
Dept. of Diagnostic and Interventional Radiology
Hoppe-Seyler-Str. 3
72076 Tübingen
Germany
Tel.: +49 7071 29 81212
thomas.beyer@cmi-experts.com

http://health.siemens.com/isi/index.php
http://health.siemens.com/isi/index_eng.php

Whole-Body MR/PET Hybrid Imaging: Technical Considerations, Clinical Workflow, and Initial Results

Harald H. Quick, PhD[1]; Ralf Ladebeck, PhD[2]; Jens-Christoph Georgi, PhD[2]

[1]*Institute of Medical Physics (IMP), Friedrich-Alexander University Erlangen-Nürnberg, Erlangen, Germany*
[2]*Siemens AG Healthcare Sector, Erlangen, Germany*

MR/PET – Advent of a new hybrid imaging modality

These days we are eyewitnesses to an exciting new hybrid imaging modality to enter the clinical arena, namely simultaneous whole-body MR/PET imaging. Envisioning the combination of the excellent soft tissue contrast, high spatial and temporal resolution, and functional tissue parameters that MR provides with the high sensitivity of PET, different technical approaches have been pursued by researchers and by the industry to work on the integration of two formerly 'non-integrable' imaging modalities. With the recent introduction of the Biograph mMR, Siemens has launched a 3.0 Tesla whole-body MR hybrid system that hosts in its isocenter a fully integrated PET detector and that with its 60 cm patient bore enables whole-body simultaneous MR/PET imaging.
Researchers, radiologists, and nuclear medicine physicians have been waiting and actively been working on the advent of this hybrid imaging modality for a long time [1–3]. A detailed overview about the pre-clinical developments, the rationale to combine MR and PET as well as the steps which were necessary for integrating these imaging modalities to allow simultaneous scanning can be found in the article by Beyer et al. 'MR/PET – Hybrid Imaging for the Next Decade', published in the supplement of issue 3/2010, RSNA edition of MAGNETOM Flash. Now that whole-body MR/PET has entered clinical practice, we have a starting point to evaluate the full clinical potential of the modality, to research for and to validate new imaging applications, and to ultimately establish this imaging modality in early diagnosis of oncologic, neurologic, cardiologic, and many more diseases.
As more and more research and clinical sites come on board during the months and years ahead, let's take a first look into the technology and explore what specifics such an integrated MR/PET hybrid system brings with it. We will then also explore the workflow of a MR/PET whole-body hybrid exam and present first image examples from clinical findings.

Technical integration of MR and PET

The Biograph mMR hybrid imaging system fully integrates the MR and the PET imaging modality into one imaging system. In order to ensure such a high level of integration, we have to overcome numerous physical and technical preconditions and challenges. The potential physical interactions of both modalities in both directions – PET on MRI and MRI on PET – are manifold. Full integration of a PET system into an MRI environment requires technical solutions for three groups of potential electromagnetic interaction:

1) the strong static magnetic B_0-field for spin alignment,
2) the electromagnetic changing fields of the gradient system (G_{xyz}) for spatial signal encoding, and
3) the radiofrequency (RF) B_1-field for MR signal excitation and MR signal readout.

→ The QR code is your direct link to Thomas Beyer's article on the history of combining PET with MRI, the rationale to do so and challenges which had to be overcome. You will also find the article at **www.siemens.com/magnetom-world**

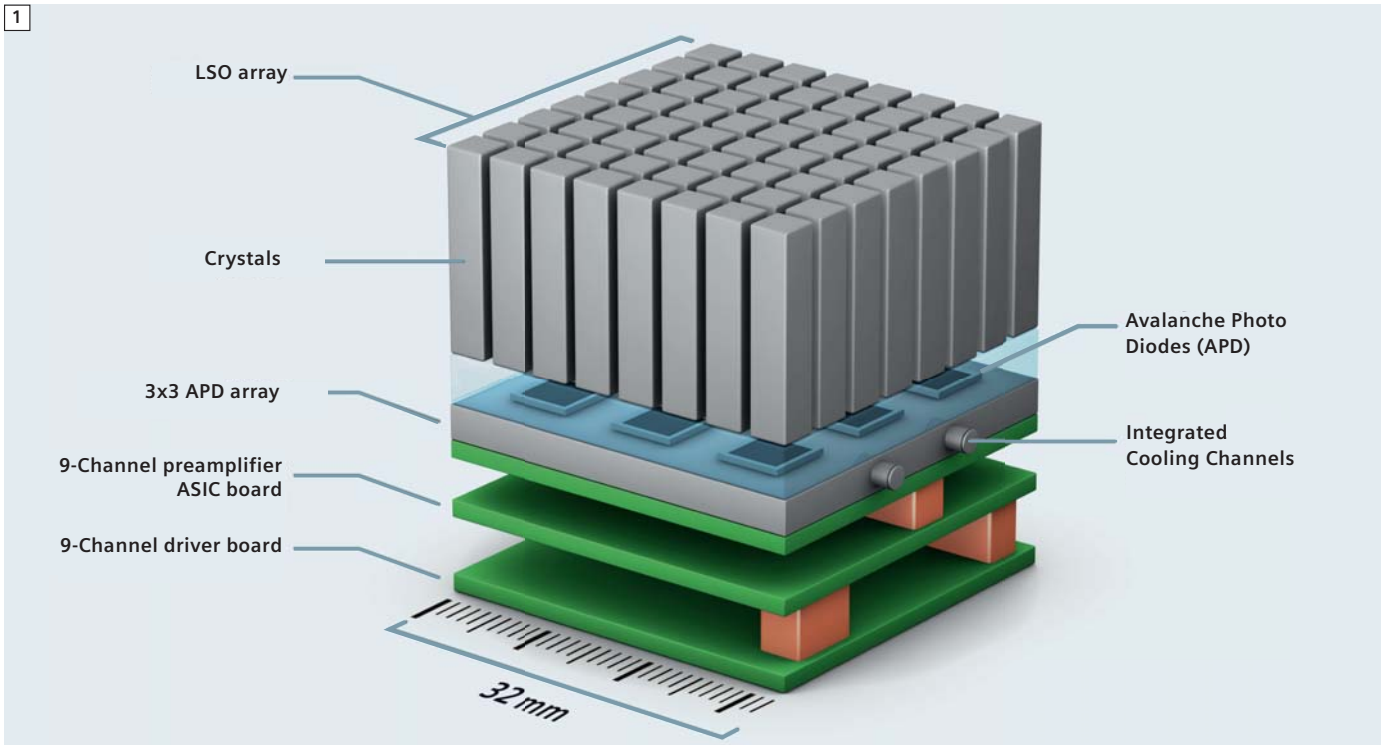

1 Pet detector assembly for mMR. 64 Lutetium Oxyorthosilicate (LSO) crystals form one block that transforms 511 keV gamma quanta into light flashes. Light events in the LSO crystals are detected by a 3x3 array of avalanche photo diodes (ADP). 9-channel preamplifiers and driver boards as well as integrated water cooling completes each detector block. This detector assembly is characterized by its small size, can be designed free of magnetic components, and performs in strong magnetic fields. 56 such blocks form one detector ring, 8 rings form the PET detector assembly in the Biograph mMR that spans a longitudinal field-of-view (FOV) of 25.8 cm.

PET hardware and PET signals must not be disturbed by any of these fields. Equally, for full and unlimited MRI system performance, PET must not disturb any of these electromagnetic MR fields and signals.
Numerous technical solutions were thus required for PET integration into an MRI system. The most important key technology enabler was the development of detectors and photo diodes that are able to detect the 511 keV PET gamma quanta following an annihilation event inside of a strong magnetic field. What worked well in established PET and in hybrid PET/CT systems in the form of scintillation crystal blocks read out by photomultiplier tubes (PMT), had to be replaced for the MR/PET integration since the PMTs are very susceptible to magnetic fields. The current detector solution for simultaneous MR/PET is a combination of Lutetium Oxyorthosilicate (LSO) crystals and Avalanche Photo Diodes (APD) able to detect gamma quanta even inside strong magnetic fields and convert the detected events from scintillation light to electrical signals (Fig. 1A) [4]. Another advantage of the combination LSO crystal and APD diodes compared to PMT is that they do not require as much space and thus can be integrated inside of an MRI bore. Siemens' 70 cm magnet bore technology is clearly another precondition to integrate the PET detectors inside the limited space of an MRI system and at the same time to leave enough space to eventually end up with an inner whole-body bore diameter of 60 cm – as has been clinical standard for MRI magnet bore diameter in the past. In the Biograph mMR hybrid system, 56 LSO-APD detector blocks, each with a block area of 32 x 32 mm^2, are aligned circumferentially to form one PET detector ring. 8 rings form the full PET detector unit, spanning a length of 25.8 cm in z-direction (for comparison: conventional/standard PET-CT systems have an axial field-of-view (FOV) of less than 20 cm and high-end PET-CT systems nowadays have a FOV of approximately 22 cm). Each LSO crystal, which are put together to form than the LSO-APD block, has a size of 4 x 4 x 20 mm^3 which is the finest crystal dimension in the market for clinical PET systems; the crystal size has a direct impact on the achievable PET resolution.

2

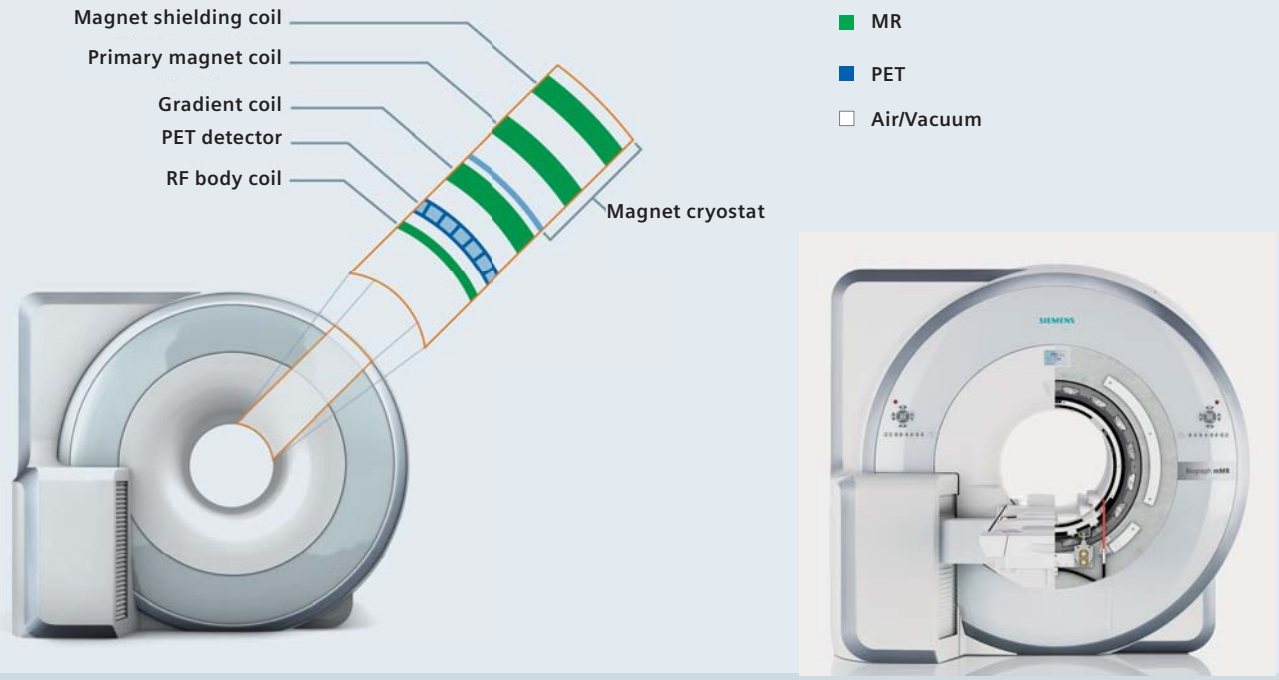

2 Schematic drawing and photograph showing the integration of the PET detectors in the MR hardware structure of the Biograph mMR. From the inside to the outside: RF body coil, PET detector, gradient coil assembly, primary magnet coil, and magnet shielding coil. The latter two magnet coil assemblies are contained in the helium filled magnet cryostat. The MR/PET integration as shown requires that the PET detector works within strong static and dynamic magnetic fields, and does not disturb any of the associated electromagnetic MR fields. The PET detector must not disturb the static B_0-field, the gradient fields nor the RF transmission and reception. Additionally, in this configuration the RF body coil needs to be designed 'PET transparent' with little attenuation of gamma quanta.

How has the integration of the PET detector unit into the MR environment been performed technically? Seen from the perspective of the signals emitting patient, the hardware layer structure of the hybrid system is as follows: The innermost layer in the magnet bore is formed by the signal transmitting and receiving RF body coil with its RF shield, shielding the RF coil towards the other structures in the bore. The PET detector rings are located behind the RF coil and its RF shield. The layer behind the PET detector unit is formed by the gradient coil assembly encompassing gradient coils for spatial MR signal encoding in all three dimensions of the scanner coordinate system. The outer layer structure is formed by the magnet cryostat containing the liquid helium for magnet cooling as well as the superconducting magnet winding producing the 3.0 Tesla static magnetic B_0-field (Fig. 2). The individual hardware components as well as the whole hardware assembly are optimized towards MR and PET signal detection with no signal disturbances in either direction. A technical precondition to fulfill these requirements is that the RF body coil should be 'PET transparent' such that gamma quanta emitted by the patient are not attenuated by the RF body hardware. An additional consequence is that the PET detectors need to be non-magnetic and 'gradient transparent' in order to not distort the linearity of the fast switching gradient fields. The PET detectors require stable temperatures over time of around 20°C temperature, which has been achieved by implementing water cooling into the APDs (Fig. 1). Analog electrical signals and water cooling are conducted from the PET detector in the isocenter of the magnet bore to the back end of the MR/PET system. All PET detector electronics are hermetically shielded by copper elements in order not to emit RF signals that potentially could disturb the weak MR RF signals or contribute to increased overall RF noise, leading to decreased signal-to-noise-ratio (SNR) in MRI measurements. With regard to potential interaction with the three groups of electromagnetic fields in an MRI surrounding, all components of the PET detector and electronics must be absolutely non-magnetic, must be absolutely RF shielded and must be optimized to eliminate susceptibility to eddy currents. Eddy currents potentially interact with the strong and fast switching magnetic gradient fields for spatial MR signal encoding. When switching gradient fields, according to Lorentz' induction law, eddy currents are induced into neighboring electrically conducting structures. Unwanted eddy currents thus counteract the effect of fast switching linear gradient fields, potentially leading to reduced rise times, reduced amplitudes, and reduced gradient linearities, resulting in an overall reduced gradient performance and non-linear geometrical distortions in MR imaging.

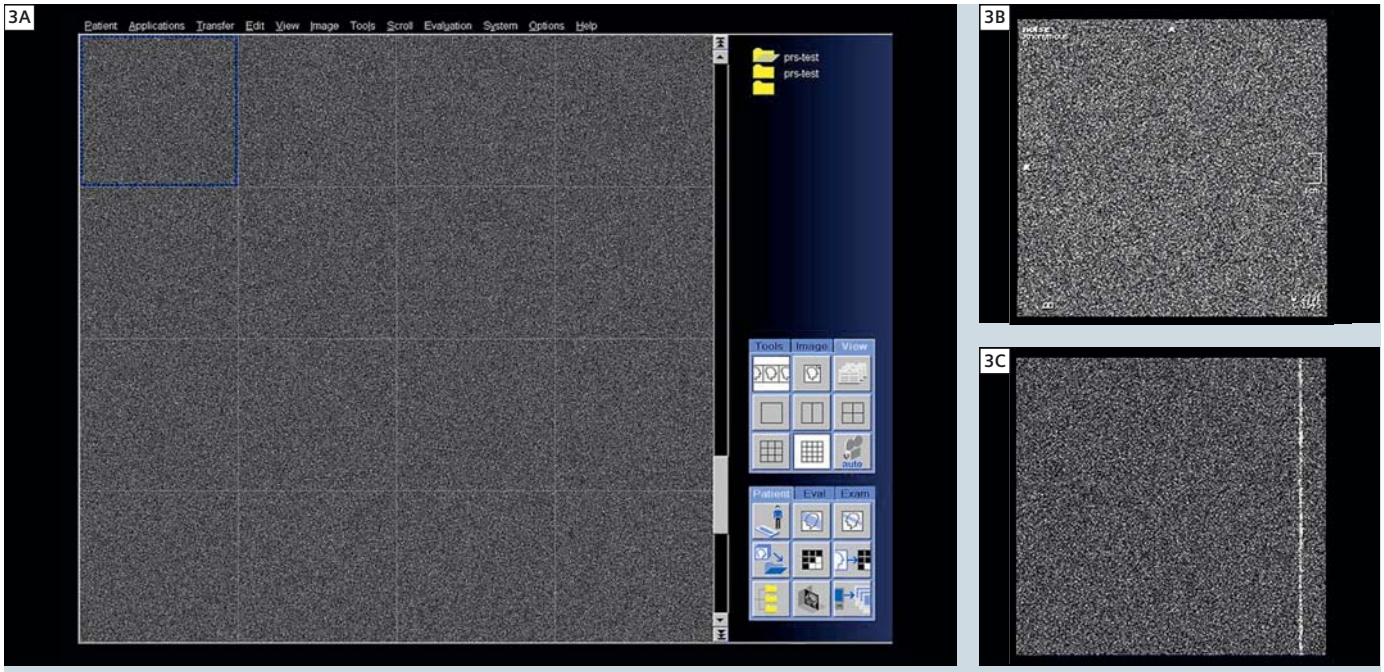

3 System integration testing: RF noise check. Images in **(A)** show results of an RF noise detection routine in MR imaging that was acquired while the PET detector unit was simultaneously activated. In this noise check, the RF receivers of the MR system are stepped through a frequency range of ±250 kHz around the Larmor center frequency in intervals of 10 kHz. The panel in **(A)** shows a selection of 4x4 images, each representing a frequency range of 10 kHz. The individual noise images here show neither increased noise nor any other discrete enhancement. Zoom-in **(B)**. This result of the RF noise check indicates uncompromised shielding of the electronic PET components over the whole receiver bandwidths of the MR system. Just to demonstrate the effect of disturbing RF noise, image **(C)** shows a single measurement disturbed by a discrete RF signal (vertical stripe on the right side of the image) that has been provoked by opening the two doors of the RF cabin during measurement.

System integration testing

Early system integration testing of the Biograph mMR hybrid MR/PET system has been performed at the Institute of Medical Physics (IMP), University of Erlangen, Germany, in close collaboration with Siemens Healthcare, Erlangen, Germany. Successful system integration needs to be explored and verified in numerous systematic technical and phantom testing experiments. This requires testing in both directions to answer the following questions: Is PET performance influenced by the MR? Is MR performance influenced by the PET? MR testing encompasses testing for potential interactions with RF, B_0, and G_{xyz}, and related artifacts. PET testing encompasses testing for count rates, detector performance, signal homogeneity, and artifacts [5].

Figure 3 shows RF noise testing – a routine system performance test in MRI. In this test, the RF receiver chain is set to a high receiver gain and then stepped in steps of 10 kHz through a varying bandwidth ranging from -250 kHz to +250 kHz around the Larmor center frequency of the 3.0 Tesla MR system. This is performed twice: Once with PET switched off, and again with the PET hardware switched on. Thus subtle differences in the overall noise level or discrete RF noise frequencies with/without PET can be detected.

Static magnetic B_0-field homogeneity testing encompasses measurements of the static magnetic field homogeneity with/without PET detectors inside of the system. The difference between both measurements can be visualized and evaluated in B_0 difference field maps in three spatial dimensions. Thus subtle differences in the B_0 static magnetic field homogeneity can be detected and displayed within ppm accuracy. In the Biograph mMR system the magnetic field homogeneity is specified with ≤6 ppm standard deviation V_{rms} (volume root-mean square) over an elliptical volume of 50 cm diameter in the x-y-plane and 45 cm in z-direction. In system integration testing the measurements with/without PET detector installed did not reveal any influence of the PET detector on the B_0-field homogeneity of the MR system.

Also the gradient system performance with its parameters amplitude (mT/m), slew rate (T/m/s) and overall linearity has to be evaluated twice with/without PET detectors to determine possible variations from the gradient systems specifications. Measurements have confirmed that the gradient systems performance in the Biograph mMR system is in the specifications – 45 mT/m maximum amplitude for all three gradient axes, 200 T/m/s maximum slew rate, and thus compares well to a system without PET integrated in the magnet bore. This is a major precondition to take full advantage of numerous whole-body imaging

4

4 The Biograph mMR system installation at the Institute of Medical Physics, University of Erlangen. Both imaging modalities – MR and PET – are fully integrated into one MR/PET hybrid system.

5

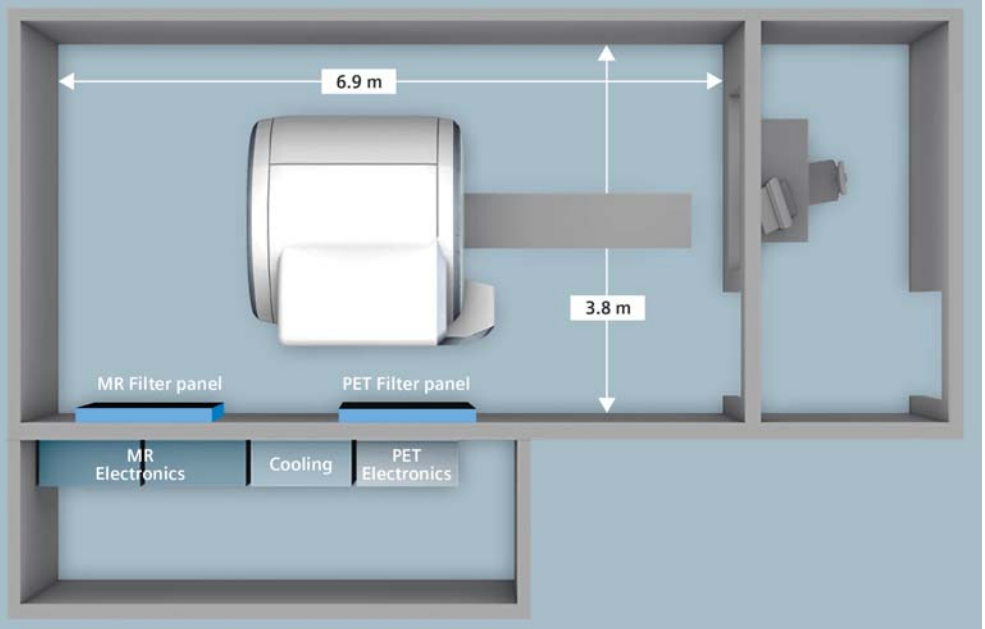

5 Schematic showing the compact siting of the Biograph mMR system and its hardware components. In comparison to an MR-only installation, the MR/PET installation adds only another filter panel and one extra cabinet for the PET electronics to the installation site.

sequences providing anatomical and functional tissue information simultaneously with a combined data acquisition with PET: Diffusion-weighted imaging (DWI), diffusion tensor imaging (DTI), arterial spin labeling (ASL), functional MRI (fMRI), MR spectroscopy, time-of-flight angiography (TOF-MRA), dynamic cardiac acquisitions, etc., to name only a few. Finally the PET systems performance has also to be tested for the potential influences of the strong magnetic field by gradient fields, or by RF interactions. Such testing performed according to NEMA standards [5] twice outside and inside of the MRI system and during system integration testing did not reveal any deviations from the PET performance without MRI surrounding.

Siting specifics

With this new hybrid imaging systems generation, combining the non-radiating imaging modality MRI with the nuclear medicine imaging modality PET, a couple of technical and logistical particularities have to be considered when it comes to siting of such a hybrid system. The high degree of system integration in case of the Biograph mMR helps to reduce the space that is required for system installation. This holds true for the scanner room as well as for the technical equipment room. The installation only requires a minimum of 33 m^2 of installation space for the scanner, electronics and console room. Figure 4 shows the Biograph mMR installation at the Institute of Medical Physics (IMP), University of Erlangen, Germany. When compared to the installation of a conventional standalone MR system, the MR/PET hybrid system does not require additional space in the scanner room and only requires one additional cabinet in the technical equipment room (Fig. 5). Water cooling infrastructure is shared for both the gradient system and for the PET detectors. The additional cabinet in the technical equipment room contains the PET electronics and computers for signal processing and image reconstruction, respectively. Another requirement for the MR/PET hybrid system installation is a second filter panel in the RF cabin to

feed the PET signals and associated cables through the wall between the system room and the technical equipment room. During the MR/PET systems installation at the Institute of Medical Physics, University of Erlangen, a second RF shielded door was installed in the RF cabin. Although not a necessity, this installation at the IMP enables a patient to be brought directly from the 'active waiting' controlled area into the scanner room which then becomes a temporal control area and thus not affecting the operator room with radiation at any time. Thus personnel, researchers and potential visitors can stay in the operator room while switching patients in the scanner room.

RF coils and associated attenuation correction

Like its MR-only siblings, the Biograph mMR MR/PET hybrid system is equipped with a full set of RF coils and associated RF architecture – the well established Tim technology (Tim, Total imaging matrix, Siemens Healthcare). The Tim RF system provides seamless coverage of the patient's body with integrated surface coils from head to toe (Fig. 6). The coils are each equipped with multiple RF coil channels providing a high coil element density for high SNR gain as well as parallel imaging capabilities with high acceleration factors in three spatial dimensions. While this integrated RF surface coil concept today is well established in MRI, its use in a combined MR/PET hybrid imaging system is a novelty and prerequisite for seamless whole-body MR/PET acquisitions. The RF surface coils that cover the patient's body for optimal MR signal performance are at the same time in the FOV of the PET detectors. Thus all RF surface coils now have to be also optimized towards PET-transparency, i.e. such coils should attenuate gamma quanta to only a minor extent, for optimized PET performance. This also holds true for all other hardware equipment – MR or PET related – that potentially accompanies the patient's body when traveling through the PET-FOV, e.g. RF surface coils, the patient table, cables, connectors, patient monitoring equipment, etc. [6]. Here one can differentiate between 'rigid and stationary' equipment such as the patient table, the RF spine array coil as well as the RF head coil, and between 'flexible and non-stationary' equipment such as the flexible RF Body Matrix array coils. 'Rigid' here means stable in its form and geometry. 'Stationary' in this context means non-moving relative to the patient table whose position is known to the imaging coordinate system at any point in time when moving in the scanner bore.

The PET signal attenuation and scatter of rigid and stationary equipment can be compensated for by straightforward attenuation correction (AC) methods. For example, the RF head coil (Fig. 7A) is scanned in a CT (computed tomography)

6

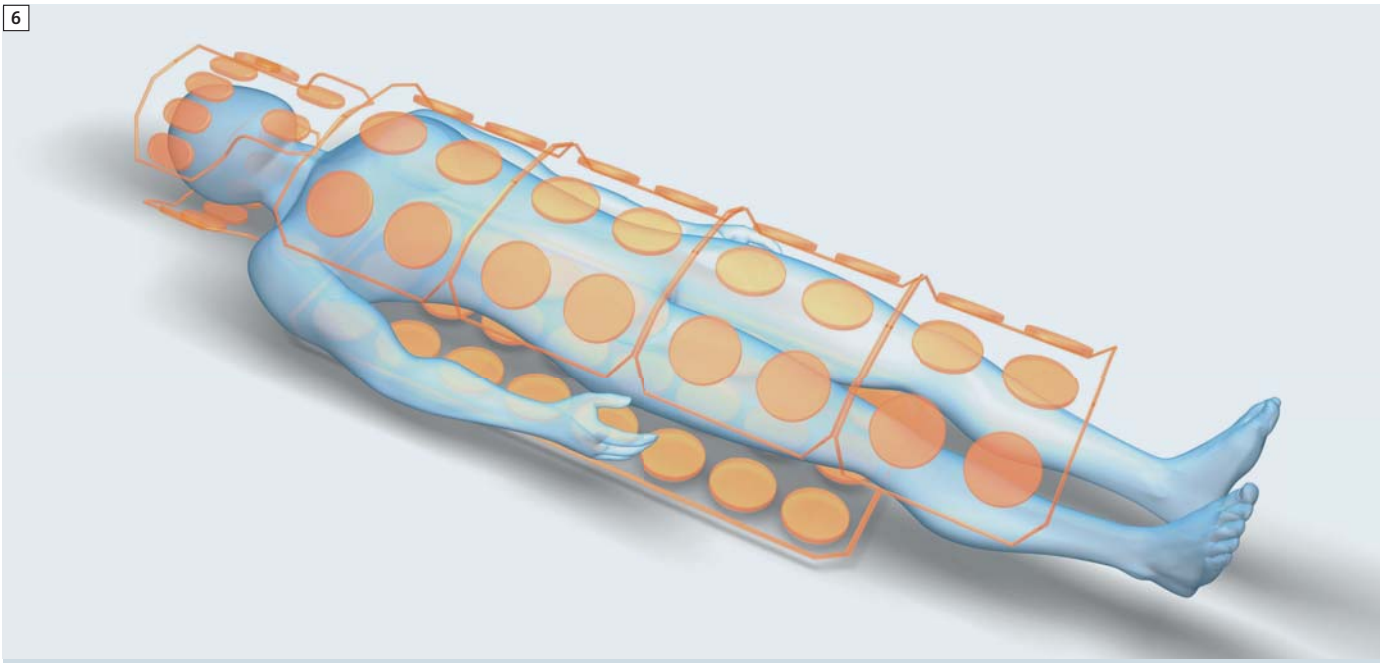

6 The Biograph mMR is equipped with the Tim (Total imaging matrix) RF coil technology consisting of multiple integrated surface coils that cover the patient's body from head to toe with up to 102 RF coil elements connected to 32 RF receivers. This multi-channel phased array RF coil configuration enables parallel imaging and whole-body MR data acquisition with optimized signal-to-noise (SNR) performance. In simultaneous MR/PET hybrid imaging, the surface RF coils are located between the radioactivity emitting patient and the PET detectors. As a consequence, the RF coils should be designed to be as PET-transparent as possible.

7A

7B

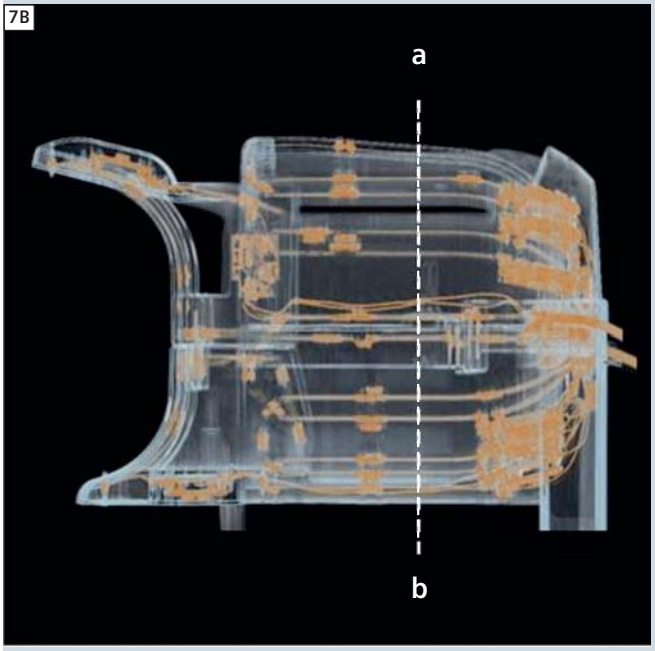

7C

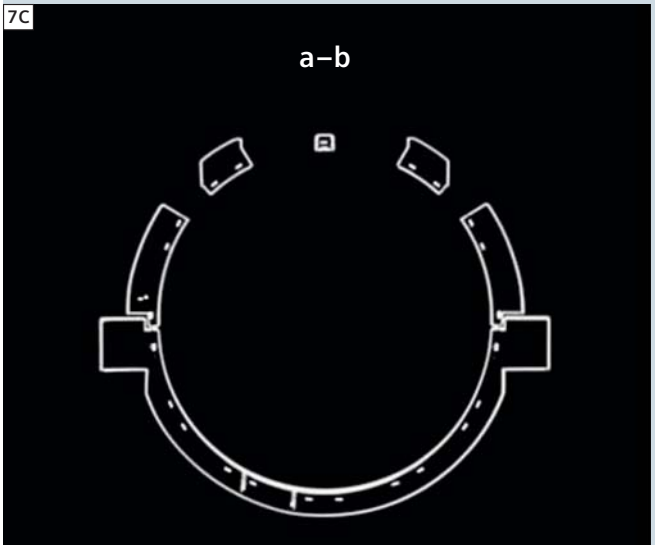

7A **(A)** A head/neck RF coil that was designed and optimized towards PET-transparency for use in simultaneous MR/PET hybrid imaging. This RF coil serves as an example of a rigid hardware component that is stationary at its known position with regard to the patient table. **(B)** 3D CT-scan of this rigid RF coil. Such a CT-scan provides hardware attenuation values that can be transformed from the CT's 100 keV energy level to the 511 keV energy level of PET in order to derive a PET-equivalent attenuation map (μ-map), shown in image **(C)**. The μ -map in **(C)** has been acquired at level a–b as shown in image **(B)**.

system once and a 3-dimensional map of attenuation values is thus generated (Fig. 7B). X-ray based CT attenuation values in general are in the energy range of about 70–120 keV and thus have to be converted to the 511 keV energy level of the gamma quanta emitted in PET. A 3D graphical representation of the obtained attenuation values 'μ-map' with 511 keV attenuation values is then generated (Fig. 7C). This CT-based registration of 3D attenuation values has to be performed once for each rigid hardware component and then the according μ-map becomes part of the PET image reconstruction process. By linking the RF spine – or RF head coils – position relative to the patient's table position, the relevant AC μ-map for each table position is automatically selected by the system for PET image reconstruction. The flexible and non-stationary Body Matrix RF array coils covering the patient's body cannot be attenuation-corrected in the same manner. Here the geometry and position of the coils attenuating structures depend on the patient's individual anatomy and on the individual situation of the patient exam and thus cannot be easily predicted by MR imaging. Here the emphasis lies on designing flexible and moving RF coils as PET-transparent as possible. For the Biograph mMR system, the associated RF coils have been further optimized in this regard. Potential design parameters for RF coil optimization are the choice of materials, the geometry, and the overall assembly. The ultimate goal of such an RF coil design optimization process is to maximize SNR and signal performance for MR while not disturbing PET-imaging.

Attenuation correction for tissue

A necessity in PET-based imaging is the correction for attenuation and scatter resulting not just from the hardware in the PET FOV (e.g. patient table, and RF coils as described above) but also from the patient's body, i.e. the anatomic distribution of soft tissues, air, and bones in the individual patient. Such tissue AC in PET-only systems traditionally has been performed by rotation of radioac-

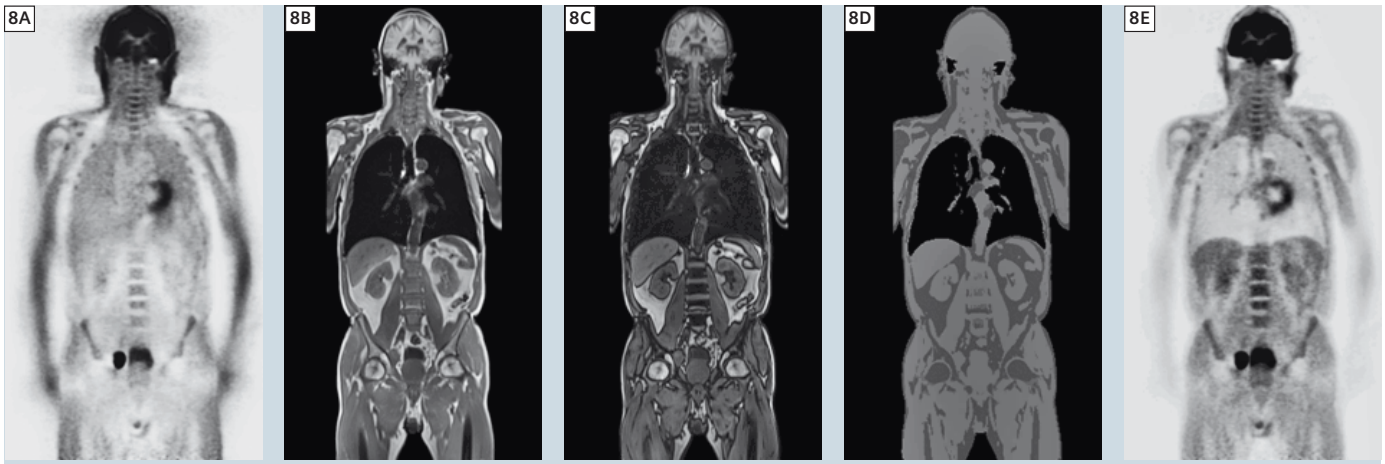

8 Soft-tissue attenuation correction (AC) based on MR imaging. **(A)** Uncorrected whole-body PET scan showing relative activity enhancement in the lungs and on the outer contours of the patient. **(B and C)** Dixon MR sequence providing separate water/fat 'in-phase' and 'opposed phase' images that serve as basis for soft-tissue segmentation. **(D)** Segmented tissue groups (air, fat, muscle, lungs) that can be assigned to 511 keV attenuation maps. **(E)** Resulting attenuation corrected whole-body PET scan of the initial data set **(A)**.

tive ^{68}Ge 511 keV sources around the patient and detection of the attenuated transmission signals 'behind' the patient. From a number of projections, a topography of attenuation values (μ-map) could be reconstructed. This was a relatively time-consuming process, since the ^{68}Ge-source needed to be rotated at a relatively slow speed in order to achieve a significant count rate for each projection angle.

In modern PET/CT hybrid systems, the hardware (e.g. patient table) and the patient tissue μ-map are generated straightforwardly from a fast (potentially low-dose) 3D CT scan provided by the build-in CT scanner. Attenuation values are converted from the 70–120 keV energy level to 511 keV and thus a fast individual and reliably AC μ-map of the patient and any hardware accessories in the PET FOV is obtained.

In a combined MR/PET hybrid system tissue attenuation has to be obtained in a completely different way. Since no CT-like attenuation information is available in such a hybrid system, tissue AC necessary for PET image reconstruction needs to be based on MR images. The problem is the non-irradiative nature of MR imaging, based on proton densities and T1 and T2 relaxation parameters, rather than on the attenuation of radiation in tissue. MR-based AC of tissues also leads to the problem that air and bone are depicted in black the vast majority of MR imaging sequences turning air and bone hardly distinguishable, in CT and PET imaging on the other hand air and bone show minimal and maximal attenuation values, respectively. Different methods have been described in the recent literature, that deal with MR-based AC for tissue [7–9]. Those methods can be separated in atlas-based or atlas-supported methods and in image segmentation based efforts. In the latter, the gray values provided by selected sequences are registered to different tissue classes resulting in tissue segmentation. Depending on the sequence type used, air, lung, fat, muscle, and bones might be segmented and provided with according PET correction values. In the current implementation of the Biograph mMR system, tissue attenuation and scatter correction is performed twice. The head/neck region is attenuation-corrected with the help of a UTE (ultrashort echo time) sequence [10, 11] providing segmentation also of the bone which in this region takes a large percentage of the imaged volume. All other body parts are attenuation-corrected by a Dixon technique providing two images where water and fat are 'in phase' and in 'opposed phase'. This allows for reconstruction of fat-only, water-only and of fat-water images and results in tissue segmentation of air, fat, muscle, and lungs (Fig. 8) [8]. Bone is not accounted for in this approach. Initial results in patient imaging have shown that this approach works reliably and provides results that are comparable to corrected images form PET/CT in the same individual. The ultimate impact of this and other MR-based AC methods on PET-quantification and determination of standard uptake values (SUV) has not yet been determined and is subject to current investigations and further research efforts.

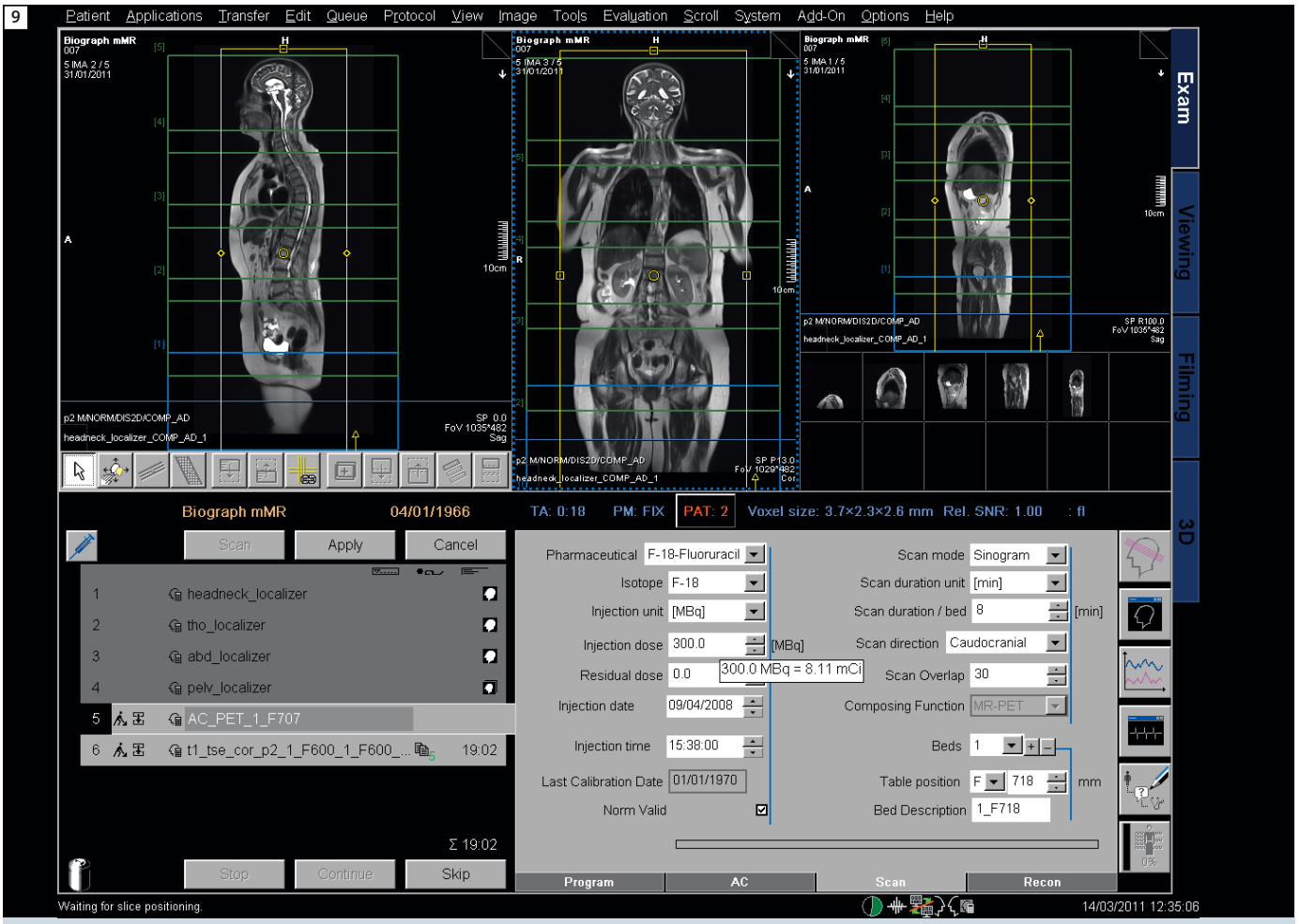

9 Screenshot of the *syngo* user interface during planning of a MR/PET examination. The image panel shows multi-station MR localizers in sagittal (left and right) and coronal (middle) orientation. Displayed with a yellow frame is the FOV of the AC MR sequence for tissue attenuation correction. Green and blue frames show graphical planning of the individual bed positions of the MR and PET data acquisition. In the lower half the planning of the MR/PET acquisition is currently ongoing.

Imaging workflow

From a procedural point-of-view the imaging workflow of a whole-body MR/PET examination on the Biograph mMR is very similar to a whole-body MRI examination. First the patient is prepared on the patient table. For that purpose the earlier described dedicated mMR Tim RF coils (head and neck coil, spine coil, and up to four body matrix coils) are positioned underneath, on and around the patient's body, respectively. In this context the Tim RF coil technology is a prerequisite for seamless whole-body imaging without RF coil replacement and patient repositioning.
Following patient preparation a localizer MR scan is performed covering the region to be examined. Making use of the *syngo* software functionality the localizer scan, as well as any further MR scan can be loaded per drag and drop from a predefined list of protocols and can also be adjusted according the user's specific needs and saved afterwards as individualized protocols, similar to customization of MR protocols. Based on the localizer scan the combined MR/PET scan then is planned.
Figure 9 shows the user interface for examination planning. The yellow boxes in the graphical slice positioning section indicate the acquisition volume for the MR sequences used in the attenuation and scatter correction. The green and blue boxes indicate the acquisition volume of the respective PET bed positions. The overlap between the bed positions is variable. When the planning for the AC sequence is finished and the scan is started, automatically the simultaneous acquisition of the PET starts as well and – bed position per bed position – the simultaneous acquisition of PET, MR AC scan, and any further MR scan for anatomy and function is performed (Fig. 10). Additional MR sequences (beyond the AC scans) for assessment of anatomy and function can be chosen individually for each bed position. For a typical MR/PET scan using ^{18}F-FDG for tumor staging, the overall scan time is defined not necessarily only by the PET acquisition time per bed and number of required

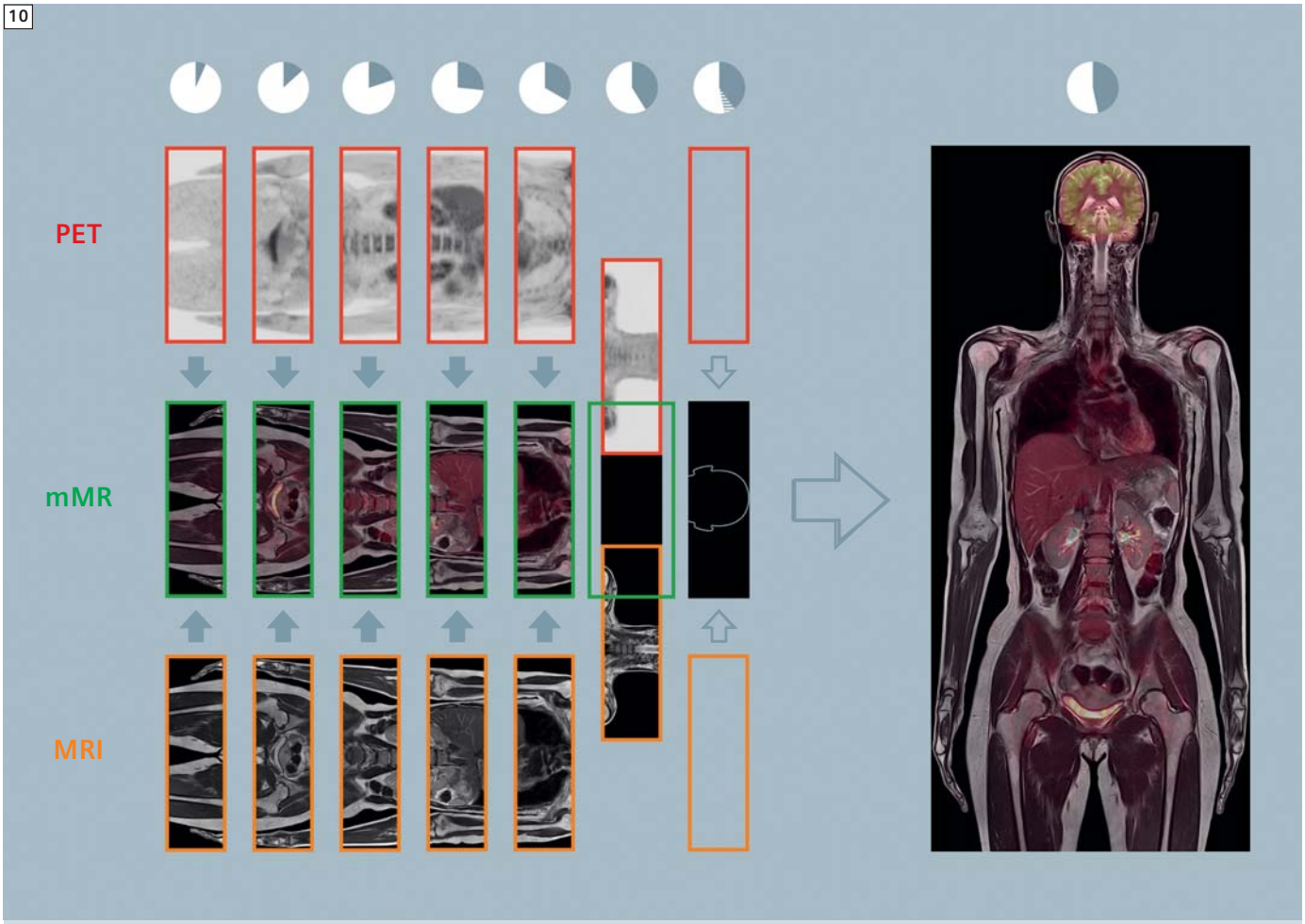

10 MR/PET simultaneous imaging workflow. MR and PET data acquisition is performed simultaneously during a multi-step examination with 6–7 bed positions for whole-body coverage. Depending on the selection of MR imaging sequences, such a whole-body MR/PET hybrid imaging study is regularly completed in about 20–30 minutes.

bed postitions to cover the region-of-interest; in contrast to PET/CT, the acquisition time necessary for MR imaging can be the limiting factor with respect to the total scan time of a mMR exam. However, the additional MR scan time is not lost: Further MR sequences may add to the acquisition time of a specific bed position. This additional time can then directly be used for longer PET data acquisition, translating not only into improved PET image quality but allowing the collection of dynamic PET data (this includes also gating / triggering of PET data). The acquisition of single bed positions for simultaneous MRI and PET, e.g. for dynamic MR/PET studies of the brain, is clinically possible and it should be emphasized that this possibility is also a direct consequence of the large z-axis coverage by the PET detectors, allowing to scan the whole brain or the liver without the need of repositioning over a longer time-period.

Combining PET data and multiple MR sequences will increase the amount of images and complexity of reading, not only for whole-body applications. Therefore an intuitive and powerful tool for evaluating mMR examinations was developed in parallel to the scanner hardware. After the acquisition of the MR/PET data the dedicated mMR Reader based on *syngo*.via and delivered with the Biograph mMR system can be used for image reading and diagnosis. It has been developed for efficient and seamless integration of the new modality into clinical workflow; this includes automatically loading and displaying images for the whole body and specific anatomical regions in MR only, PET only and MR/PET fusion. The client-server-based software supports reading and diagnosing by an MRI and a PET expert (also on different days and in different rooms) in several regards including advanced findings navigation and also by automatically merging these individual findings into one joint report.

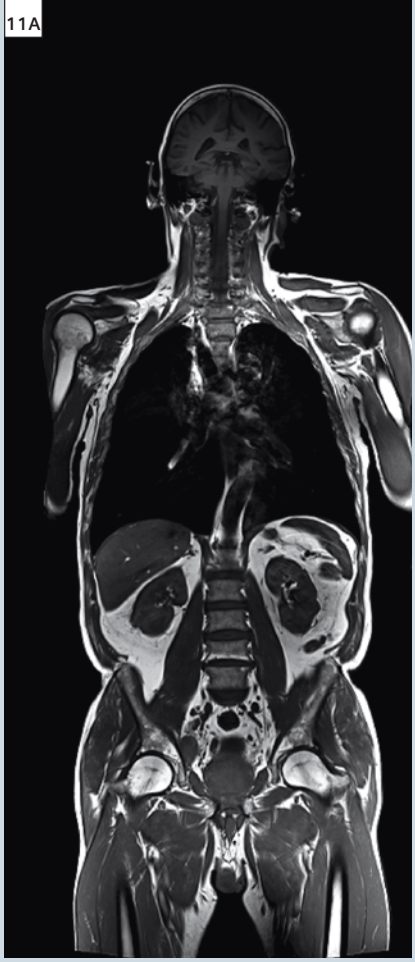

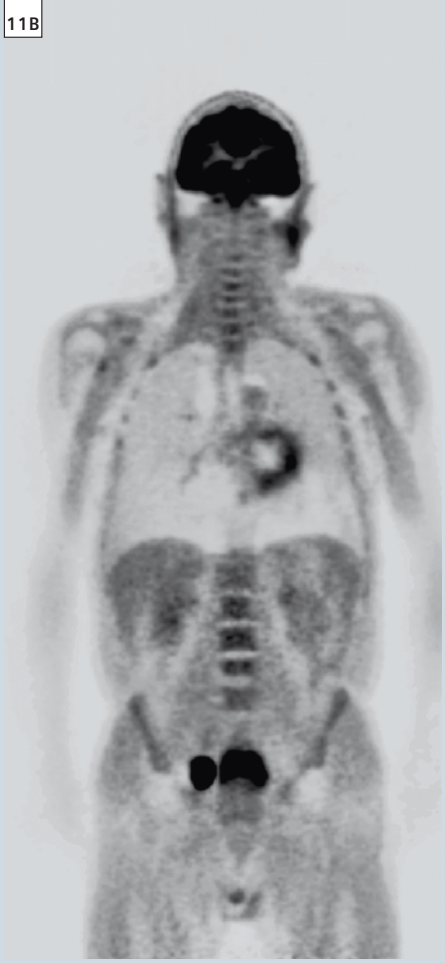

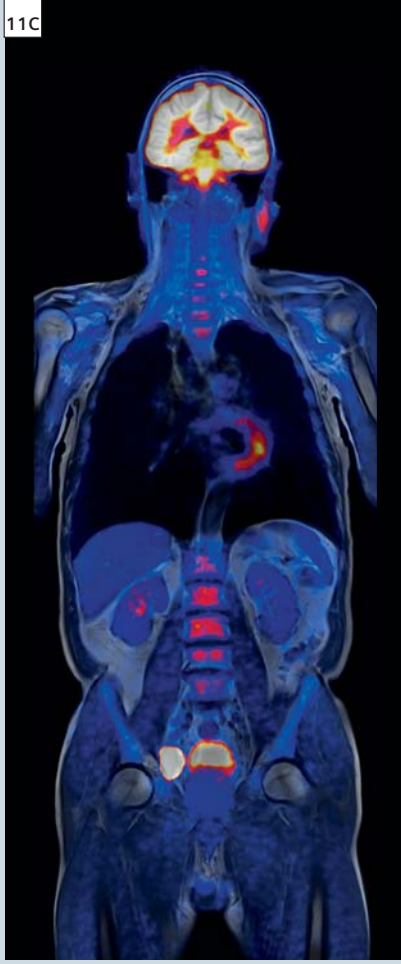

11 Patient with lymph node filiae following a history of a penis carcinoma. Images **(A–C)** show whole-body T1-weighted MR image **(A),** attenuation corrected PET **(B)**, and MR/PET hybrid images **(C)** in a coronal orientation, that were all simultaneously acquired in a multi-station/multi-bed acquisition mode. MRI in this whole-body study **(A)** displays anatomical structures with exquisite detail and excellent soft-tissue contrast. PET **(B)** and the combined MR/PET hybrid image **(C)** in this coronal overview show enhanced tracer activity in one lymph node on the right side of the patient. The axial and sagittal reformates of the MR/PET hybrid data **(D, wE)** reveal two additional lymph nodes with focal tracer activity on the right side.

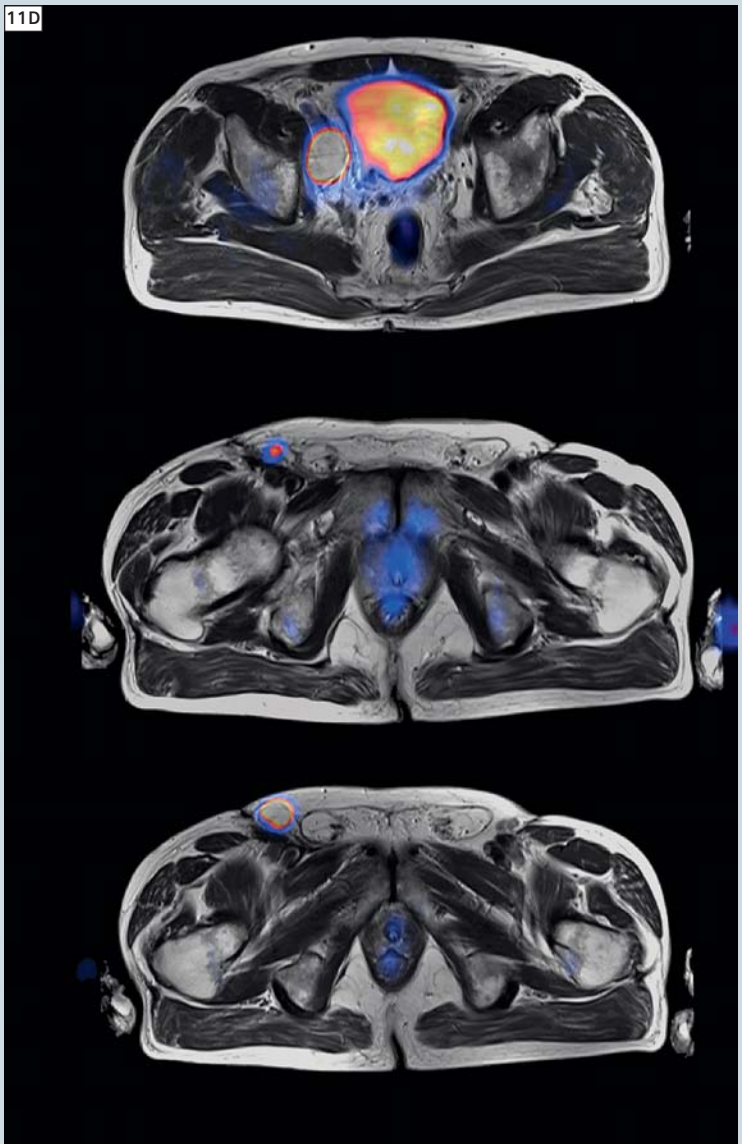

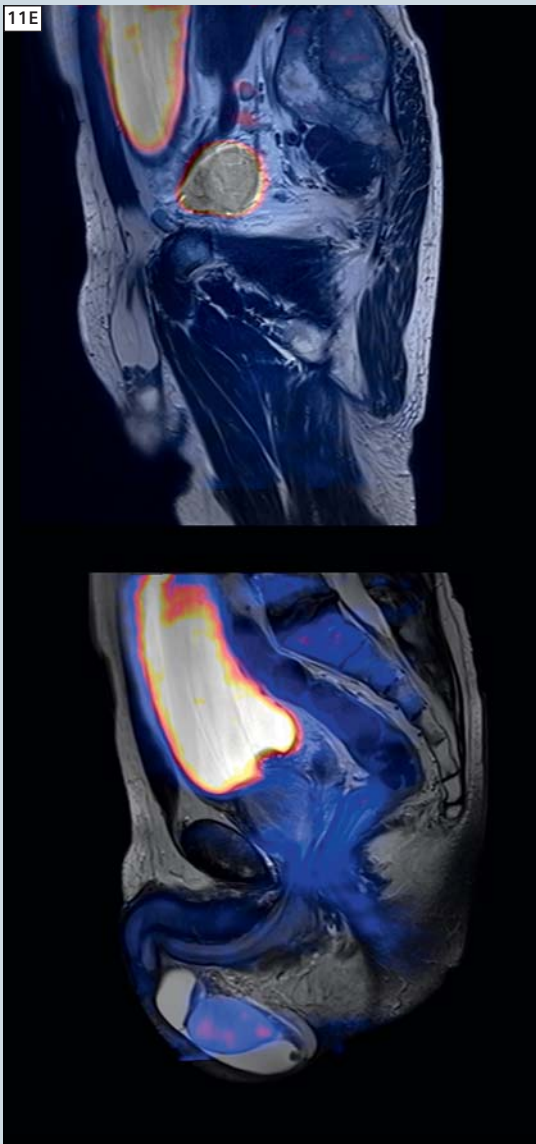

First clinical examples

An early study was initiated in 2010 at the Institute of Medical Physics (IMP), University of Erlangen, in cooperation with Siemens AG Healthcare Sector, Erlangen. This study aimed at system integration testing and at showing system performance and full operationality by scanning first patients. For acquiring these images, the study was setup as follows: Patients referred to PET/CT scanning were recruited from the Nuclear Medicine Department of the nearby University Hospital Erlangen. Patients had been injected the radioactive tracer ^{18}F-Fluordesoxyglucose (FDG) and had already undergone their PET/CT examination immediately before participating in the MR/PET hybrid imaging examination. This study design thus also had the benefit that the preceding PET/CT examination could serve as a 'gold standard' comparison for subsequent MR/PET imaging. No additional FDG injection or increased radiation dose was necessary. Due to the scanning PET/CT first, however, patients involved in this study had their MR/PET examination on average about 120 min after the injection of FDG. This is about 60 min later than the PET scan would usually have been performed after ^{18}F-FDG-injection. With the given half life time of 108 min for ^{18}F-FDG, this has the effect that activity and thus count rate have already decreased since the PET/CT examination and additionally, FDG has been metabolized during a longer time window than usual. In our study, the effect of decreased activity has been compensated for by longer PET measurement times per bed position (i.e. 6 minutes instead of 2–3 minutes per bed position).

Figure 11 shows a whole-body MR/PET study of a patient with a history of a penis carcinoma with R0 resection of the tumor and now suspicion of tumor recurrence (lymph node metastases). The MR/PET study in this case revealed multiple lymph node filiae inguinal and iliacal, which can be displayed in fine detail in PET and in MRI. These findings correlate well with the findings of the preceding PET/CT examination (not shown).
Figure 12 shows a brain MR/PET study of a lung cancer patient for therapy effectivness control with a history of 2 resected brain metastases. No increased activity or any other signs of recurrence or malignancy could be observed – neither in the PET nor in the MR images. This also correlates with the findings of the associated PET/CT examination (not shown).

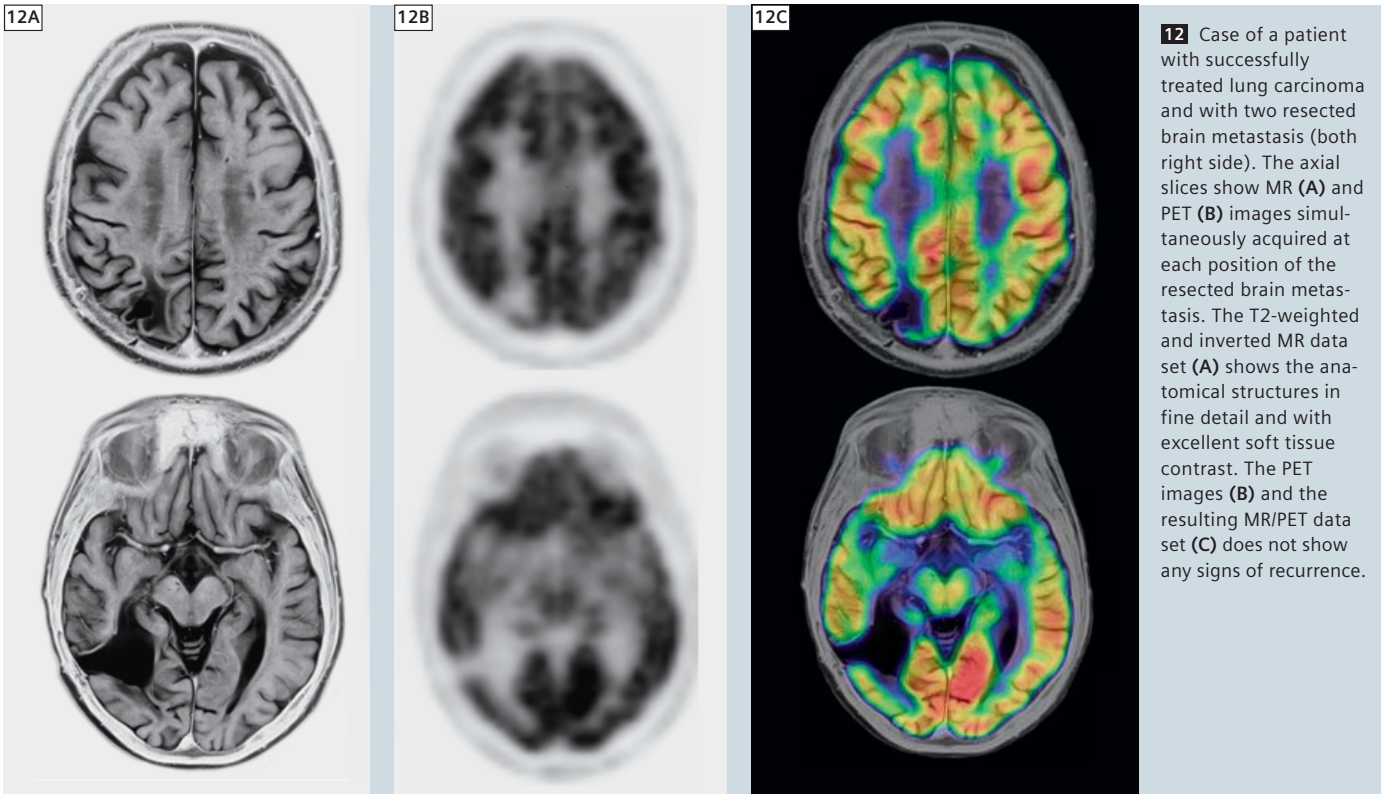

12 Case of a patient with successfully treated lung carcinoma and with two resected brain metastasis (both right side). The axial slices show MR **(A)** and PET **(B)** images simultaneously acquired at each position of the resected brain metastasis. The T2-weighted and inverted MR data set **(A)** shows the anatomical structures in fine detail and with excellent soft tissue contrast. The PET images **(B)** and the resulting MR/PET data set **(C)** does not show any signs of recurrence.

Status and outlook

The long-awaited hybrid imaging modality enabling simultaneous whole-body MR/PET imaging has entered the clinical arena. On the physics and hardware level, this opens up completely new options for clinical imaging research. MR-based hardware and tissue attenuation correction (AC) and MR-based motion correction (MC) for PET imaging are only two examples of current active fields of research. The development of RF coils intended not only for their intended diagnostic application and MR imaging performance but also for their PET-transparency is another research field. On the clinical imaging level, this new hybrid imaging modality demands clinical evaluation especially given the wealth of new diagnostic information generated by the integration of both imaging modalities. Here a special area of interest will focus on the streamlining and optimization of the imaging workflow of simultaneous MR and PET imaging. The ultimate goal is the maximization of multi-modal diagnostic information within a minimum of acquisition time.

Acknowledgements

The authors would like to thank Dr. Matthias Lichy, Dr. Jürgen Kampmeier, and Heike Weh, all Siemens Healthcare Sector, Erlangen, Germany, for in depth discussions and for their support in preparing figures for this article. The authors are also grateful to Prof. Dr. Torsten Kuwert, Prof. Dr. Michael Uder, Dr. Michael Lell, all University Hospital Erlangen, Germany, and to Dr. Alexander Cavalaro, ISI Erlangen, for their help in patient recruitment and personal support.

References

1. Pichler BJ, Judenhofer MS, Wehrl HF. PET/MRI hybrid imaging: devices and initial results. Eur Radiol. 2008; 18:1077-86. Review.
2. Antoch G, Bockisch A. Combined PET/MRI: a new dimension in whole-body oncology imaging? Eur J Nucl Med Mol Imaging. 2009; 36 Suppl 1:S113-20. Review.
3. Wehrl HF, Sauter AW, Judenhofer MS, Pichler BJ. Combined PET/MR imaging--technology and applications. Technol Cancer Res Treat. 2010; 9:5-20.
4. Pichler BJ, Wehrl HF, Kolb A, Judenhofer MS. Positron emission tomography/magnetic resonance imaging: the next generation of multimodality imaging? Semin Nucl Med. 2008; 38:199-208. Review.
5. Delso G, Martinez MJ, Torres I, Ladebeck R, Michel C, Nekolla S, Ziegler SI. Monte Carlo simulations of the count rate performance of a clinical whole-body MR/PET scanner. Med Phys. 2009; 36:4126-35.
6. Delso G, Martinez-Möller A, Bundschuh RA, Ladebeck R, Candidus Y, Faul D, Ziegler SI. Evaluation of the attenuation properties of MR equipment for its use in a whole-body PET/MR scanner. Phys Med Biol. 2010; 55:4361-74.
7. Beyer T, Weigert M, Quick HH, Pietrzyk U, Vogt F, Palm C, Antoch G, Müller SP, Bockisch A. MR-based attenuation correction for torso-PET/MR imaging: pitfalls in mapping MR to CT data. Eur J Nucl Med Mol Imaging. 2008; 35:1142-6.
8. Martinez-Möller A, Souvatzoglou M, Delso G, Bundschuh RA, Chefd'hotel C, Ziegler SI, Navab N, Schwaiger M, Nekolla SG. Tissue classification as a potential approach for attenuation correction in whole-body PET/MRI: evaluation with PET/CT data. J Nucl Med. 2009; 50:520-6.
9. Schulz V, Torres-Espallardo I, Renisch S, Hu Z, Ojha N, Börnert P, Perkuhn M, Niendorf T, Schäfer WM. Automatic, three-segment, MR-based attenuation correction for whole-body PET/MR data. Brockmann H, Krohn T, Buhl A, Günther RW, Mottaghy FM, Krombach GA. Eur J Nucl Med Mol Imaging. 2011; 38:138-52.
10. Waldman A, Rees JH, Brock CS, Robson MD, Gatehouse PD, Bydder GM. MRI of the brain with ultra-short echo-time pulse sequences. Neuroradiology. 2003; 45:887-92.
11. Robson MD, Bydder GM. Clinical ultrashort echo time imaging of bone and other connective tissues. NMR Biomed. 2006; 19:765-80. Review.

Contact

Prof. Dr. Harald H. Quick, PhD
Director of MR-Imaging
Institute of Medical Physics (IMP)
Friedrich-Alexander-University (FAU)
Erlangen-Nürnberg
Henkestr. 91
91052 Erlangen
Germany
Phone: +49 9131 85 25900
Harald.Quick@imp.uni-erlangen.de

Dr. Jens-Christoph Georgi, PhD
Global Product Manager Biograph mMR
Siemens AG Healthcare Sector
MR MK O
Karl-Schall-Str. 6
91052 Erlangen
Germany
Phone: +49 9131 84 4701
Jens-Christoph.Georgi@siemens.com

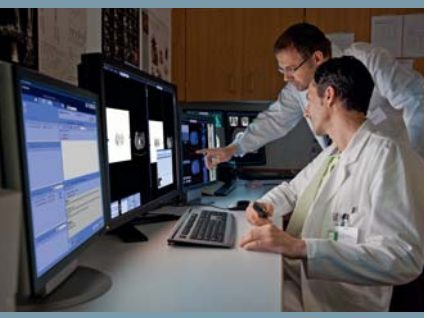

Innovative integration

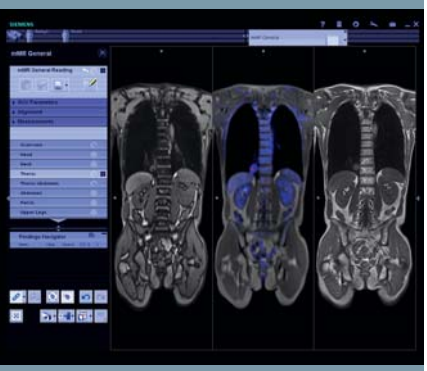

syngo.mMR General

syngo.PET Segmentation

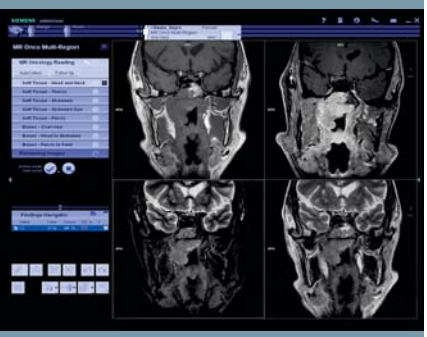

syngo.MR Onco

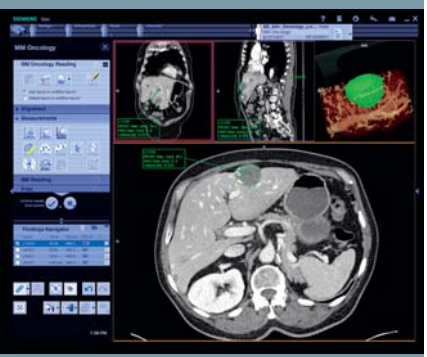

syngo.CT Segmentation

Revolutionizing image reading and evaluation in oncology

Cancer is a threat to the entire body. That is why *syngo*.via supports a multimodality approach to help maximize therapeutic outcomes.

Interdisciplinary imaging studies – such as computed tomography (CT), magnetic resonance imaging (MRI), positron emission tomography (PET) scans – have become standard in oncology diagnostic evaluations. They are complemented by new and very promising approaches like molecular MR (mMR) that are currently in the process of establishing themselves in clinical routine. Furthermore, for a clinical institution to be successful, it is essential to obtain the highest possible diagnostic accuracy while maintaining a fast and efficient oncology workflow. *syngo*.via[1], the software solution for routine 3D reading and advanced visualization from Siemens, creates an exciting experience in efficiency and ease of use. It uniquely combines innovative features and applications tailored to the oncology workflow.

Multimodality reading with confidence, accuracy, and speed

On up to two monitors, *syngo*.via provides a seamless integration of quantitative measures, automated processes, and advanced visualization into your oncology reading workflow. For example, it combines[2] more accurate and fast lesion segmentation, RECIST 1.0 and RECIST 1.1 calculation, WHO calculation, automated lesion finding and tracking, and multimodality reading. A number of quantitative parameters characterizing a segmented lesion are provided[2]. The tumor growth rates and tumor burden can be calculated automatically. And computer-aided detection (CAD) tools can be integrated as a second reader to help you increase diagnostic confidence, while maintaining a fast and efficient workflow.

Finding, not searching

In oncology imaging, keeping track of findings over the entire patient history can sometimes be quite a challenge. Multiple lesions, multiple time-points, and multiple readers can often result in countless findings. As it automatically collects the findings on-the-fly while you are reading a case, *syngo*.via's Findings Navigator makes referencing and reporting easy. The Findings Navigator thus facilitates accelerated reading and the list of findings can be effectively used as bookmarks during clinical demonstrations such as tumor board meetings.

Innovative integration abilities

syngo.via allows you to experience higher reading efficiency thanks to its client-server technology and connection with your RIS or PACS. Most of the processing and rendering of data from the connected modalities is done by the server while the client provides the user interface. This means that users can access *syngo*.via from virtually anywhere[3] within the network infrastructure and perform their tasks – whether at a workstation in a different department, at the RIS/PACS reporting workplace, at a tumor board, the reading physician's office or even at home[3].

www.siemens.com/syngo.via

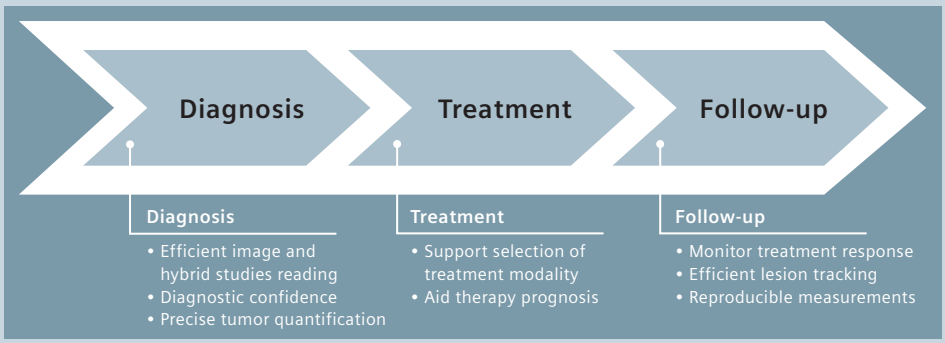

[1] *syngo*.via can be used as a standalone device or together with a variety of *syngo*.via-based software options, which are medical devices in their own rights.
[2] This functionality belongs to the *syngo*.via-based software applications *syngo*.PET&CT Oncology and *syngo*.MR Onco Engine which are medical devices in their own rights.
[3] Prerequisites include: Internet connection to clinical network, DICOM compliance, meeting of minimum hardware requirements, and adherence to local data security regulations.

Integrated Whole Body MR/PET Imaging. First Examples of Clinical Application

A. Drzezga; A.J. Beer; S. Fürst; S. Ziegler; S.G. Nekolla; M. Schwaiger

Technische Universität München, Klinik und Poliklinik für Nuklearmedizin, Klinikum rechts der Isar, Munich, Germany

Introduction

Over the last decade, development of hybrid-imaging instrumentation has been among the innovations with the strongest impact on diagnostic imaging in clinical everyday routine. The driving force behind these developments is the considerable extent to which several different imaging modalities show complementary rather than redundant features. Consequently, it is logical to bundle the particular strengths of different modalities, and to compensate particular deficits of one modality with capabilities of another by combination of the different modalities into one hybrid instrument. Hybrid PET/CT entered the market in around 2000 and became a major success, thereby quickly obviating the demand for PET-only scanners. This success has been strongly driven by oncological applications, combining the high sensitivity of PET with the anatomical precision of CT. The coupling of ^{18}F-FDG, a tracer for metabolic activity with CT, has especially proved highly valuable: FDG-PET allows the sensitive detection of tumor cells and the estimation of their viability (e.g. for therapy control); CT complements the exact anatomic localization of suspect lesions and has a very high sensitivity for small lesions which are missed by PET due to limited resolution or movement artifacts (e.g. in the lung).

However, CT has some specific limitations, the most apparent being the relatively low soft-tissue contrast. This represents a disadvantage particularly for diagnostic questions directed to body regions which are defined by a complex regional arrangement of different adjacent soft tissue structures, e.g. the brain, the head-and-neck region or the pelvis. In contrast to CT, MR-imaging is distinguished by the ability to provide excellent soft-tissue contrast. This is the main reason why corresponding diagnostic problems are typically directed to MRI as the first-line imaging procedure of choice rather than to CT. This includes questions concerning e.g. neurological disorders, brain tumors, conditions in the head and neck region, abdominal/hepatic and pelvic masses and musculoskeletal problems.

For many of these diagnostic questions, PET has demonstrated a high added value as a complementary test in itself, whilst frequently being performed in addition to mandatory MRI-tests (see A. Padhani 'Multiparametric imaging of tumors – an emerging paradime', MAGNETOM Flash #45 3/2010, Research Supplement). Thus, the value of a combination of PET with MRI seems obvious. However, the development of such hybrid MR/PET instrumentation has been hampered for a long time primarily by technical obstacles which have been harder to overcome compared to the combination of PET and CT. Whereas the latter both represent modalities working with radiation (although in different wavelengths) and can thus be combined more easily, PET and MRI are based on entirely different image acquisition principles. The strong magnetic field required for MR-image acquisition is severely affecting the acquisition of the PET-signal. In particular, the conventional photomultiplier technique commonly used for obtaining the PET signal does not work properly in a magnetic field. To circumvent this limitation, platforms have been developed in which spatially separate MR- and PET-scanners are connected by means of a moving table. The patient is positioned on this table and undergoes first PET and then MR imaging, without having to get up from the table between the scans. However, these solutions do not allow simultaneous image acquisition and they are of course associated with lengthy examination protocols and with the risk of patient movement.

With the introduction of the so-called APDs (Avalanche Photodiodes) into PET-

instrumentation this problem has been solved more elegantly. APDs function in strong magnetic fields and can be used to substitute conventional photomultipliers to acquire information in the MR-scanner. The advent of this technology has allowed the industry to produce a first generation of hybrid MR-scanners in which a true integration of both modalities in a single machine has been realized (see H. Quick 'Whole-body MR/PET hybrid imaging' page 88 in this issue of MAGNETOM Flash). This principle was first successfully demonstrated by means of small head-only PET-scanners (PET-insert) which have been installed in conventional MR-scanners (see T. Beyer et al. 'MR/PET-hybrid imaging for the next decade', MAGNETOM Flash #45 3/2010 Research Supplement). Several studies have been performed in this prototype system since and proved the practicability of the concept [1–4].

On the basis of this prototype, a dedicated whole-body MR/PET system has now been developed. In November 2010, the world's first integrated clinical whole-body MR/PET scanner (Siemens Biograph mMR) was installed in the Department of Nuclear Medicine at the Technische Universität München (TUM), in Munich, Germany. The scanner is now operated by a consortium between the directors of Nuclear Medicine (Prof. Dr. Markus Schwaiger) and Radiology (Prof. Dr. Ernst Rummeny) from TUM and the directors of Nuclear Medicine (Prof. Peter Bartenstein) and Radiology (Prof. Dr. Maximilan Reiser) from the Ludwig-Maximilians-Universität, München. The setup of the first scanner of this type in Germany (and of three identical scanners which will be established in 2011 in Essen, Leipzig and Tübingen) has been made possible by funding of the German Research Foundation (DFG, Deutsche Forschungsgemeinschaft).

The Biograph mMR MR/PET-scanner is constituted by a high end 3T MR-scanner which harbours a fully functional state-of-the-art PET system within the gantry. The PET-system covers a field of view (25.8 cm) which is larger than in any other existing PET-camera. This allows to obtain multimodal (MR&PET) image information simultaneously in an extended region and to cover the entire body with a limited number of bed positions in short time. For further technical details on the system see page 88 in this issue of MAGNETOM Flash.

Opportunities of the MR/PET-system

From a clinical point of view, this system offers a number of obvious advantages:

1. Reduction in examination time

In comparison to clinical CT-examinations, MR-scans can often be relatively time-consuming. The recently introduced whole-body MR/PET scanner now allows the acquisition of MR and PET information in a truly simultaneous approach, i.e. in regional alignment at exactly the same time, thereby reducing not only the number of examination appointments (i.e. the visits patients have to make to the imaging department) but also cutting the required examination time approximately in half (as compared to two separate examinations). This option of 'one-stop shop' examinations represents a major gain in patient comfort for patients requiring both MR and PET examinations and also reduces the required time of the medical personnel to acquire the requested imaging information.

2. Regional coregistration

The acquisition of PET and MR-information in exactly overlapping anatomical positions also offers clear advantages: Precise coregistration of the PET-signal with the underlying anatomical information is assured as the risk of patient movement or changes in organ position (e.g. in bowel positions, different bladder filling status) between the acquisition of the two modalities is reduced, and thus potential misalignment is minimized. Due to the lack of radiation exposure by the MR-image acquisition, anatomical scans can be added/repeated to achieve optimal anatomical information.

3. Simultaneity of acquisition

The newly introduced integrated MR/PET scanners for the first time allow truly simultaneous acquisition of imaging information from two different modalities of the same region at the same time. This opens a completely new dimension in hybrid imaging. Even established PET/CT technology only allows the acquisition of CT and PET in the same system but not at exactly the same time and region, as the two modalities/acquisition procedures are cascaded one after the other. The simultaneous acquisition of MR and PET information opens the opportunity to address many new scientific questions, which may be translated into clinical application, e.g. to cross-evaluate the value of different imaging tests under identical examination conditions or to improve understanding of disease pathophysiology by shedding light on the interrelation between different pathological processes. Simultaneous acquisition may also allow the following of organ and/or patient movement over time allowing for motion correction [2] and also the combination of information on motility with other functional information provided by PET (e.g. information on viability/perfusion derived from PET-imaging with information on wall movement in cardiac examinations).

4. Exposure to ionizing radiation

Radiation exposure based on clinical imaging tests is currently a much-discussed topic. Compared to PET/CT, hybrid MR/PET offers the chance to reduce ionizing radiation exposure without loss of diagnostic information. MRI will probably allow anatomical allocation of the PET-signal with comparable precision as known from CT. In some cases the combination of PET-imaging with appropriate diagnostic MR-imaging procedures may be of superior diagnostic value with considerably lower radiation exposure as compared to the combination of PET and diagnostic CT.

5. **Complementary/superior diagnostic value of MR/PET compared to PET/CT**
   It is well known that MRI has complementary features to CT. The most obvious being the higher soft-tissue contrast. As mentioned above, combined MR/PET may be of obviously higher diagnostic value compared to PET/CT for indications and in body regions which would usually be approached using MRI rather than CT (see clinical examples below). In this regard MR/PET may represent a complementary imaging technique to PET/CT in the future just as MR itself represents a complementary imaging technique to CT nowadays.
6. **Opportunities for scientific applications**
   The MR/PET-system opens a large number of potential scientific applications. Among these is the unique option to establish previously unknown interrelations between different measures of pathology and physiology in the human body such as structure and function, perfusion and metabolism, tissue diffusivity and cell proliferation etc. This may allow to improve the understanding of healthy organ function and to detect causal relationships in disease pathogenesis potentially leading to new therapeutic approaches.
   For clinical diagnosis, combined MR/PET may allow the development of integrated multiparametric markers for more sensitive and more specific diagnosis, therapy planning and evaluation [5]. Several previous studies using separate modalities point to a potentially high scientific and clinical benefit from multimodal imaging approaches using MR/PET [e.g. 5–7].

Challenges of the MR/PET system

Like every new system, combined MR/PET still has a number of apparent challenges:

1. **Attenuation correction**
   In PET/CT systems, low-dose CT scans are used to estimate the expected attenuation of the radiation emitted from a specific body region. In contrast to CT, MR imaging does not provide information on tissue specific photon absorption, but rather on tissue type/class. However, it has been demonstrated that by means of a set of specific MR-sequences (Dixon imaging or chemical shift imaging) suitable attenuation maps can be calculated, which allow an approximation of 511 keV photon attenuation correction with sufficient reliability [8]. The dual point VIBE T1-weighted Dixon sequence used for attenuation correction in the Biograph mMR can be acquired quickly for each bed position (e.g. in the thorax during one breathhold), practically not increasing the examination time. However, the current approach of tissue classification with the Dixon sequence is not yet fully satisfying, it is prone to metal artifacts, attenuation by bones is not considered and truncation artifacts may occur due to the limited transaxial field-of-view of the MR/PET scanner (particularly of the upper limbs). The compensation for these artifacts is currently a matter of ongoing research. Moreover, it can be anticipated that different sequences for attenuation correction will be used in specific areas of the body. For the head e.g., bone probably cannot be neglected completely for truly accurate AC, especially for the skull base. Therefore in this region, the application of ultrashort TE (UTE) sequences might be favourable, which allows for delineation of the bone, thus leading to more exact attenuation maps (μ-maps) as compared to the Dixon imaging approach.
2. **Anatomical allocation of PET-findings**
   The low dose CT scan of the whole body as acquired in conventional PET/CT provides limited diagnostic information but it allows a rough anatomical allocation of suspect PET-findings with sufficient reliability in many cases. For precise attribution diagnostic contrast-enhanced CT scans can be acquired in very short time and provide excellent anatomical information. By contrast, MR-sequences can be comparably slow and it may not be feasible to always acquire whole-body MR-information with high resolution in due time. However, it seems likely that the Dixon-sequences used for attenuation correction of the PET-data also can be used for anatomical allocation of PET-findings with very satisfying results. These whole-body images can then be complemented by added high-resolution MR-sequences in particular regions of interest.
3. **MR-specific diagnostic limitations**
   It is expected that MR/PET will be inferior to PET/CT for indications which are commonly addressed with better diagnostic value by CT, e.g. small pulmonary lesions. It remains to be evaluated for which indications MR/PET is superior or equal to PET/CT and for which indications PET/CT will remain the method of choice.
4. **Workflow**
   The high costs for this type of imaging instrumentation will require elaborate logistics regarding patient flow, occupancy of the scanner, selection of examination procedures etc., to assure efficient utilization of the scanner. The combined acquisition of MR and PET information defines the need for specially educated medical personnel experienced with both modalities.
5. **Design of suitable imaging protocols**
   The large number of available MR-sequences and of different PET-tracers exponentiates the number of potential combinations of imaging tests. This will define the need to develop optimized imaging algorithms for specific diagnostic questions, which ensure the selection of the most beneficial combinations.

Examples for clinical applications

1. Oncology

Case 1 Patient with a cervical Non-Hodgkin lymphoma.

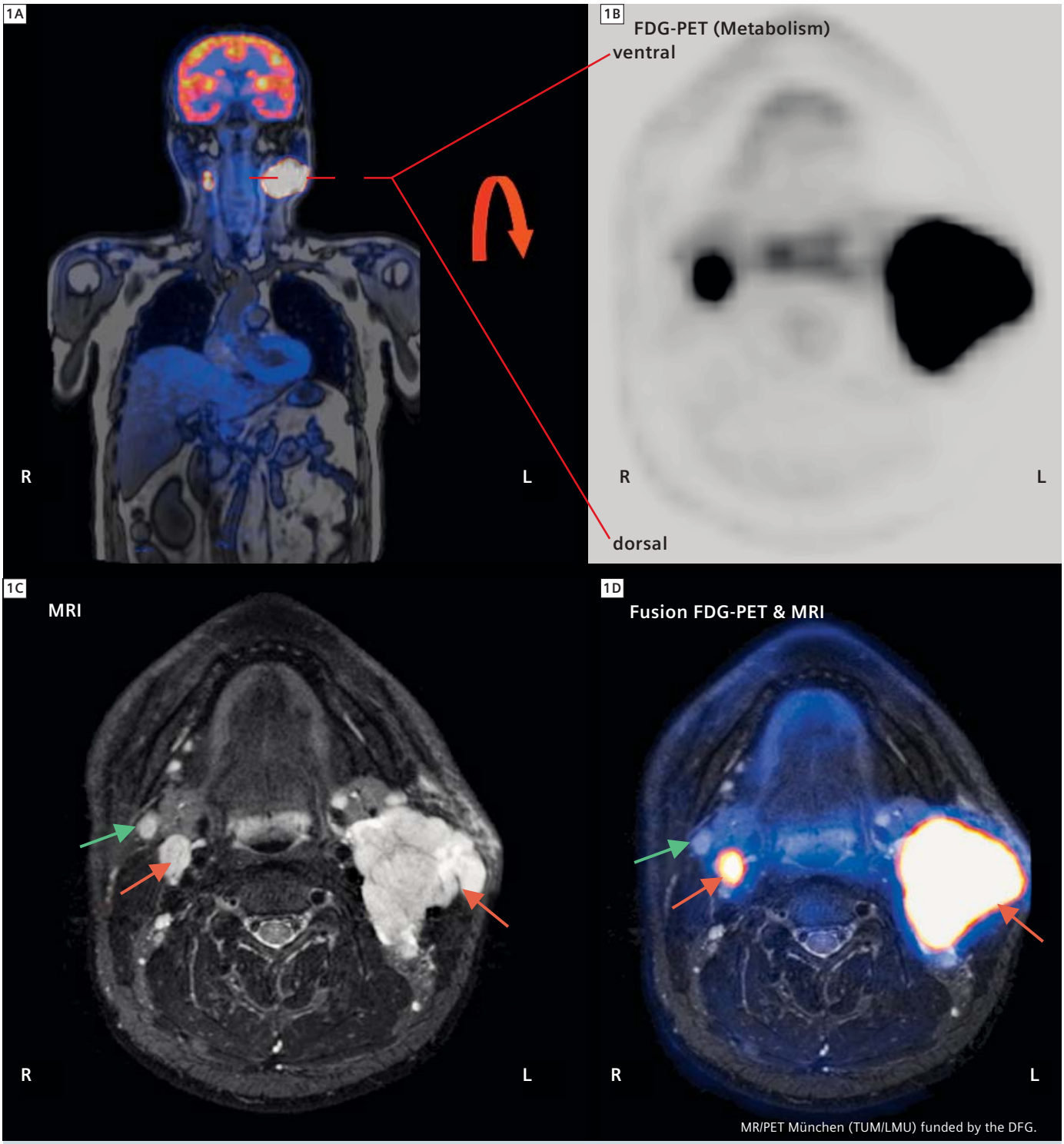

1 **A:** Overview using the opposed phase of the MR AC Dixon sequence. **B:** Axial slice of the ^{18}F-FDG-PET image, demonstrating tumor-suspect increased metabolism in two lesions (left and the right lateral). **C:** Axial MRI (STIR sequence) demonstrating the high tissue contrast. Several cervical lymph nodes are apparent, some enlarged. **D:** Overlay of PET and MRI, easily tumor-typical (red arrows) and non tumor-typical findings (green arrow) can be identified and allocated anatomically.

Case 2 Patient with a Neuroendocrine tumor.

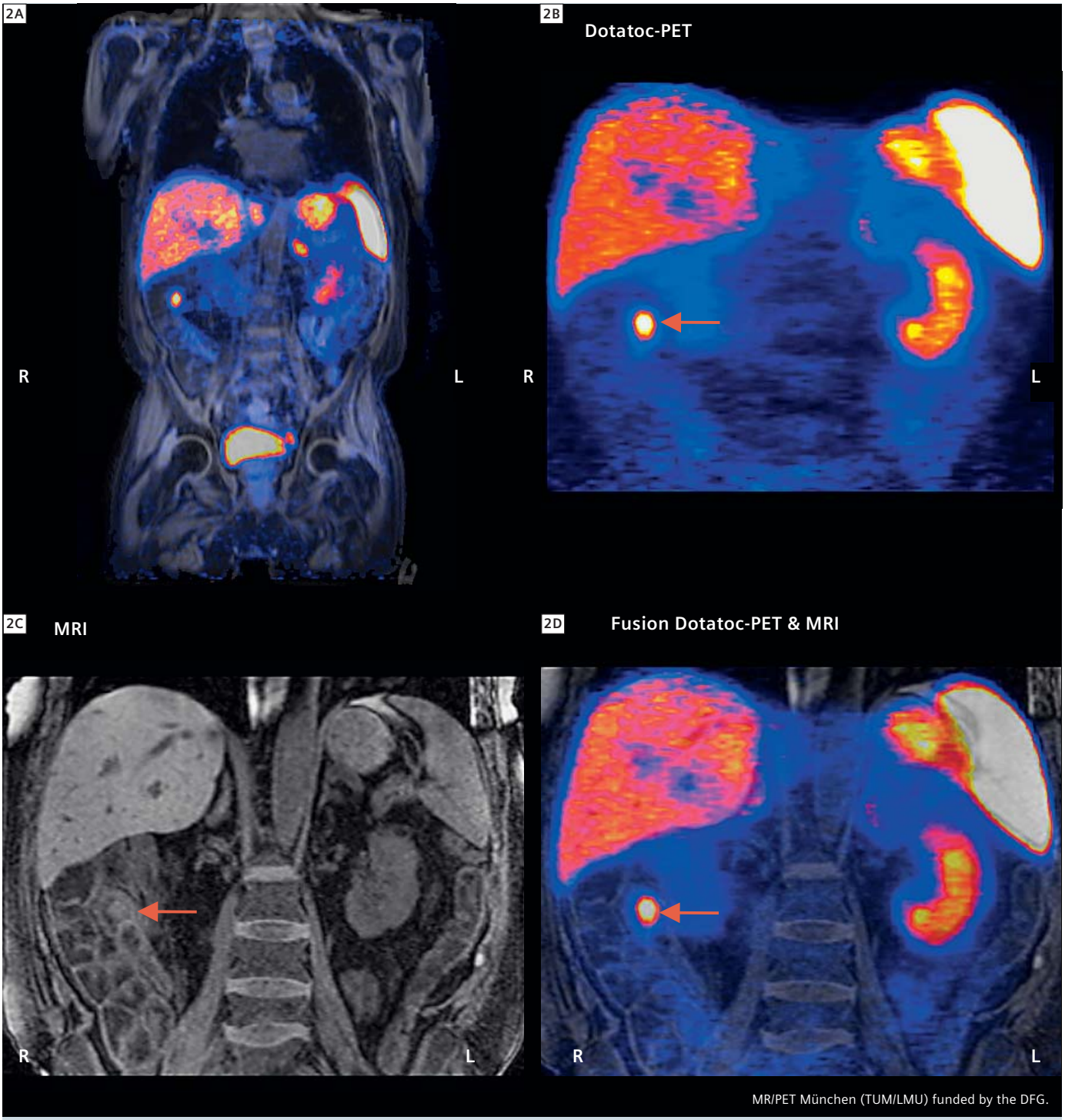

2 **A:** Overview using the water image of the MR AC Dixon sequence. Note the area of intense focal tracer uptake in the right upper quadrant of the abdomen, projecting on the region of the terminal ilium. There is a small bladder diverticulum of the left lateral bladder wall with tracer retention as accidental finding. **B:** PET-findings with ^{68}Ga-DOTATOC, a tracer binding to somatostatine-receptors which are expressed frequently on neuroendocrine tumors. An intense focal tracer-uptake can be found in the abdomen. **C:** MR-image, fat-suppressed coronal T1w breathold VIBE sequence. **D:** Fusion of PET and MR-findings. An excellent identification and anatomical allocation of the tumor is possible by combination of PET and MRI findings. No additional suspect lesions are apparent.

Case 3 Patient with bone metastases of a prostate cancer.

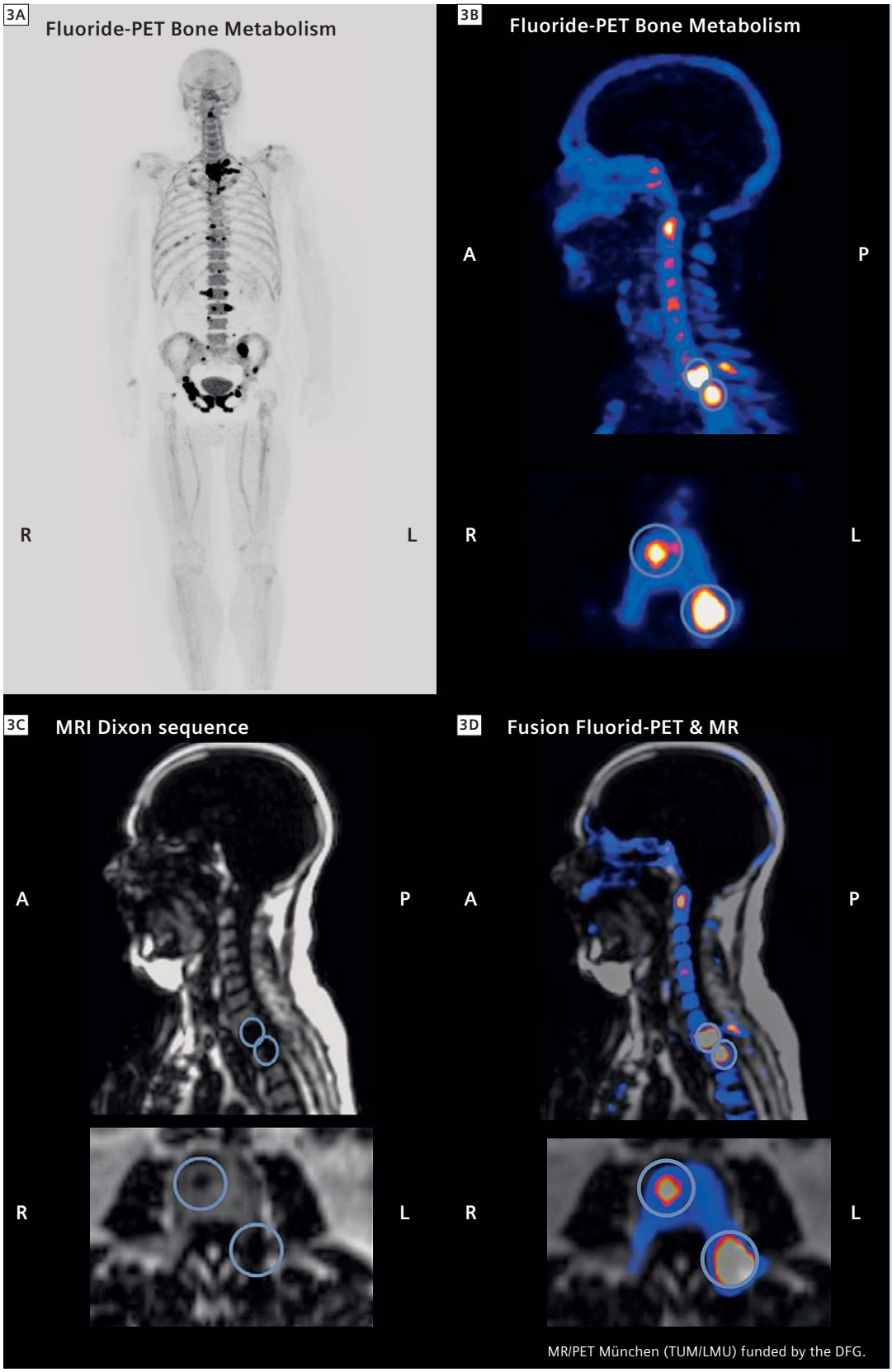

3 **A:** Overview of the ^{18}F-Fluoride PET scan. **B:** PET-findings. **C:** MR-image, sagittal fat-weighted MR AC Dixon sequence. **D:** Fusion of PET and MR-findings. Upper row: sagittal slices, Lower row: axial slices. The Fluoride-PET scan shows a number of suspect lesions in the skeleton, likely corresponding to bone metastases of the prostate-cancer. On the MR- and the fusion-images it is apparent that in the region of the increased PET-tracer uptake, displacement of the bone marrow has occurred, underlining the suspicion of bone metastases.

MR/PET München (TUM/LMU) funded by the DFG.

2. Neurology
Case 4 Patient with a glioblastoma multiforme.

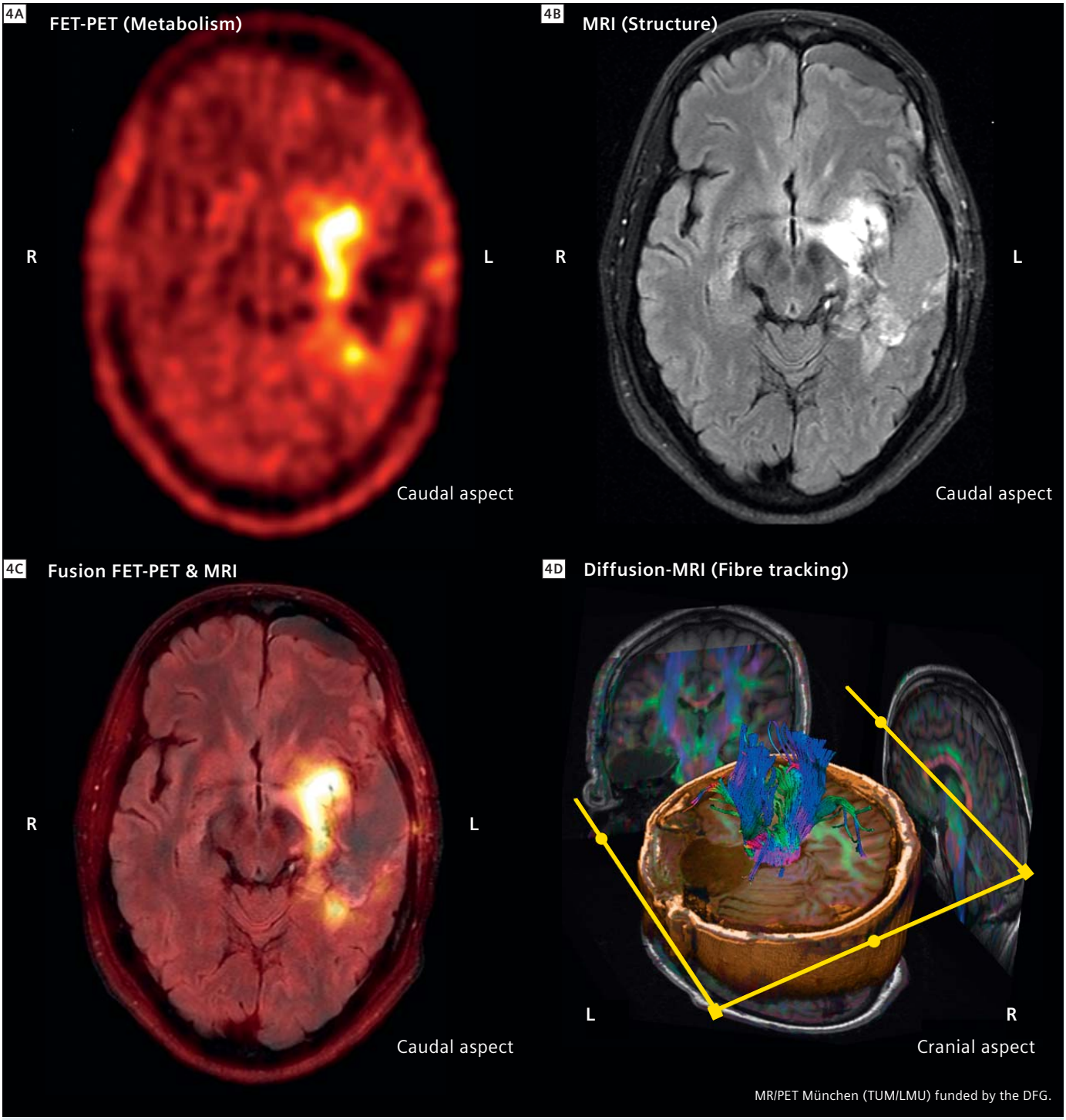

4 **A:** ^{18}F-FET PET scan. The tracer FET represents a measure of the amino acid metabolism and allows the sensitive identification of brain tumor tissue which is characterized by high amino acid turnover, in contrast to healthy brain tissue. A strong tracer uptake is visible around a previous resection area, suspect for remaining/recurrent brain tumor tissue. **B:** MR-image, axial FLAIR-sequence, demonstrating a region of hyper intensity around the area of resection, potentially representing edema and/or gliosis, but also vital tumor tissue cannot be excluded. Moreover, a left frontopolar hygroma is seen. **C:** Fusion of PET and MR-findings, allowing excellent anatomical allocation of the vital tumor tissue in reference to anatomical structures and abnormalities in the MR-image. **D:** Fibre-tracking based on a diffusion-tensor MR dataset, demonstrating the course of neuronal axons alongside the resection area.

Case 5 Patient with Alzheimer's disease.

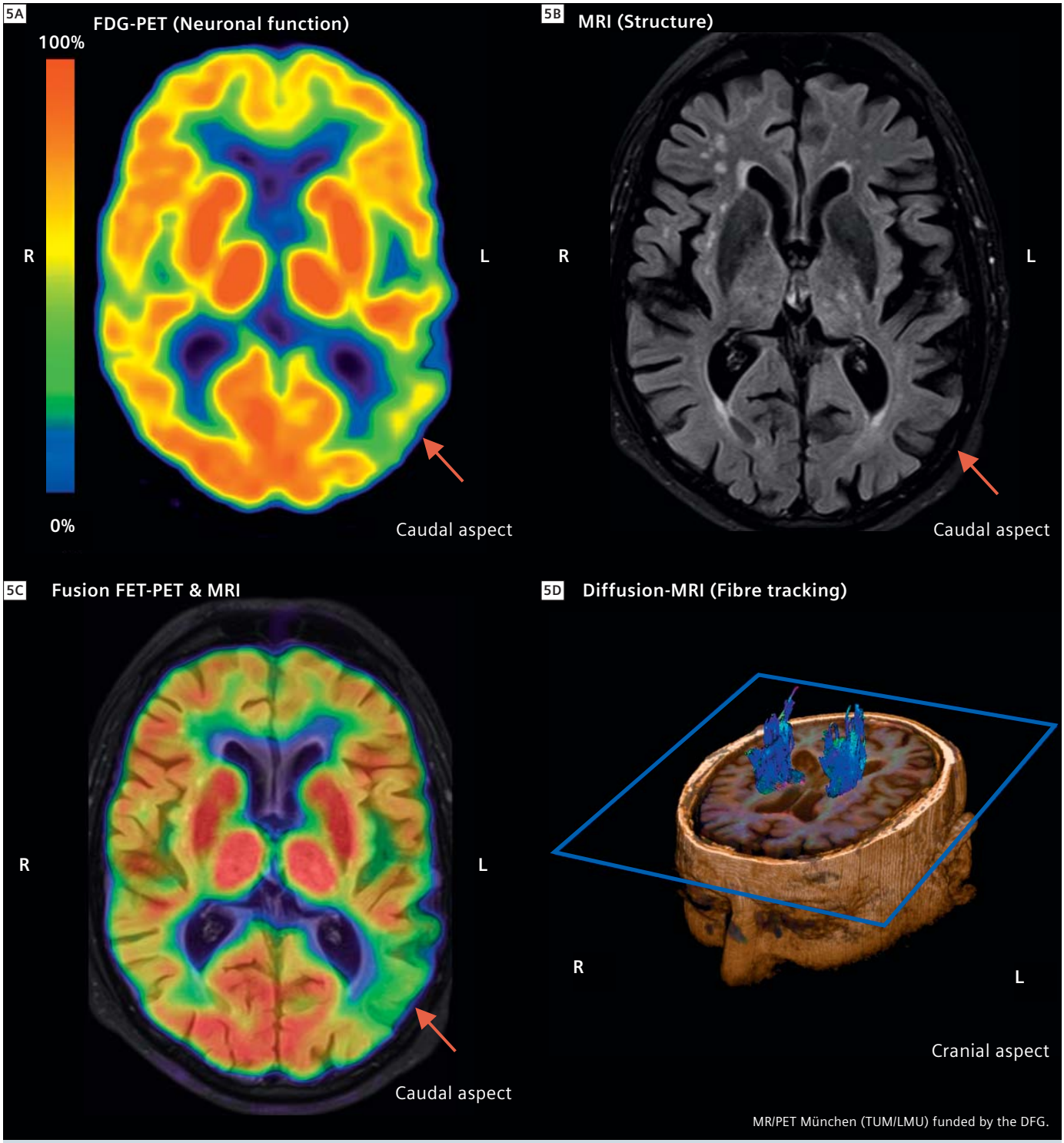

5 **A:** ^{18}F-FDG-PET of the brain, which represents a measure of neuronal function. Areas with reduced neuronal function in consequence of ongoing neurodegenerative processes are displayed in green-yellow (left temporoparietal cortex, see red arrow), healthy brain regions in orange-red. **B:** MR-image, axial FLAIR-sequence. Brain anatomy can be displayed in high resolution, cerebral atrophy is apparent in widespread regions, predominantly on the left side. **C:** In the MR/PET fusion regional allocation of hypometabolism and brain substance loss is possible. **D:** Fibre-tracking based on a diffusion-tensor MR dataset, demonstrating the course of neuronal axons in the brain of the patient.

3. Cardiology

Case 6 MR/PET of the heart.

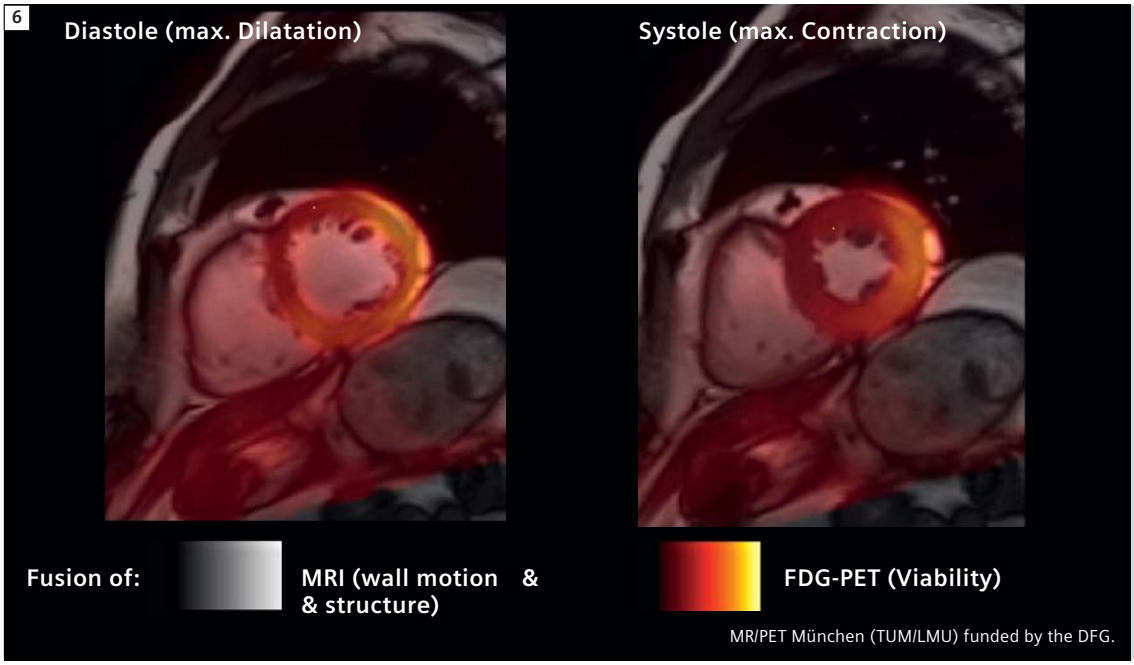

6 Assessment of the metabolism of cardiac tissue with the tracer ^{18}F-FDG allows the identification of viable myocardium. Simultaneous acquisition of wall motion and myocardial anatomy can be performed using MRI. The combination allows the exact attribution of functional aspects to underlying regional metabolic conditions/viability.

Conclusions

- First clinical imaging studies demonstrate successful clinical applicability of integrated whole body MR/PET.
- Attenuation correction of the PET signal using appropriate MR-derived attenuation maps appears to be feasible with sufficient reliability for most cases. Some problems (lack of accurate bone-detection, truncation artifacts) are a matter of ongoing research.
- From a diagnostic perspective, superiority of MR/PET compared to PET/CT can be foreseen for indications/body regions, which would preferably be approached by MRI rather than by CT, due to the superior soft tissue contrast of MRI. Examples are:
  Oncology: Head and neck tumors, masses in the pelvis/abdomen (e.g. prostate cancer), carcinoma of unknown primary, whole-body imaging
  Neurology: Brain tumors, epilepsy, dementia, stroke
  Cardiology: Regional function (wall motion) and scar detection (late enhancement) versus myocardial perfusion and tissue viability
- It remains to be evaluated for which indications MR/PET is superior or equal to PET/CT and for which indications PET/CT will remain the method of choice. MR/PET will probably be inferior to PET/CT for indications which are commonly addressed with better diagnostic value by CT, e.g. pulmonary lesions.
- The expected high costs for this type of imaging procedure will require elaborate logistics regarding patient flow, examination procedures, occupancy of the scanner etc., to ensure efficient utilization.
- The large number of available MR-sequences and of different PET-tracers exponentiates the number of potential combinations of imaging tests. This will define the need to develop optimized imaging algorithms for specific diagnostic questions.

References

1 Catana, C., et al., MRI-assisted PET motion correction for neurologic studies in an integrated MR-PET scanner. J Nucl Med. 52(1): p. 154-61.
2 Catana, C., et al., Toward implementing an MRI-based PET attenuation-correction method for neurologic studies on the MR-PET brain prototype. J Nucl Med. 51(9): p. 1431-8.
3 Herzog, H., et al., High resolution BrainPET combined with simultaneous MRI. Nuklearmedizin. 50(2).
4 Schlemmer, H.P., et al., Simultaneous MR/PET imaging of the human brain: feasibility study. Radiology, 2008. 248(3): p. 1028-35.
5 Beer, A.J., et al., Radionuclide and hybrid imaging of recurrent prostate cancer. Lancet Oncol. 12(2): p. 181-91.
6 Metz S, Ganter C, Lorenzen S, van Marwick S, Herrmann K, Lordick F, Nekolla SG, Rummeny EJ, Wester HJ, Brix G, Schwaiger M, Beer AJ. Phenotyping of tumor biology in patients by multimodality multiparametric imaging: relationship of microcirculation, alphavbeta3 expression, and glucose metabolism. J Nucl Med. 2010 Nov; 51(11):1691-8. Epub 2010 Oct 18.
7 Drzezga A, Becker AJ, Van Dijk K, Sreenivasan A, Talukdar T, Sullivan C, Schultz AP, Sepulcre J, Putcha D, Greve D, Johnson KA, Sperling RA. Neuronal dysfunction and disconnection of cortical hubs in non-demented subjects with elevated amyloid-burden. Brain. 2011, in press.
8 Martinez-Moller, A., et al., Tissue classification as a potential approach for attenuation correction in whole-body PET/MRI: evaluation with PET/CT data. J Nucl Med, 2009. 50(4): p. 520-6.

Contact
Alexander Drzezga, MD
Technische Universität München
Klinik und Poliklinik für Nuklearmedizin
Klinikum rechts der Isar
Ismaninger Str. 22
D-81675 Munich
Germany
phone: +49 89 4140 7722
a.drzezga@lrz.tum.de

Missing information?

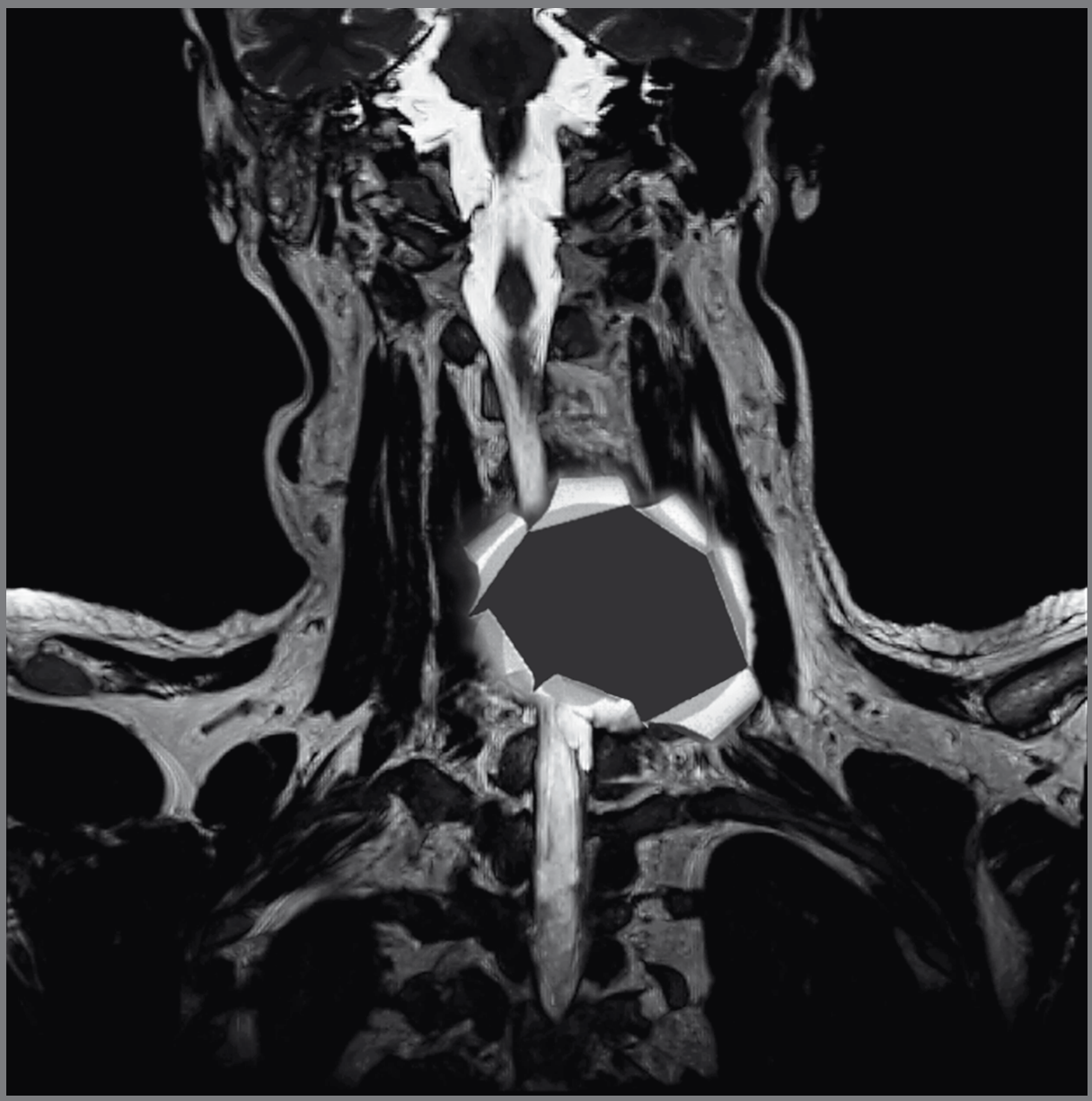

To make sure you have all the information you need, register for our free monthly newsletter on clinical MRI information.
Check out case reports from MAGNETOM users around the world and stay up-to-date with Siemens software applications.

Register at
www.siemens.com/magnetom-world
Go to
Publications > Subscriptions

Simultaneous MR/PET – Clinical Reality?

Nina Schwenzer; Christina Pfannenberg; Holger Schmidt; Bernd Pichler; Claus D. Claussen

University of Tübingen, Department of Diagnostic and Interventional Radiology and Department of Preclinical Imaging and Radiopharmacy, Tübingen, Germany

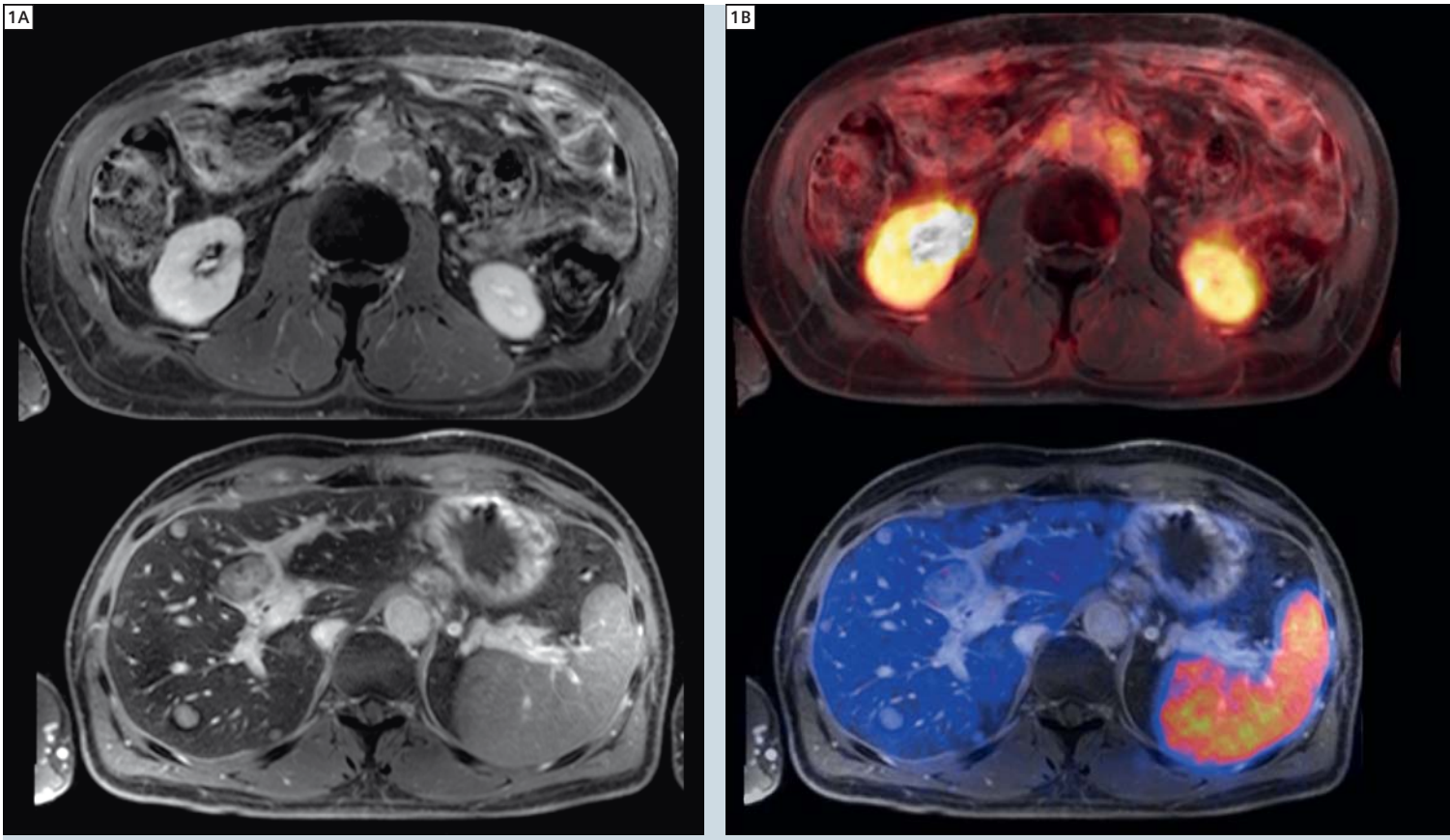

1A–B **1A**: Contrast-enhanced T1w 2D FLASH with fat saturation showing extensive retroperitoneal and hepatic tumor spread of the NET with partially necrotic areas. Corresponding DOTATATE PET in figure **1B**, acquired during simultaneous MR/PET, shows only slightly increased uptake/receptor upregulation of the retroperitoneal metastases and no focality within the liver.

Background

Much has already been written about the technology, the basic ideas as well as the potential clinical needs behind the combining of MR and PET. As with all new imaging methodologies, there is debate as to how much this technology is really needed (similarly, for example, with the availability of PET/CT) and the discussion regarding MR/PET in particular concerns the level of integration and, even more fundamentally, the question whether the simultaneity of MRI and PET acquisition is really required.

It should be pointed out that now that the MR/PET technology is available in the Biograph mMR, real simultaneous imaging with different methodologies is possible in a clinical setting for the first time – a clear paradigm shift in how we acquire information about patients and their diseases. The combining of functional information derived by MR and the possibility to influence PET information and vice versa is stimulating researchers worldwide and hopefully this will also clearly impact on how we provide biomarkers for therapy decisions throughout the continuum of patient care. But also from a purely clinical and very practical perspective, simultaneity

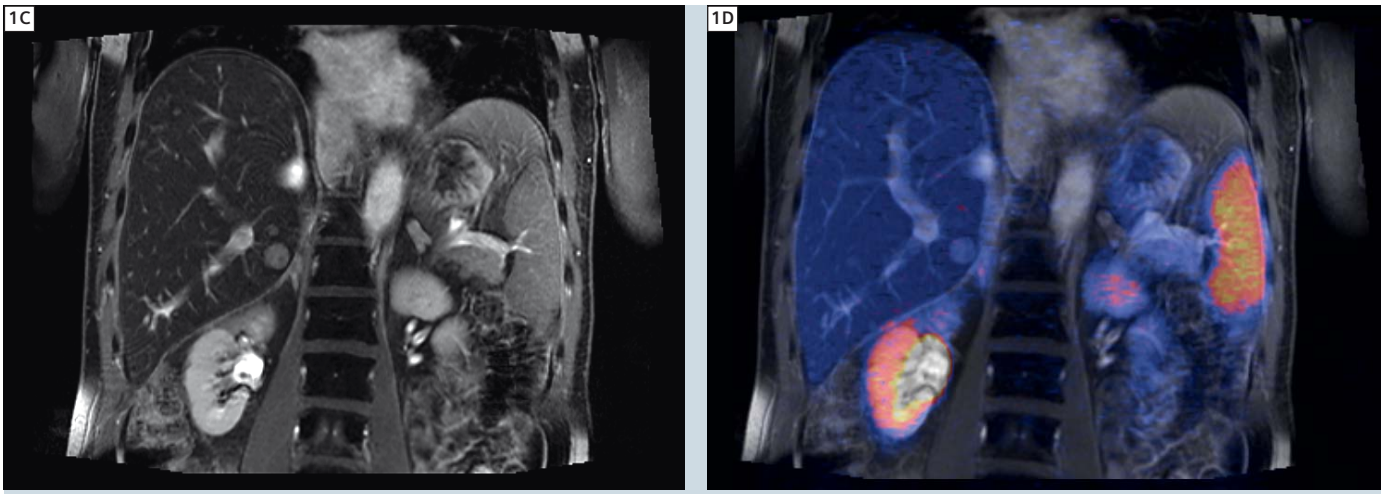

1C–D Corresponding coronal MR/PET.

of acquisition promises definite advantages over sequential acquisition – independently of how this sequential approach is organized (main concepts: a) different scanners and combination of results with software only, b) different scanners in different rooms with patient transport solution, or c) different scanners in the same room with patient transport solution). More detail about concepts and technology of MR/PET can also be found in the research supplement of the MAGNETOM Flash issue 3/2010 and in the MAGNETOM Flash issue 1/2011.

Impact of MRI on mMR imaging protocols

MRI has one main disadvantage when combining MR and PET in addition to not providing quantitative information about tissue density (a fact which has to be taken into account for attenuation correction of PET data): Data acquisition speed is limited compared, for example, to today's CT. MR imaging speed can of course be improved to some extent by increasing the strength of the B_0 field; by using different sequence techniques; by applying parallel imaging; and through its combinations (e.g. T2w 3D acquisition is only feasible within clinical routine as a turbo-spin-echo technique by the combination of variable flip angle evolutions with long echo trains and parallel imaging; *syngo* SPACE). In addition, the need for multiple contrasts and the capability to derive functional parameters like perfusion (T2* dynamics), cellularity (diffusion-weighted imaging, *syngo* REVEAL), microvessel density and permeability (T1w DCE; *syngo* VIBE or *syngo* TWIST for acquiring 4D data sets, *syngo* Tissue 4D for pharmaceutical modelling) are resulting in complex and relatively long examination times. For example, a comprehensive brain scan for tumor resection planning with MRI involves not only morphology scans (multiplanar T1w and T2w contrast including contrast media application) but possibly also fiber tracking and functional MRI to evaluate, for example, the tumor's involvement of essential areas like the motor cortex. An MRI exam that provides the required information can easily exceed half an hour and complex whole-body scans with MRI can easily take one hour.

Furthermore, these scans also generate a huge volume of imaging data. A standard whole-body MRI protocol in our clinical daily practice comprises 1,000 to 1,500 images; and this amount is increased dramatically by adding information from DWI, T1w DCE, etc. To provide another example of the level of complexity of these multimodal MRI approaches: A state-of-the-art prostate MRI exam aimed at local tumor staging / detection includes not only multiplanar / 3D high-resolution T2w TSE images but also T1w DCE, 3D MR spectroscopy, and DWI (including ADC calculations). Leaving aside the necessary post-processing, more than 2,000 images are acquired and have to be taken into account for diagnoses. But what does this mean to the simultaneously acquired PET data, and how is this influenced by such a relatively time-consuming and complex MRI exam?

In today's sequential PET/CT routine, PET can be regarded as a stand-alone imaging acquisition. CT (independent if only as a native low-dose or multi-phase contrast-enhanced scan) is acquired completely independently from the PET. Consequently, long PET measurement times are not desirable. Furthermore, the relatively small dimensions of the PET beds in a larger number of PET/CT scanners and physiological processes like filling of the bladder, bowel movement and uncomfortable patient fixation require the shortest possible PET scan times, in overall terms and per bed, especially also to limit the time-difference between the "snap-shot" CT (a whole-body scan with the latest CT generation can be done in less than 10 seconds at sub-millimetre resolutions) and the corresponding metabolic / PET information. As a further consequence of the time-constraints on PET measurements, dynamic

and late PET scans can be considered as wishful thinking and are not yet part of clinical routine, despite the promising results reported over recent years. This also applies to some degree to gated PET acquisition. Another problem is the relatively small number of patients included in these reports which makes it difficult to apply these techniques in daily patient care on a larger scale and thereby make economies of scale. But how do the relatively long MRI examination times, the need for complex functional information and the simultaneous acquisition of MR and PET data fit together? How will MR influence the PET acquisition and vice versa?

- The used PET detector for simultaneous MR/PET is characterized by a large field-of-view (in fact the largest available for clinical routine) which allows us to cover large areas if not the whole organ (brain, liver) in one go. Furthermore, the high sensitivity allows for fast PET scans per bed and in total. However, the relatively long MR imaging time and the high sensitivity of the detector results in an 'oversampling' of PET data, allowing gated PET scans (e.g. by adding information of the diaphragm movements derived from the simultaneous acquired MRI) or even longer dynamic PET acquisition when focusing on one organ. And whilst such an exam will take longer than a standard PET/CT, such a patient would have to undergo an MRI anyhow, and a dynamic PET scan would not really be possible in clinical routine for a PET/CT scanner aiming for a high patient through-put.
- PET information can be used to reduce the required amount of MR information; in fact, MR and PET point out different aspects of biology and so far it is more a question of diagnostic power of an individual biomarker and their combination that will determine the content of future MR/PET protocols. The 3D in-phase / opposed phase T1w sequence for attenuation correction will replace its counterparts in the MR protocol only in rare cases. Also, thanks to the 3D VIBE with Dixon technique, this is nowadays a simple one breathhold scan and does not really extend the overall scan time. Nevertheless, information derived from this MR sequence is of a diagnostic nature as it is for any low-dose attenuation CT scan for PET/CT.
- Of course, simultaneous MR/PET does offer multiple chances to improve PET performance, for example by adding information about perfusion information to dynamic PET data, or by allow for motion or volume correction. It is evident that these techniques are especially appealing for very specific PET tracers (e.g. for dementia evaluation) or for obtaining dedicated biological information for therapy adoption, for example the presence and adoption to hypoxic stress of tumor tissue.

Clinical examples
Study design and equipment

At a given point in time, all patients examined with the Biograph mMR are included in clinical studies. In the first phase, imaging capabilities of the system are evaluated to derive important information for advanced imaging protocols. We also want to compare the clinical performance of MR/PET with PET/CT for existing PET/CT indications. Because of the convincing results of the first phase of the clinical testing and after

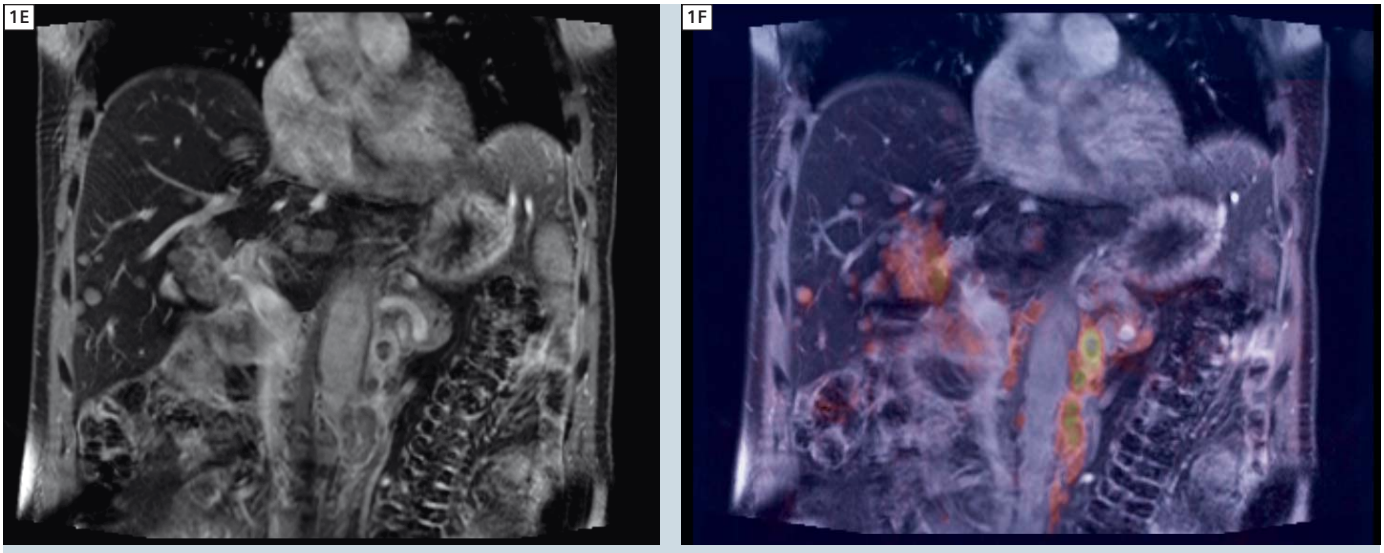

1E–F **1E** (MR only) and **1F** (b=800 s/mm^2 overlaid) show the extensive retroperitoneal tumor spread. In contrast to PET, DWI demonstrates areas with restricted diffusion as an expression of high cellularity which is not directly linked to the receptor expression but more to cell density. Not shown in this case are the quantitative ADC maps which are used to separate T2-shine through effects from real restriction of diffusion. These effects can both contribute to the signal in the original b-value images.

receiving the CE-label for the Biograph mMR, we expanded our IRB approval for the use of our system for imaging children* and now regularly use contrast-media for, for example, dynamic liver evaluations.

All patients have an indication for PET/CT and are scanned at the PET/CT and at the mMR. We apply body-weight adjusted PET tracers according to our clinical PET/CT protocols; the second scan is performed with the residual activity. Most of our patients received the PET/CT scan first. However, for some indications we now change this order. The installation of the Biograph mMR at our institution was the second world-wide, and the BrainPET prototype the first, used for advanced neuro-research and basic / methodology evaluation of the MR/PET technology. This scanner is placed in our radiopharmaceutical laboratories, which can produce all common radiopharamaceuticals in clinical imaging and research. The Biograph mMR is placed in a different building, but short delivery ways allow us to apply ^{11}C labelled tracers and other tracers than FDG within the framework of clinical pilot studies.

*MR scanning has not been established as safe for imaging fetuses and infants under two years of age. The responsible physician must evaluate the benefit of the MRI examination in comparison to other imaging procedures.

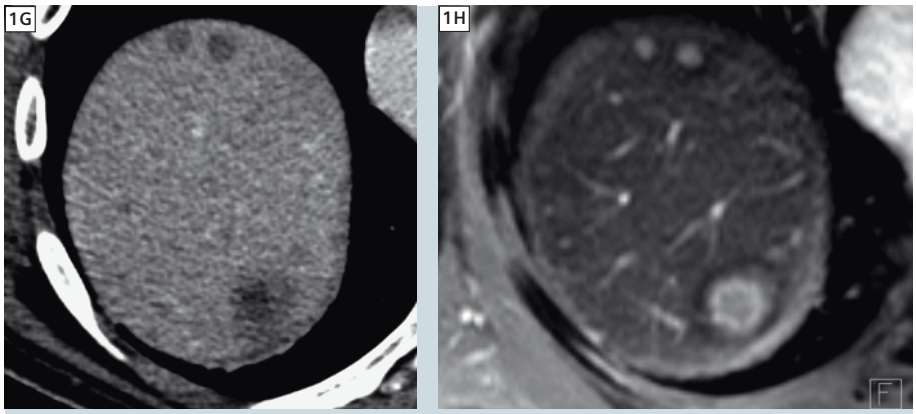

1G–H **1G**: Contrast-enhanced CT scan (late phase) and corresponding MRI in **1H** (contrast-enhanced late phase) show the superior soft contrast of MRI which enables detailed information about regional differences within the metastases.

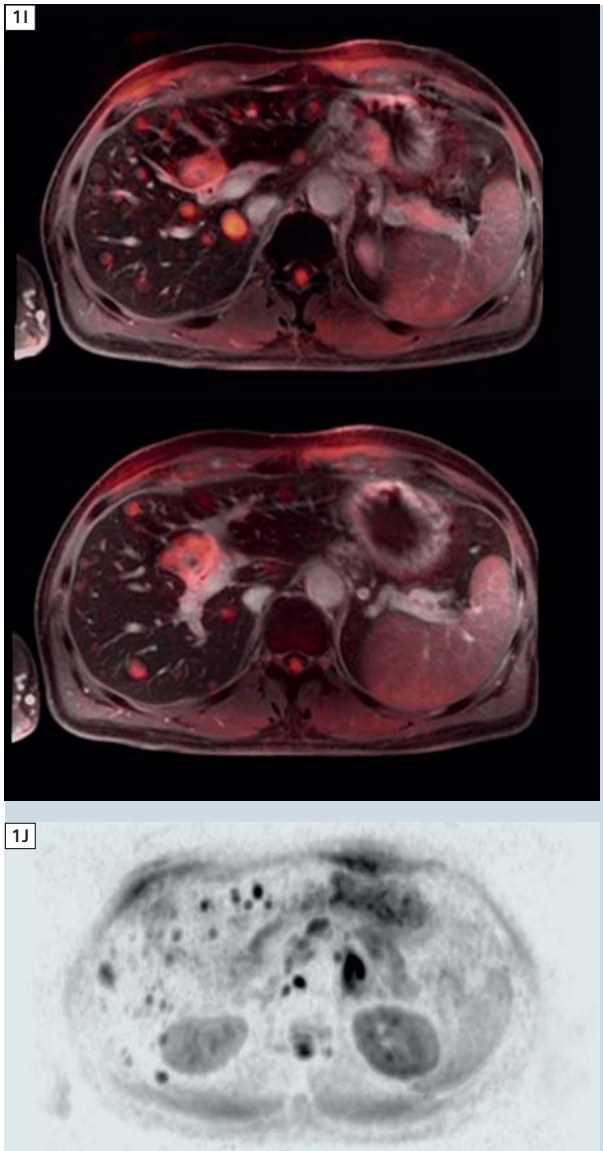

1I–J **1I** (DWI superimposed on contrast-enhanced T1w ce FLASH) and **1J** (thick-slice MIP of original b-value images) show the potential of DWI to provide detailed information about the total tumor load. Nevertheless, simply based on the original b-value images, a differentiation between tumor and reactive tissue, e.g. after surgery, as seen in the ventral abdominal wall, can be challenging. There is an additional finding of increased fat content of the liver.

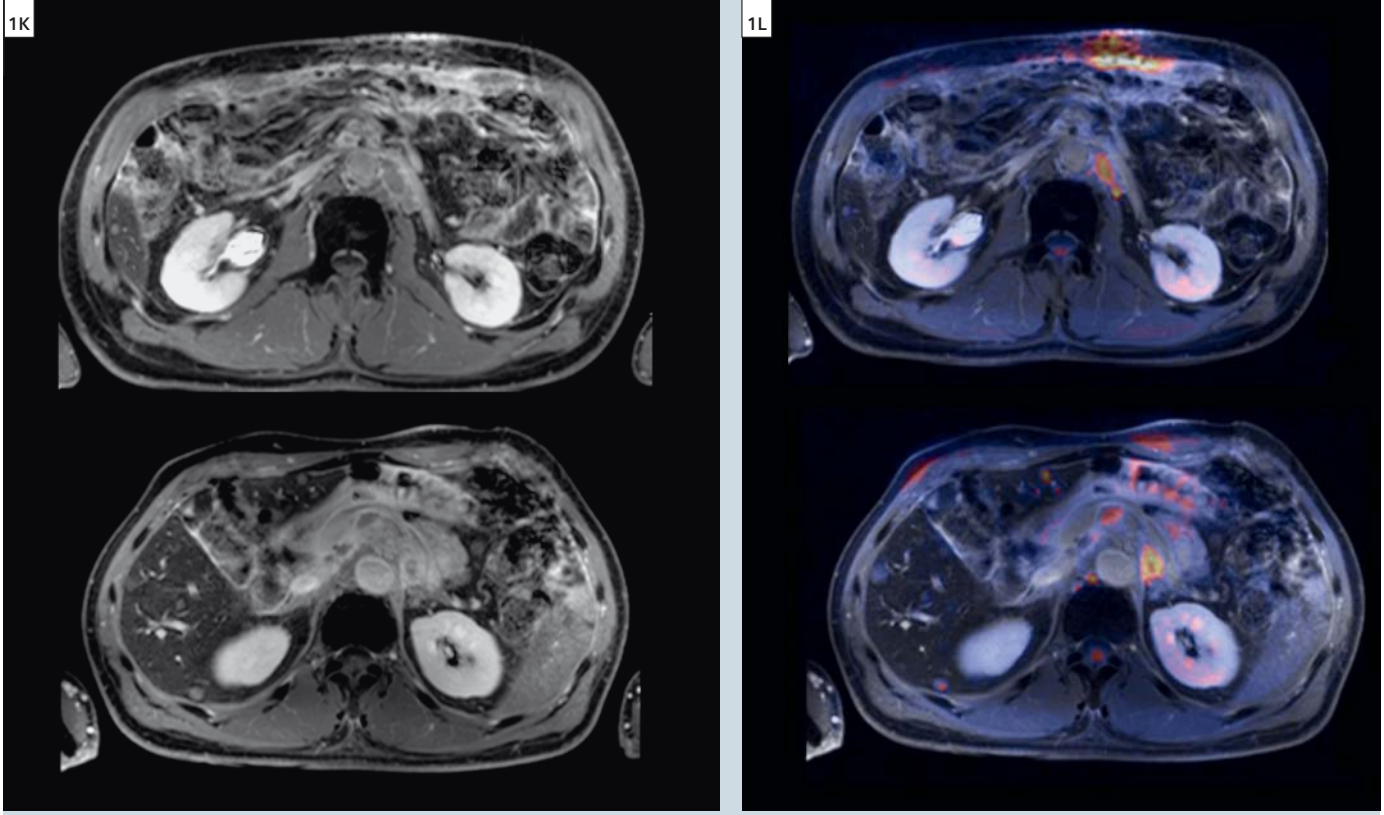

1K–L T1w contrast-enhanced MRI demonstrating extensive spread and involvement of paraortic lymph nodes stages with necrosis. In addition, diffuse enhancement of the peritoneum can be seen **(1K)**. Overlayed high b-value images do show however different aspects of metastases than T1w scan **(1L)**. Compare with figure 1B for evaluation of receptor status of the metastases.

MR/PET imaging protocols

We are now still in the evaluationary phase for different MR/PET protocols depending on clinical indications and patients' capabilities. In general, we try to focus more on clinically relevant combinations than to rigidly adhere to our imaging protocols. This approach can best be compared to the modules for whole-body MRI proposed by several working groups, which take into account clinical patterns of disease as well as the diagnostic power of MRI sequences, e.g. dynamic liver scans for colorectal cancers, coronal whole-body TIRM in case of high probability of bone metastases and FLAIR and post-contrast scans of the brain in case of lung cancer, etc., are added to a basic protocol. Our MR/PET protocols aim first at acquiring a comprehensive overview that is more comparable to conventional PET/CT and comprises basic MR sequences including the sequence for attenuation correction and then add a focused scan. Here we limit the scan range to smaller areas of interest and perform the specific MR protocols that also allow us to acquire dynamic PET data.
In the following case reports we describe two typical cases from our patient cohort. Both patients were scanned first with the PET/CT and then with the Biograph mMR.

Case 1
Evaluation of metastatic spread in case of a neuroendocrine tumor (NET)

This exam had to answer three important questions: First, what is the total tumor load; second, can this NET be treated by an internal radiotherapy; and finally, are there any complications that would cause an adoption of the therapy (e.g. recommendation of supportive actions in case of congestion of the biliary tract, obstruction of the urinary tract etc.). As one of the few clinical available 'therapeutics', ^{68}Ga DOTATATE was used in this patient. Over-expression of Somatostatine receptors of NET are a common finding. DOATATE has similar characteristics to DOTATOC and is used for imaging NETs. If labelled with ^{68}Ga, DOTATOC as well as the applied DOTATAE can be used as a tracer specific PET tracer to provide not only information about degree of receptor expression but also an evaluate the effectiveness of potential systemic ^{90}Y labelled DOTATOC/DOTATATE application for internal radiotherapy. However, as is the case for other tumors, metabolism and in this case receptor expression may vary not only between patients but also between different metastases of the same tumor within one individual. In addition, a common organ for metastastic spread of NET is the liver, but small filiae can easily be missed even when showing higher DOTATOC uptake because of the high background activity of liver tissue. Furthermore, since limited disease would potentially allow a more radical and curative approach e.g. atypical resection of liver metastases, a precise detection of filiae is essential for therapy assessment. It has been shown that MRI (using arterial phase of dynamic liver scans and / or diffusion weighted imaging) is the most accurate imaging method for an accurate evaluation of liver metastases of a NET. But DWI in particular also has

the potential to provide fast assessment of the total tumor load. By quantifying diffusion restriction it has already proved itself as an early therapy response biomarker for other tumor entities.

The images shown are from a 47-year-old male patient. With a weight of 82 kg and body height of 195 cm (BMI 21.56 kg/m^2), 167 mBq of ^{68}Ga DOTATATE was injected. After an uptake time of 20 min, a PET/CT was acquired including contrast-enhanced diagnostic CT scans and 78 min after tracer injection, the MR/PET examination was started (due to low residual activity, time per bed was 8 min, 3 beds were measured). PET/CT and MR/PET showed both multiple hepatic, coelical and retroperitoneal filiae of the known NET with only slightly increased receptor expression, most evident for the ceolical / retroperitoneal metastases. As expected, MRI could visualize more hepatic filiae and also allow for a more sensitive evaluation of diffuse reactions of the great omentum due to both advanced tumor spread and to the surgical approach before the patient was sent to our department. For the hepatic filiae, only discrete uptake could be seen in some larger metastases. However, this is not visible within the normal range of standard uptake values as used for images with overlaid PET; clear focal uptake is not seen and multiple metastases show no increased uptake compared to the liver background. As expected, the diagnostic performance of the PET/CT is inferior to MRI (MR/PET) but the information derived from MRI and DWI also show different aspects of tumor biology than PET; DWI reveals areas with higher cellularity that are not necessarily linked to a higher level of receptor expression.

Alongside the clinically comprehensive information derived from a combined MR/PET, this case shows clearly the high image quality achievable in challenging cases in the abdomen where MRI at 3T not only has the advantage of a high SNR but must also take into account potential negative effects. We do not apply to this patient the motion-freezing techniques which we also evaluate at our institution in a clinical setting. Motion-freezing and correction will unquestionably have an impact on diagnostic accuracy, especially for brain and liver MR/PET exams. However, in this clinical example no change of therapy would be evident: The extent of disease and the missing clear increase of uptake of the liver metastases compared to the residual normal liver parenchyma and the massive tumor load negates any further surgical approach.

Case 2
Evaluation of lung cancer

Lung cancer is perhaps the most evident indication for a PET/CT scan. MRI has not played a role in the diagnostic work-up so far, although the diagnostic accuracy of MRI has improved dramatically over recent years. The potential to detect small lung nodules is size-dependent but especially for the therapeutic relevant lesions with diameters >4 mm is comparable to state-of-the-art helical CT techniques. By adopting MR sequence techniques, lung MRI at 3T is clinical reality. Furthermore, MRI can add important information about, for example, infiltration of the chest wall, or provide detailed knowledge about vessel impairment which can be used for a detailed

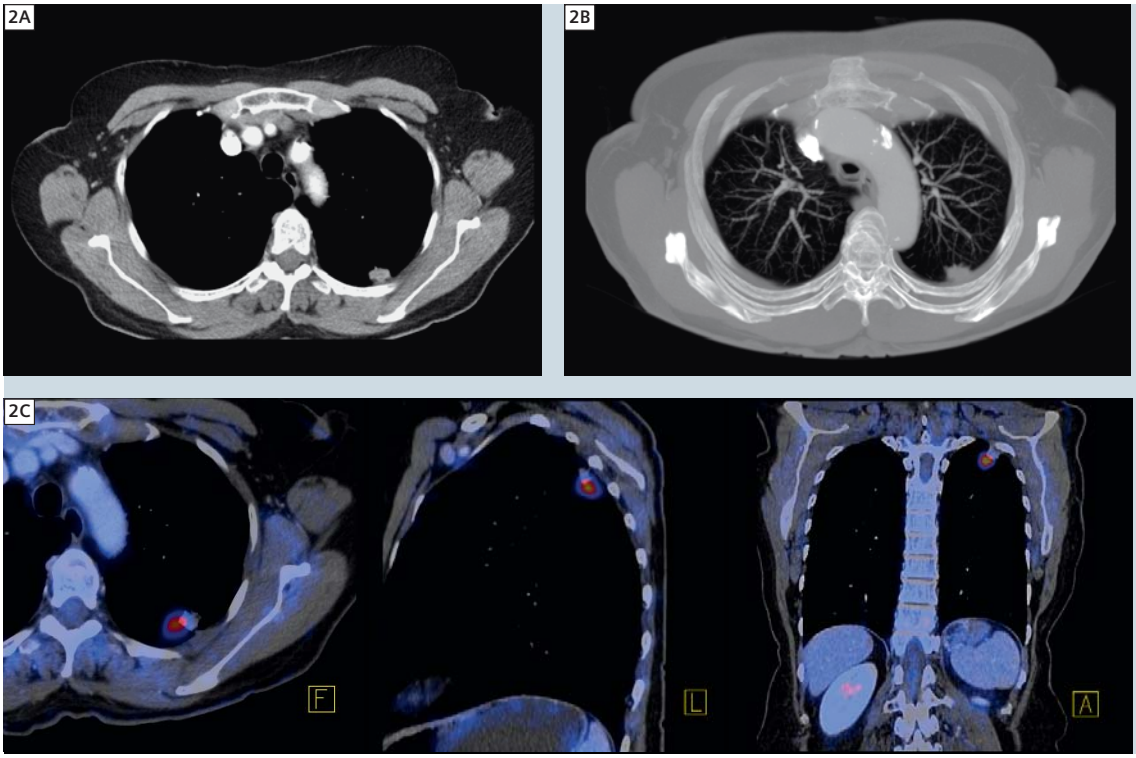

2A–C Contrast-enhanced CT scan (**2A** soft-tissue window and **2B** lung window) demonstrates the left apical lung nodule. As expected clear focal FDG uptake can be seen, however, fused on the contrast-enhanced diagnostic CT scan, a mismatch between PET (which is acquired during free breathing) and the cancer is seen in **2C**. However, fused on the native attenuation correction CT, this mismatch is as expected less evident (not shown).

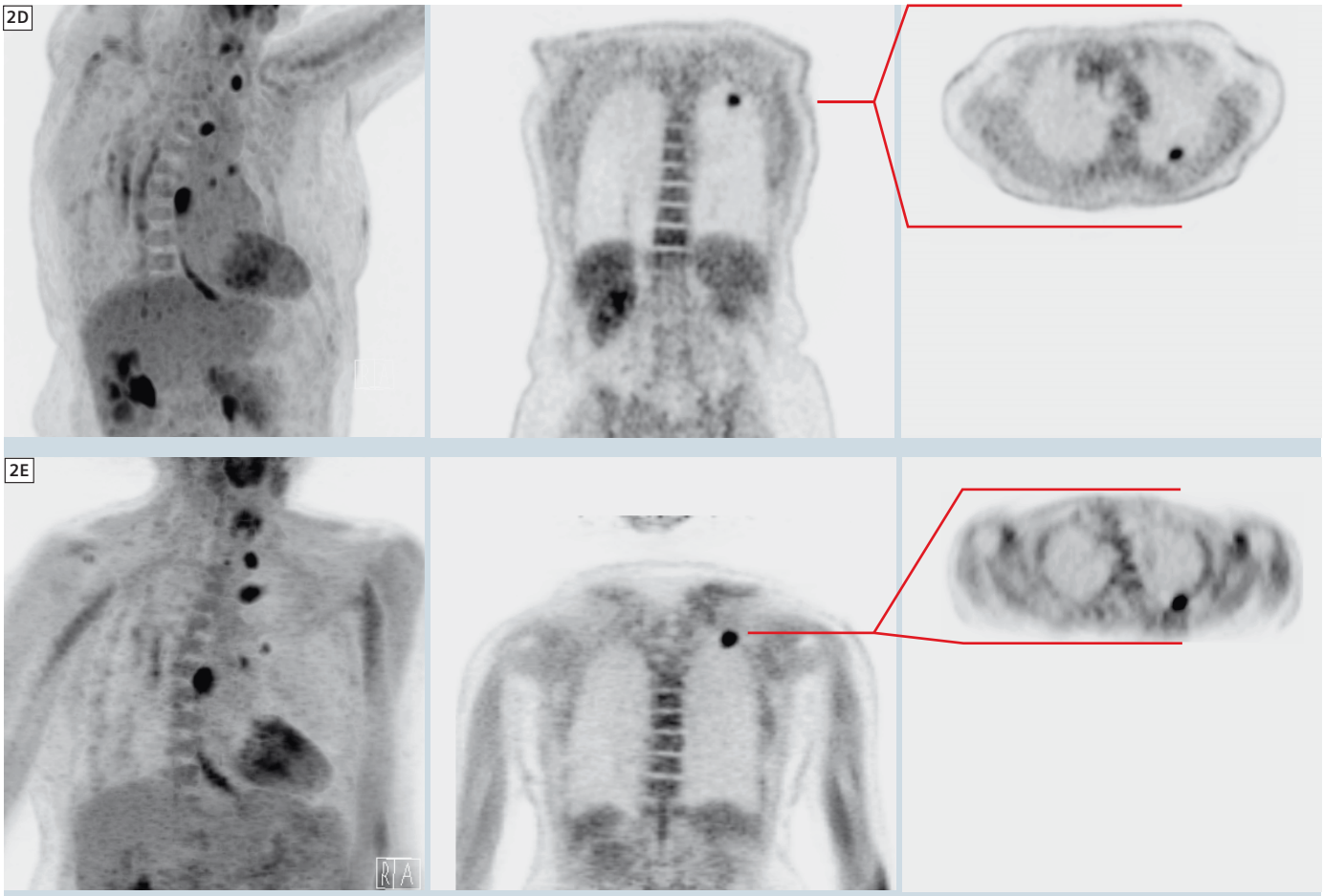

2D–E **2D** shows MIP and MPR of the PET derived from the PET/CT scan. Corresponding PET derived from the MR/PET in **2E**. Note that the MR/PET scan had to utilize the residual activity of the first acquired PET/CT. Note also that for MR/PET the arms can be positioned more comfortably without negative impact on image quality even if positioned outside the MRI's FOV. Findings details are given in the text.

surgical therapy assessment. In addition, MRI can provide functional parameters such as:

- cellularity by DWI,
- 3D motion patterns of the lesions by dynamic MRI (TrueFISP techniques, in development are sequences with radial k-space sampling schemes in combination with compressed sensing; evaluation of motion is feasible with CT, too, especially in an elderly patient undergoing radiotherapy this is a clinically realistic setting. However, especially for young female patients, additional radiation should be avoided)
- perfusion (again, radiation is a topic for CT scans when applied to young patients but also information derived especially by T1w DCE scans does differ from CT acquired perfusion data. DCE MRI was successfully applied to differentiate benign versus malignant lung lesions).

Especially in the evaluation of lung lesions of unknown origin in younger patients, MRI has to be considered as a clear alternative to conventional CT exams.

In this case, a 70-year-old female (weight 60 kg, height 165 cm, BMI 22,04 kg/m^2) – after injection of 381 mBq ^{18}F-FDG and an uptake time of 55 min – underwent a PET/CT, including multi-phase contrast-enhanced CT scans, for staging of a suspected lung cancer. The patient was than referred to our MR/PET unit. Simultaneous MR/PET was started 122 min after injection of FDG; PET acquisition time per bed was adapted to 6 min to compensate for the low residual tracer activity (2 bed positions were acquired which covered the whole thorax as well as the cervical region).

PET/CT and MR/PET showed both the left apical lung cancer neighbouring the pleura but without clear evidence of an affection of the thorax wall; also no signs of a pleural infiltration are seen. In addition, two small hiliar lymph nodes are present as well as paraoesphagel lymphnodes which were all rated as metastases because of their high and

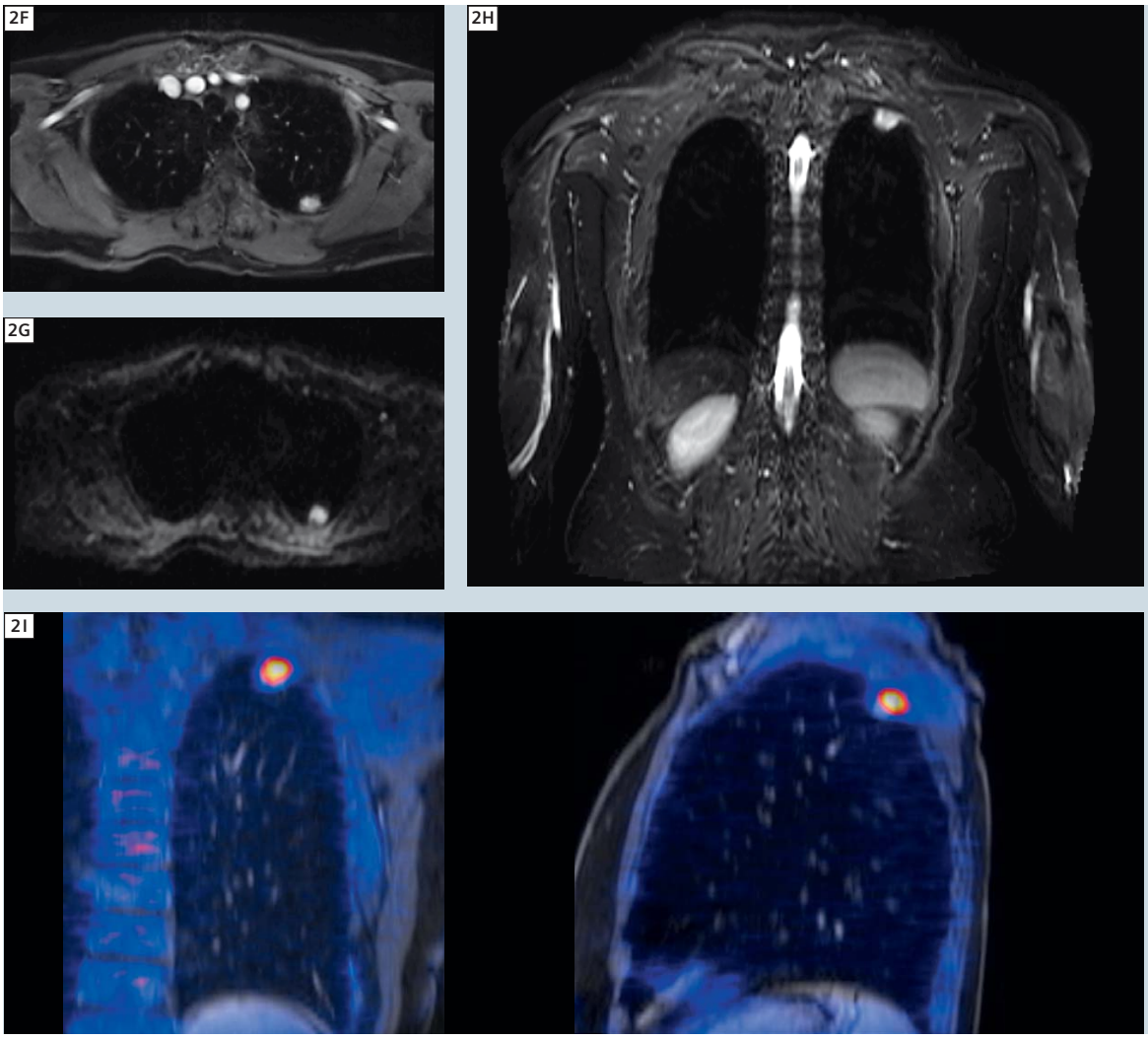

2F–I Transversal arterial phase T1w 3D VIBE scan is shown in **2F**. **2G** shows corresponding original b = 400 s/mm² DWI measurement. In **2H** coronal T2w STIR reveals the contact of the lesion to the very apical border of the pleura. Figure **2I** demonstrates focal uptake of the lesion also with the MR/PET examination. PET information is displayed with the simultaneously acquired contrast-enhanced 3D VIBE which demonstrates the high perfusion of the lesion.

focal FDG uptake. Both PET data sets also show a focal uptake within the oesophagus which has to be considered as a potential second malignoma. Both exams also demonstrate an increased but non-focal uptake of the lower oesophagus as often seen in case of recurrent inflammation which would also increase the possibility of a malignancy.

Another finding which corresponded to nodular formation in morphology was a small focal FDG uptake within the thyroid gland. Southern Germany is considered as an iodine-deficient area and therefore findings within the thyroid gland are common, however, a focal uptake within the gland can be linked also to thyroid cancer and a further evaluation of this finding is required, too.

Attenuation correction of PET data derived from the MR/PET examination is based on a segmentation approach. A direct comparison between of PET/CT and MR/PET is challenging in a clinical setting; different bio-distribution when measuring at different time-points is perhaps the main factor, but the problems associated with the measurement itself as well as different reconstructions of the PET images, etc., are also potential factors influencing the comparability of the two scans. With a SUVmax / SUVavg of 8.1 / 4.1 for the PET/CT and 8.8 / 4.3 for the MR/PET for the primary lung cancer lesion, a good correlation between the two scans is evident. However, it also shows that quantification of PET data is dependent on various factors which have to be taken into account, together with the error level that is deemed to be clinically acceptable, and these issues require an increased awareness especially from us clinicians.

This case clearly demonstrates that simultaneous MR/PET is clinically feasible at high quality and diagnostic accuracy, even where PET/CT would otherwise be considered as standard. MR/PET is a also a clear alternative for evaluation of lung lesions where radiation exposure is relevant, especially in young female patients. This clinical example comprises only basic MR techniques, but

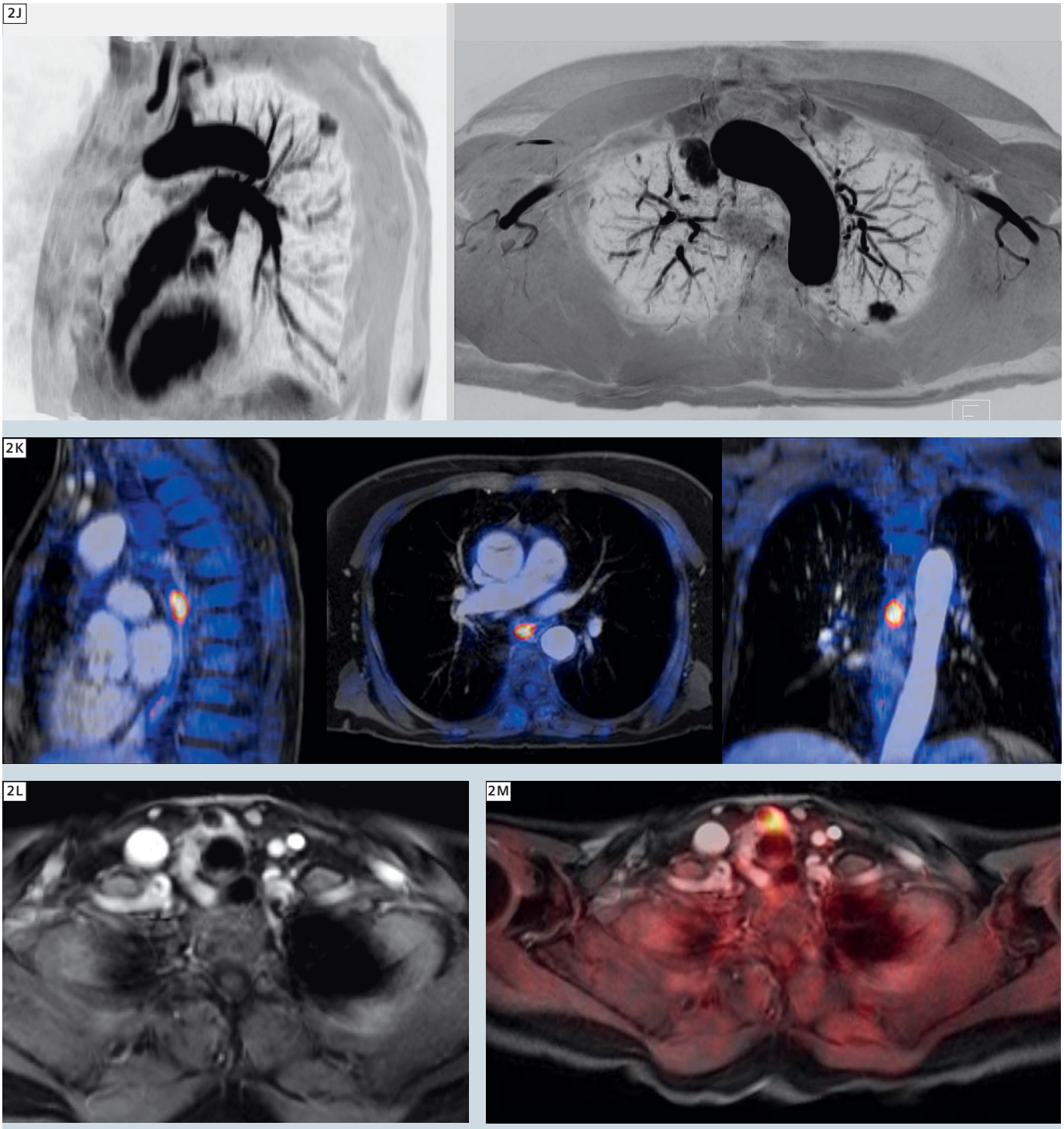

2J–M **2J** shows the relative relationship to the lung vessels. Images are thick-slice MPR and based on arterial phase 3D VIBE MR acquisition. In **2K** a multiplanar reconstruction based on the same MR sequence is shown, superimposed on the PET data and visualizing the focal uptake within the oesophagus of unknown origin. **2L** shows nodular changes within the thyroid gland and **2M**) superimposed with the PET the focal appearance of the increased FDG uptake in this area.

MRI can already deliver variable functional parameters. In this particular case, motion-freezing or correction would have been favourable but not clinically essential. However, especially for follow-up of small lung lesions, it has to be considered as an integral part of simultaneous MR/PET examinations.

Conclusion

As shown by the two cases in our ongoing clinical evaluation study, simultaneous MR/PET has already proven its potential to deliver outstanding image quality and offer all the advantages of MRI and PET in one examination. It is also evident that simultaneous MR/PET is about much more than just adding a radiation-free imaging modality to PET and that we have only begun to understand the clinical benefits of molecular MR. There is no doubt that it has huge potential to advance imaging in patient care and to provide detailed biomarkers for a vast range of diseases and therapies.

References

1 Thorwarth D, Henke G, Müller AC, Reimold M, Beyer T, Boss A, Kolb A, Pichler B, Pfannenberg C. Simultaneous 68Ga-DOTATOC-PET/MRI for IMRT treatment planning for meningioma: first experience. Int J Radiat Oncol Biol Phys. 2011 Sep 1 ;81(1):277-83. Epub 2011 Feb 6.

2 Werner MK, Brechtel K, Beyer T, Dittmann H, Pfannenberg C, Kupferschläger J. PET/CT for the assessment and quantification of (90)Y biodistribution after selective internal radiotherapy (SIRT) of liver metastases. Eur J Nucl Med Mol Imaging. 2010 Feb;37(2):407-8. Epub 2009 Dec 9.

3 Gehler B, Paulsen F, Oksüz MO, Hauser TK, Eschmann SM, Bares R, Pfannenberg C, Bamberg M, Bartenstein P, Belka C, Ganswindt U. [68Ga]-DOTATOC-PET/CT for meningioma IMRT treatment planning. Radiat Oncol. 2009 Nov 18;4:56.

4 Plathow C, Staab A, Schmaehl A, Aschoff P, Zuna I, Pfannenberg C, Peter SH, Eschmann S, Klopp M. Computed tomography, positron emission tomography, positron emission tomography/computed tomography, and magnetic resonance imaging for staging of limited pleural mesothelioma: initial results. Invest Radiol. 2008 Oct;43(10):737-44.

5 Plathow C, Aschoff P, Lichy MP, Eschmann S, Hehr T, Brink I, Claussen CD, Pfannenberg C, Schlemmer HP. Positron emission tomography/computed tomography and whole-body magnetic resonance imaging in staging of advanced nonsmall cell lung cancer-initial results. Invest Radiol. 2008 May;43(5):290-7.

6 Lichy MP, Aschoff P, Plathow C, Stemmer A, Horger W, Mueller-Horvat C, Steidle G, Horger M, Schafer J, Eschmann SM, Kiefer B, Claussen CD, Pfannenberg C, Schlemmer HP. Tumor detection by diffusion-weighted MRI and ADC-mapping--initial clinical experiences in comparison to PET-CT. Invest Radiol. 2007 Sep;42(9):605-13.

7 Judenhofer MS, Wehrl HF, Newport DF, Catana C, Siegel SB, Becker M, Thielscher A, Kneilling M, Lichy MP, Eichner M, Klingel K, Reischl G, Widmaier S, Röcken M, Nutt RE, Machulla HJ, Uludag K, Cherry SR, Claussen CD, Pichler BJ. Simultaneous PET-MRI: a new approach for functional and morphological imaging. Nat Med. 2008 Apr; 14(4) :459-65. Epub 2008 Mar 23.

8 Schraml C, Schwenzer NF, Martirosian P, Bitzer M, Lauer U, Claussen CD, Horger M. Diffusion-weighted MRI of advanced hepatocellular carcinoma during sorafenib treatment: initial results. AJR Am J Roentgenol. 2009 Oct;193(4):W301-7.

9 Boss A, Stegger L, Bisdas S, Kolb A, Schwenzer N, Pfister M, Claussen CD, Pichler BJ, Pfannenberg C. Feasibility of simultaneous PET/MR imaging in the head and upper neck area. Eur Radiol. 2011 Jul;21(7):1439-46. Epub 2011 Feb 10.

10 Pichler BJ, Kolb A, Nägele T, Schlemmer HP. PET/MRI: paving the way for the next generation of clinical multimodality imaging applications. J Nucl Med. 2010 Mar;51(3):333-6. Epub 2010 Feb 11.

11 von Schulthess GK, Schlemmer HP. A look ahead: PET/MR versus PET/CT. Eur J Nucl Med Mol Imaging. 2009 Mar;36 Suppl 1:S3-9.

12 Schlemmer HP, Pichler BJ, Schmand M, Burbar Z, Michel C, Ladebeck R, Jattke K, Townsend D, Nahmias C, Jacob PK, Heiss WD, Claussen CD. Simultaneous MR/PET imaging of the human brain: feasibility study.Radiology. 2008 Sep;248(3):1028-35.

13 Catana C, van der Kouwe A, Benner T, Michel CJ, Hamm M, Fenchel M, Fischl B, Rosen B, Schmand M, Sorensen AG. Toward implementing an MRI-based PET attenuation-correction method for neurologic studies on the MR-PET brain prototype. J Nucl Med. 2010 Sep;51(9):1431-8.

14 Wehrl HF, Judenhofer MS, Thielscher A, Martirosian P, Schick F, Pichler BJ. Assessment of MR compatibility of a PET insert developed for simultaneous multiparametric PET/MR imaging on an animal system operating at 7 T. Magn Reson Med. 2011 Jan;65(1):269-79.

15 Guérin B, Cho S, Chun SY, Zhu X, Alpert NM, El Fakhri G, Reese T, Catana C. Nonrigid PET motion compensation in the lower abdomen using simultaneous tagged-MRI and PET imaging. Med Phys. 2011 Jun;38(6):3025-38.

16 Catana C, Benner T, van der Kouwe A, Byars L, Hamm M, Chonde DB, Michel CJ, El Fakhri G, Schmand M, Sorensen AG. MRI-assisted PET motion correction for neurologic studies in an integrated MR-PET scanner. J Nucl Med. 2011 Jan;52(1):154-61.

17 Eiber M, Martinez-Möller A, Souvatzoglou M, Holzapfel K, Pickhard A, Löffelbein D, Santi I, Rummeny EJ, Ziegler S, Schwaiger M, Nekolla SG, Beer AJ. Value of a Dixon-based MR/PET attenuation correction sequence for the localization and evaluation of PET-positive lesions. Eur J Nucl Med Mol Imaging. 2011 Sep;38(9):1691-701. Epub 2011 Jun 18.

18 Delso G, Martinez-Möller A, Bundschuh RA, Ladebeck R, Candidus Y, Faul D, Ziegler SI. Evaluation of the attenuation properties of MR equipment for its use in a whole-body PET/MR scanner. Phys Med Biol. 2010 Aug 7;55(15):4361-74. Epub 2010 Jul 20.

Contact
Assoc. Professor Nina Schwenzer, M.D.
University of Tübingen
Department of Diagnostic and Interventional Radiology
Hoppe-Seyler-Straße 3
72076 Tübingen
Germany
nina.schwenzer@med.uni-tuebingen.de

Clinical Experience with Simultaneous MR-PET Acquisition: Developing Optimal Protocols for Anatomically Focused and Whole-Body Examinations

Kathryn Fowler, M.D.[1]; Farrokh Dehdashti, M.D.[1]; Tammie L.S. Benzinger, M.D., Ph.D.[1]; Michelle Miller-Thomas, M.D.[1]; Jonathan McConathy, M.D., Ph.D.[1]; Matthew Parsons, M.D.[1]; Vilaas Shetty, M.D.[1]; Constantine Raptis, M.D.[1]; Perry Grigsby, M.D.[1]; Pamela K. Woodard, M.D.[1]; Richard Laforest, Ph.D.[1]; Robert J. Gropler, M.D.[1]; Vamsi Narra, M.D.[1]; Barry A. Siegel, M.D.[1]; John Kotyk, Ph.D.[1]; Agus Priatna, Ph.D.[2]; Robert McKinstry, M.D., Ph.D.[1]

[1]Mallinckrodt Institute of Radiology, Washington University School of Medicine, St Louis, MO, USA
[2]R&D Collaborations, Siemens Healthcare, St Louis, MO, USA

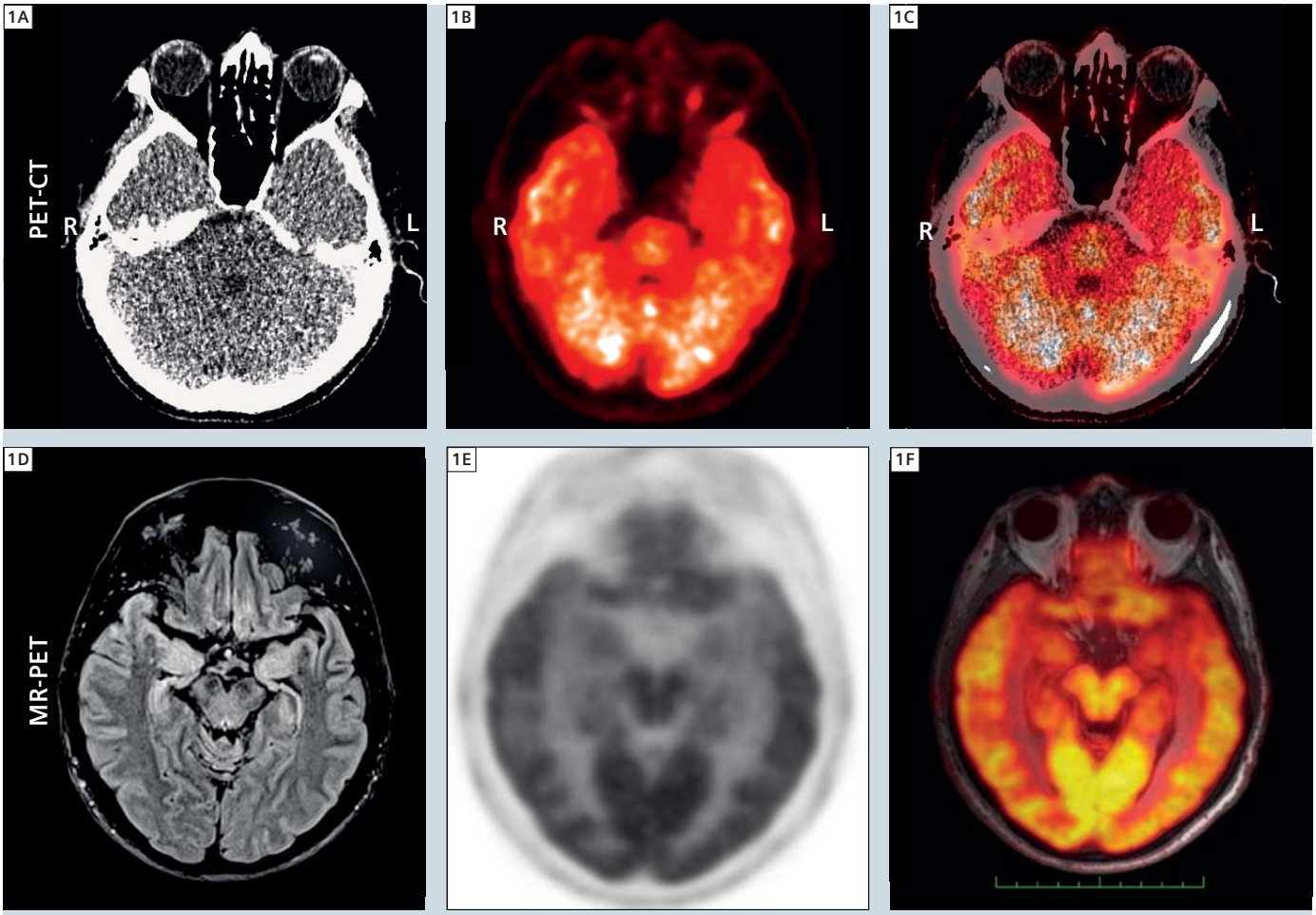

1 65-year-old male with a 1-year history of memory loss and episodic acute confusion; brain MRI demonstrated possible bilateral temporal lobe hyper intensity on FLAIR, without associated volume loss. FDG PET recommended for further evaluation. **(1A–C)** conventional FDG PET/CT shown: **(1A)** low-dose CT for attenuation correction, **(1B)** FDG PET, **(1C)** image fusion; **(1D–F)** simultaneous MR/PET of the same patient: **(1D)** FLAIR, **(1E)** FDG PET data, **(1F)** overlay of metabolic information.

Introduction

The new Biograph mMR offers simultaneous acquisition of PET and MR imaging data of potential added benefit in oncologic, neurological and other medical imaging [1–3]. The inherent benefit of the simultaneous acquisition is improved registration allowing optimal localization of PET findings to anatomic imaging and shortened overall imaging times through acquisition of PET and MRI in a single session. The purpose of this article is to present initial clinical experience with development of neurological protocols, anatomically focused MR-PET imaging protocols of body organs, including pelvic, thoracic, and liver oncologic imaging, and cardiac imaging experience. Initial experience, validation with PET-CT, challenges, and insights into protocol development are presented through representative examples.

Methods

Following IRB approval, patients scheduled for standard of care clinical FDG-PET-CT were recruited and consented for additional MR-PET imaging. The simultaneous MR-PET imaging was acquired on a Biograph mMR system recently installed in the Center for Clinical Imaging Research (CCIR) at Washington University School of Medicine, with total imaging matrix, with attenuation body array and spine matrix coils. By incorporating Avalanche Photodiodes (APDs) into the bore of a 3T magnet, the Biograph mMR system fully integrates the acquisition of state-of-the-art PET and MR images. Attenuation correction imaging was performed utilizing a dual echo VIBE Dixon sequence that separates water and fat with TE1/TE2 1.23 msec / 2.46 msec, TR 3.6 msec, left-right field-of-view (FOV) 500 mm and anterior-posterior FOV 300 mm. The acquisitions were performed in either a single station or a multiple station mode as indicated. Depending on the applications, PET images were simultaneously acquired with the anatomical sequences

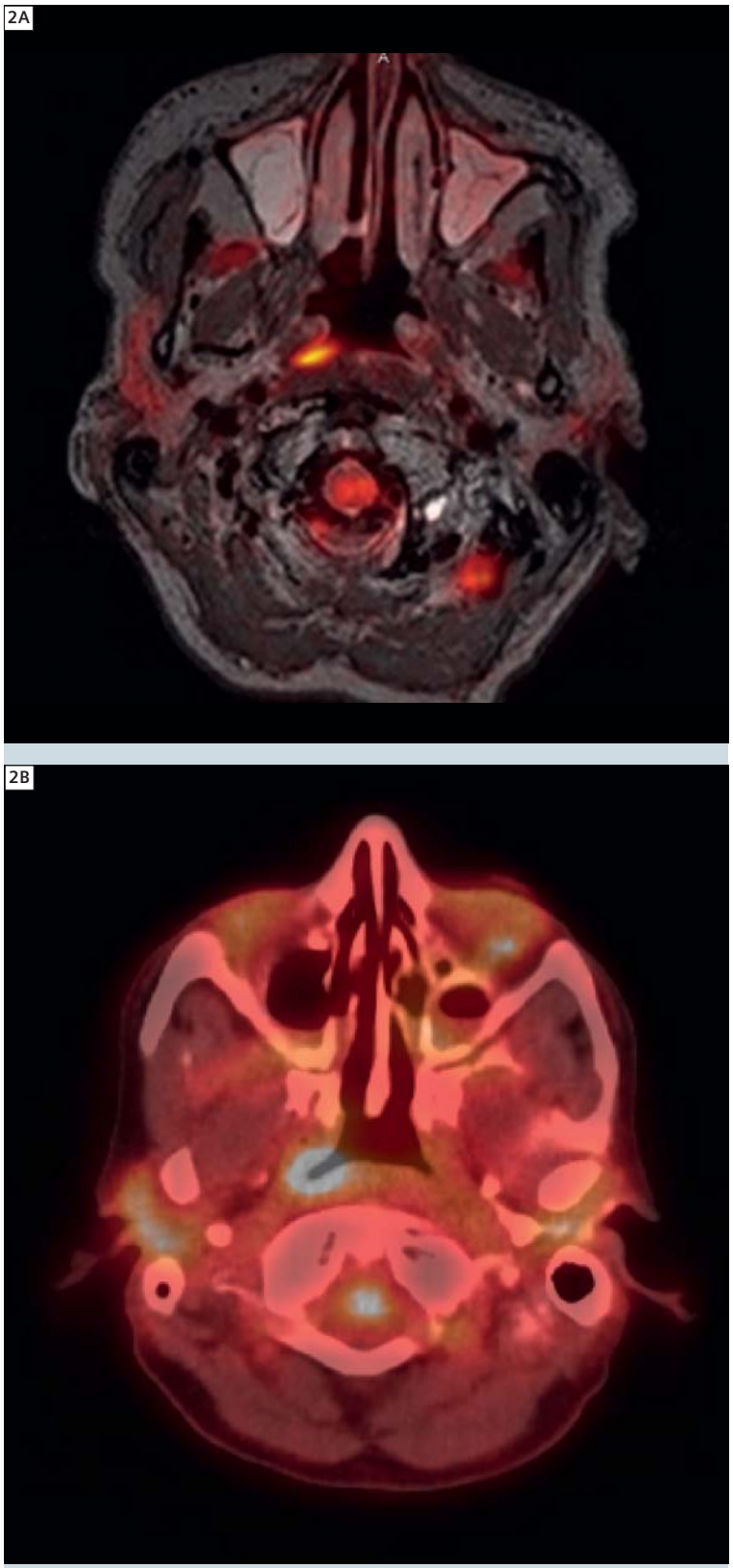

2 Poorly differentiated nasopharyngeal carcinoma with bilateral cervical nodal (and liver) metastases is shown. Simultaneous MR-PET demonstrated excellent MR image quality and excellent localization of FDG uptake. **(2A)** FDG PET overplayed on T1w **(2B)** corresponding PET/CT exam.

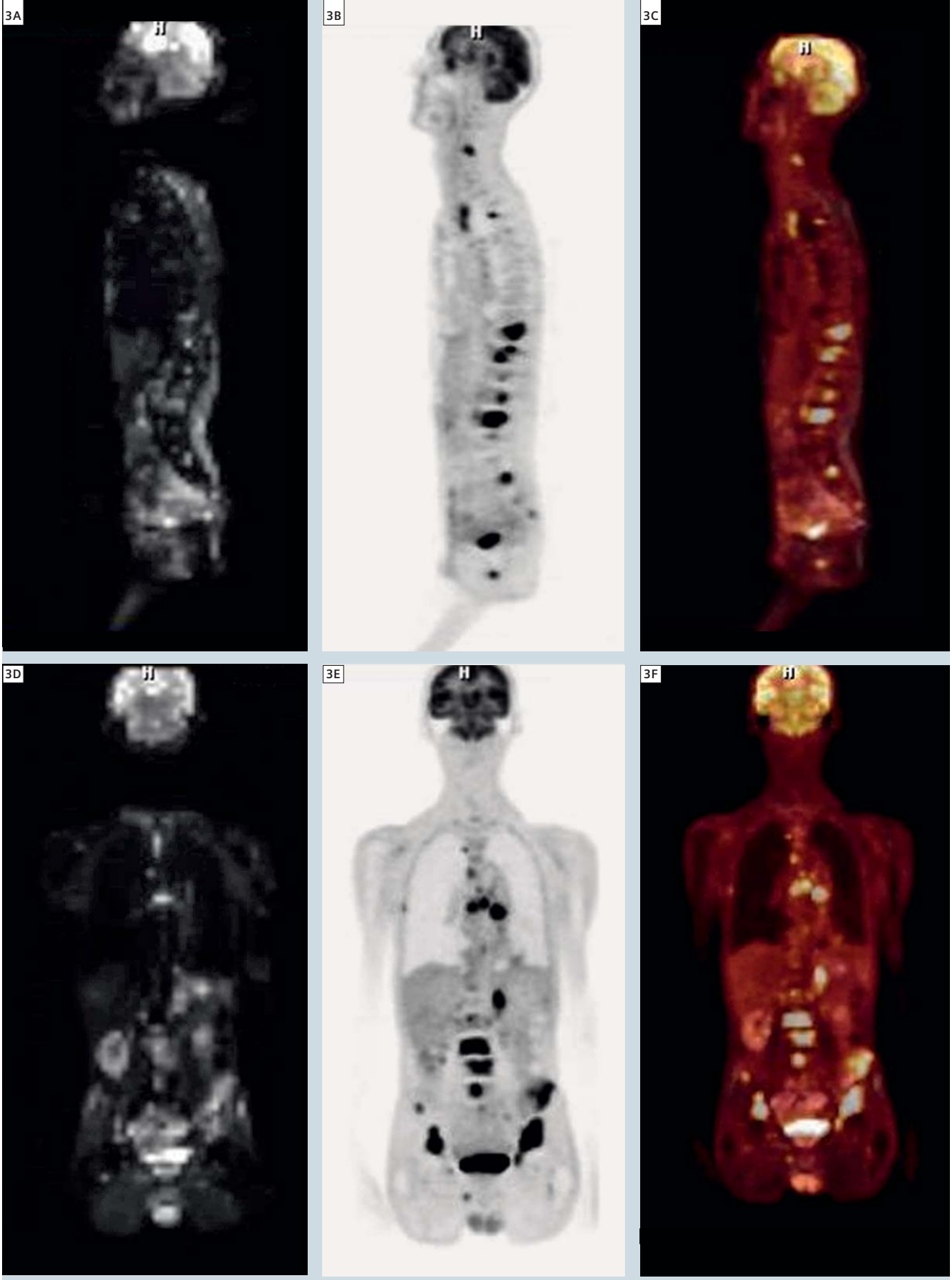

3A–F Patient with metastatic lung cancer; primary tumor is present in the left lower lobe (see arrow in **3H**). Metastatic disease is shown in the mediastinum (lymph nodes), spine, and bony pelvis (osseous metastases). MR images include a STIR acquisition as well as diffusion-weighted imaging. Sagittal reconstructions: **(3A)** DWI, **(3B)** PET, **(3C)** MR/PET fused to DWI; coronal reconstructions: **(3D)** DWI, **(3E)** PET, **(3F)** MR/PET fused to DWI.

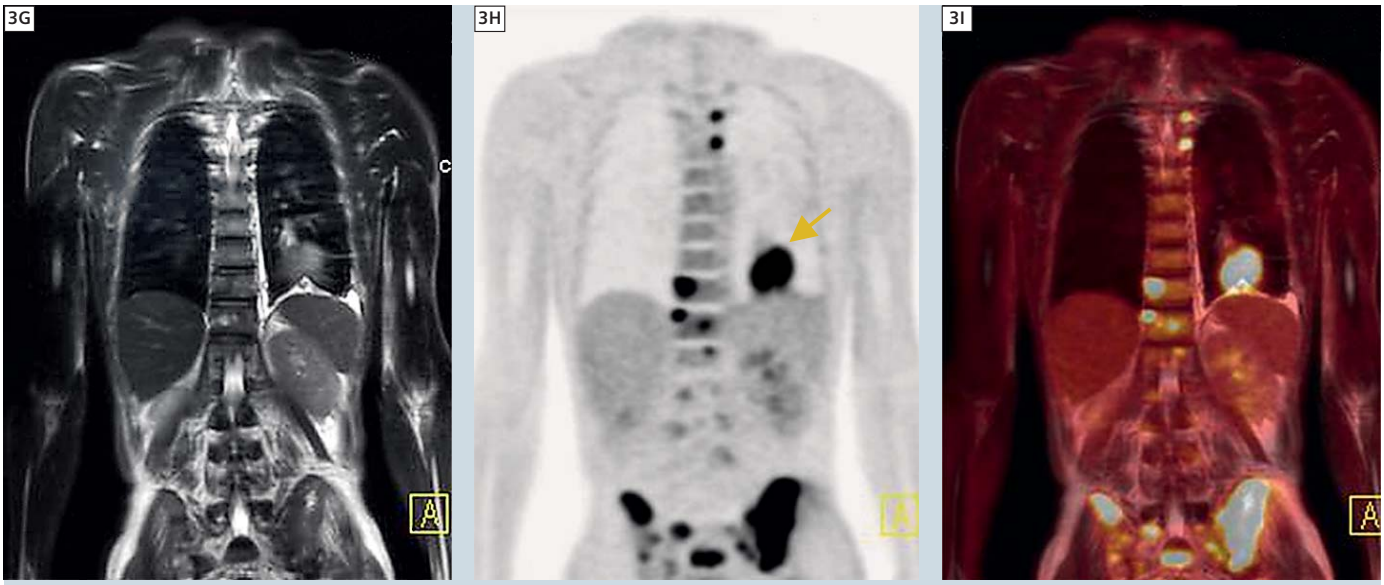

3G–I **(3G)** Coronal T2w HASTE for morphology, **(3H)** corresponding PET MPR, **(3I)** image overlay of PET and HASTE.

from MR such as HASTE for whole-body acquisition, MPRAGE for brain imaging, SPACE or HASTE for pelvic application, or delayed enhancement for cardiac imaging. Additional examinations using high-resolution MR were added for the focused examination such as high resolution T2 TSE, diffusion-weighted imaging or diffusion tensor imaging (DTI) and other sequences depending on the applications.

Clinical cases

The following are some examples of the clinical cases acquired for anatomically focused and whole-body examinations with the Biograph mMR.

Brain imaging

Although fusion of separately acquired brain MR and FDG-PET is readily available with offline software tools, a combined examination can allow for streamlined patient care and potentially improved diagnostic specificity, as illustrated by this case. A 65-year-old male with a 1-year history of memory loss and episodic confusion presented for workup at our institution (Fig. 1). A clinical MRI was interpreted as normal; however, there was a question of subtle FLAIR hyperintensity in the mesial temporal lobes. FDG-PET was recommended for further correlation of the MR findings and clinical presentation. The PET acquisition was acquired simultaneously with MRI. Brain MRI shows subtle bilateral mesial temporal lobe hyperintensity on FLAIR. FDG-PET shows mild bilateral mesial temporal lobe hypometabolism. Further clinical workup was then ordered which generated a final diagnosis of limbic encephalitis with voltage-gated potassium channel antibodies (VGKC). In this case, subtle findings on PET and MR performed independently, could be simultaneously reviewed and confirmed with PET/MR, leading to diagnostic confidence and initiation of the correct pathologic workup.

Head and neck oncology

Simultaneous head and neck MR-PET performs well compared with PET-CT in our initial experience. In the head and neck, MR-PET combines the metabolic and biochemical information from PET with high spatial resolution, anatomic localization, and soft tissue contrast from MR. The advantages of MR imaging in oral cavity and skull base neoplasms, the superior ability of MR to detect perineural spread of tumor, and improved coregistration of PET imaging with MR imaging during simultaneous acquisition make this a promising new technology for staging and follow-up of select head and neck neoplasms.

Patient is a 51-year-old woman with poorly differentiated nasopharyngeal carcinoma with bilateral cervical nodal and liver metastases. Simultaneous MR-PET demonstrated excellent MR image quality and excellent localization of FDG uptake. MR provided superior soft tissue resolution in the nasopharynx compared

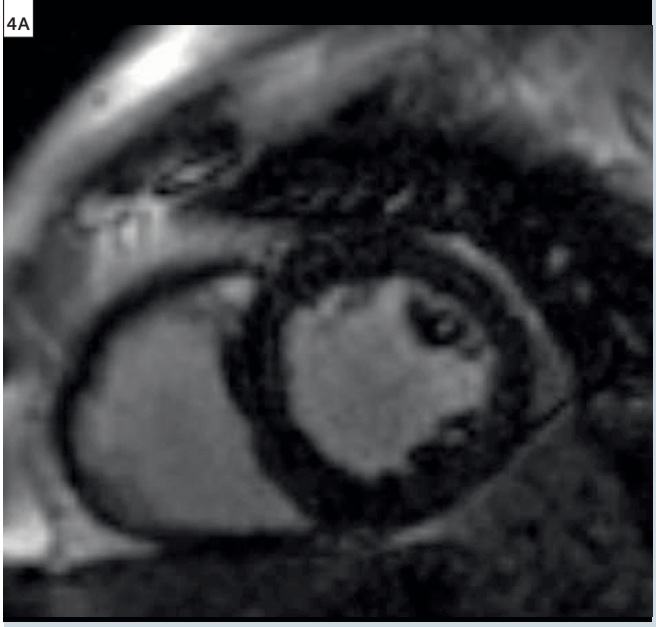

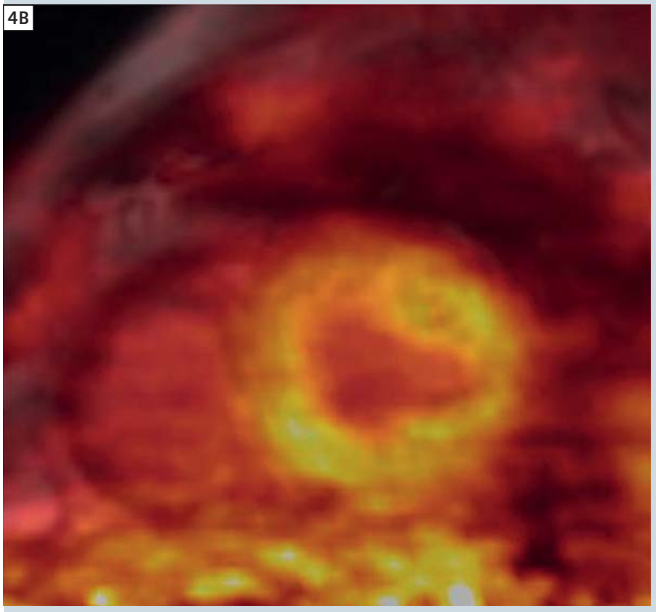

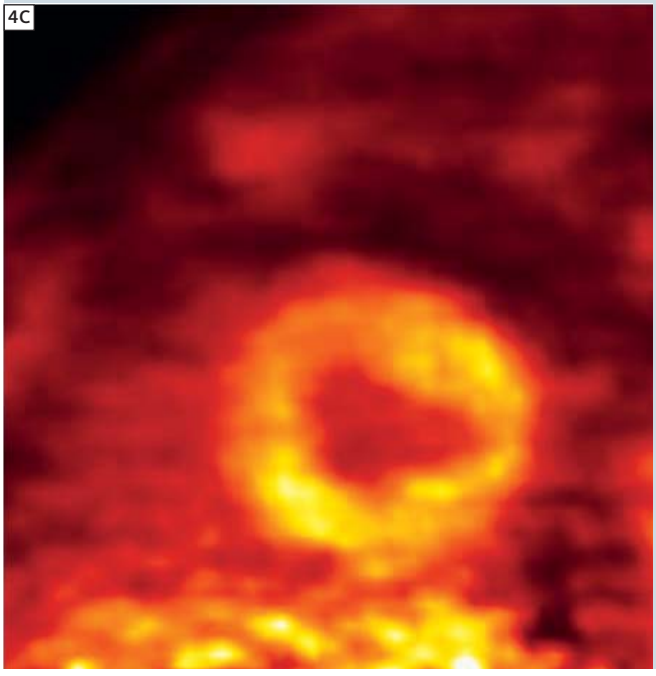

4A Simultaneous acquisition of ECG-gated PET and delayed contrast enhanced (DCE) cardiac MR images (simultaneous acquisition of MR 2-point Dixon also acquired for AC). PET data acquired in list mode and binned. DCE MR images acquired in diastole are fused with diastolic PET data to create the center image. Patient has a normal heart. **(4A)** MRI, **(4B)** fused MR/PET, **(4C)** FDG PET.

to PET-CT. Lesion detection based on FDG uptake on the MR-PET was equivalent to PET-CT in this case (Fig. 2).

Lung cancer with metastatic disease

While MRI can be used in the assessment of lung cancer, it has typically been reserved for specific cases in which CT and PET-CT, the first-line modalities for the assessment of lung cancer patients, are not able to answer a specific question, such as whether a lesion is invading the chest wall or a vascular structure. One of the key reasons for the secondary role for MRI is the fact that whole-body MR imaging is cumbersome and time consuming, thus preventing assessment of the full extent of disease. MR-PET for lung cancer has the potential to foster the development of new imaging protocols that allow for detailed assessment of the primary tumor while still providing the information regarding more distant metastatic disease. In addition, simultaneously acquired diffusion MR and PET data may prove useful both in the initial evaluation of tumors as well as in follow up after treatment.
Figure 3 shows a 50-year-old man with metastatic lung cancer. Primary lesion is present in the left lower lobe. Metastatic disease is shown in the mediastinal lymph nodes, spine, and bony pelvis. MR images include a HASTE acquisition as well as diffusion-weighted image obtained at a b-value of 600.

Cardiac imaging

Cardiac MR-PET imaging has the potential to play a role both in cardiac ischemia and viability assessment. Potential clinical protocols include stable chest pain assessment, playing on the strengths of both modalities, performing MR cine cardiac function assessment, ^{13}N-ammonia or rubidium-82 PET myocardial perfusion and delayed contrast-enhanced inversion recovery infarct imaging in a single examination. Combined FDG and delayed contrast-enhanced inversion recovery cardiac

imaging may play a role in co-localized, simultaneously acquired functional and anatomic viability assessment that, theoretically, could play a role in imaging-directed ventricular tachycardia radiofrequency ablation or direct biventricular pacing in dyssynchrony.
A 68-year-old man injected with FDG for oncologic imaging was recruited immediately after his whole-body PET-CT examination to undergo a cardiac MR-PET imaging for protocol development (Fig. 4). Simultaneous acquisition of ECG-gated PET and delayed contrast-enhanced (DCE) cardiac MR images (simultaneous acquisition of MR 2-point Dixon also acquired for AC) allow for precise fusion of imaging. PET data was acquired in list mode, binned and reconstructed into 3 phases. DCE MR images acquired in diastole are fused with diastolic PET data to create the center image (Fig. 4B). This patient has a normal heart.

Cervical and vulvar cancers
PET-CT and MRI are established modalities in initial staging and monitoring treatment response in patients with cervical cancer and other pelvic malignancies. PET can provide estimated tumor volumes for treatment planning and diagnosis of nodal metastases. High resolution MR imaging of the pelvis can detect parametrial spread of tumor, an essential feature in determining surgical resectability. The combination of metabolic information derived from PET with high resolution MR imaging of the pelvis shows promise in both clinical management and potential research opportunities in correlating functional MRI with tumor metabolism.
Given the complex anatomy of the pelvis, high resolution T2-weighted imaging is best performed utilizing a 3D isotropic dataset, such as SPACE. Isotropic acquisition allows for infinite multiplanar reformations without loss of resolution. Diffusion-weighted imaging, pre- and dynamic post-contrast volumetric interpolated breath-held examination (VIBE), and inversion recovery T2 fat suppressed images complete a diagnostic MR examination of the pelvis providing additional staging information regarding local invasion, tumor size, and regional metastases.
Figure 5 shows a 47-year-old woman with biopsy-proven cervical cancer. Given the large size of the patient's cervical malignancy and presence of metabolically active nodal metastases, the patient subsequently underwent radiation therapy.
Figure 6 is a 31-year-old woman with vulvar carcinoma. A small focus of residual tumor within the pelvis could be missed on MR imaging alone and is in a difficult location with PET alone given the potential for contamination in this

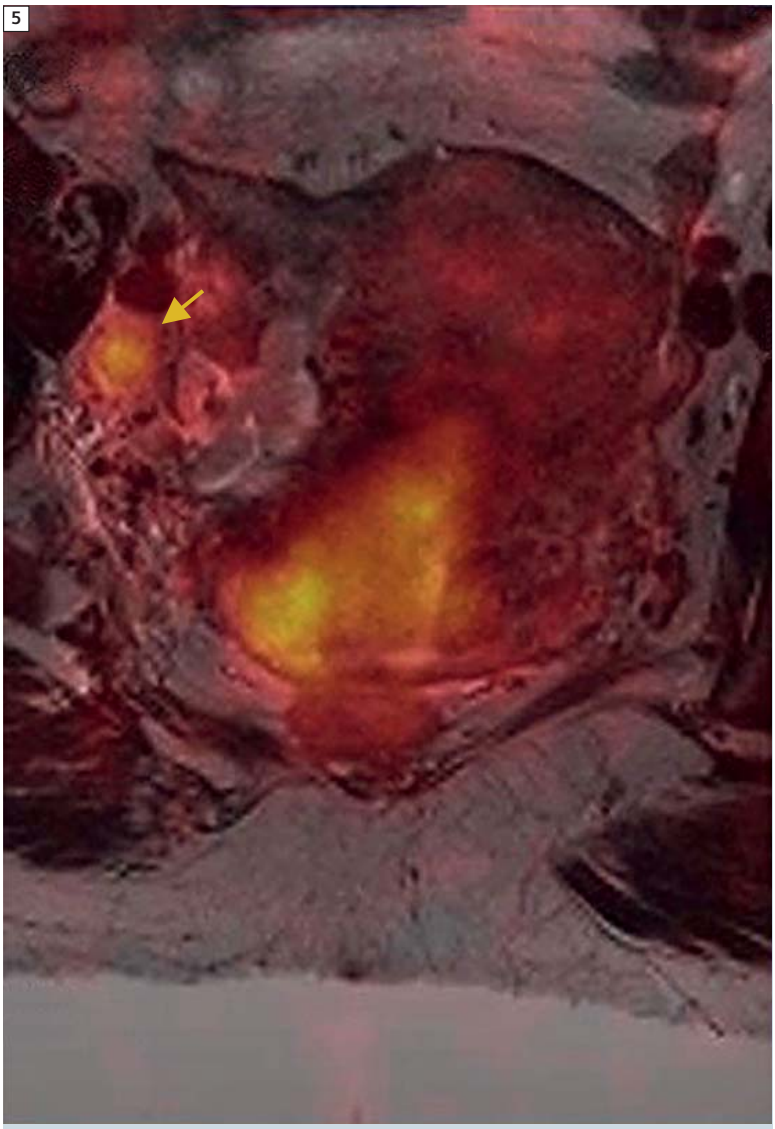

5 Primary cervical cancer and involved adjacent right external iliac lymph node (arrow); overlay of PET on T2 TSE is shown.

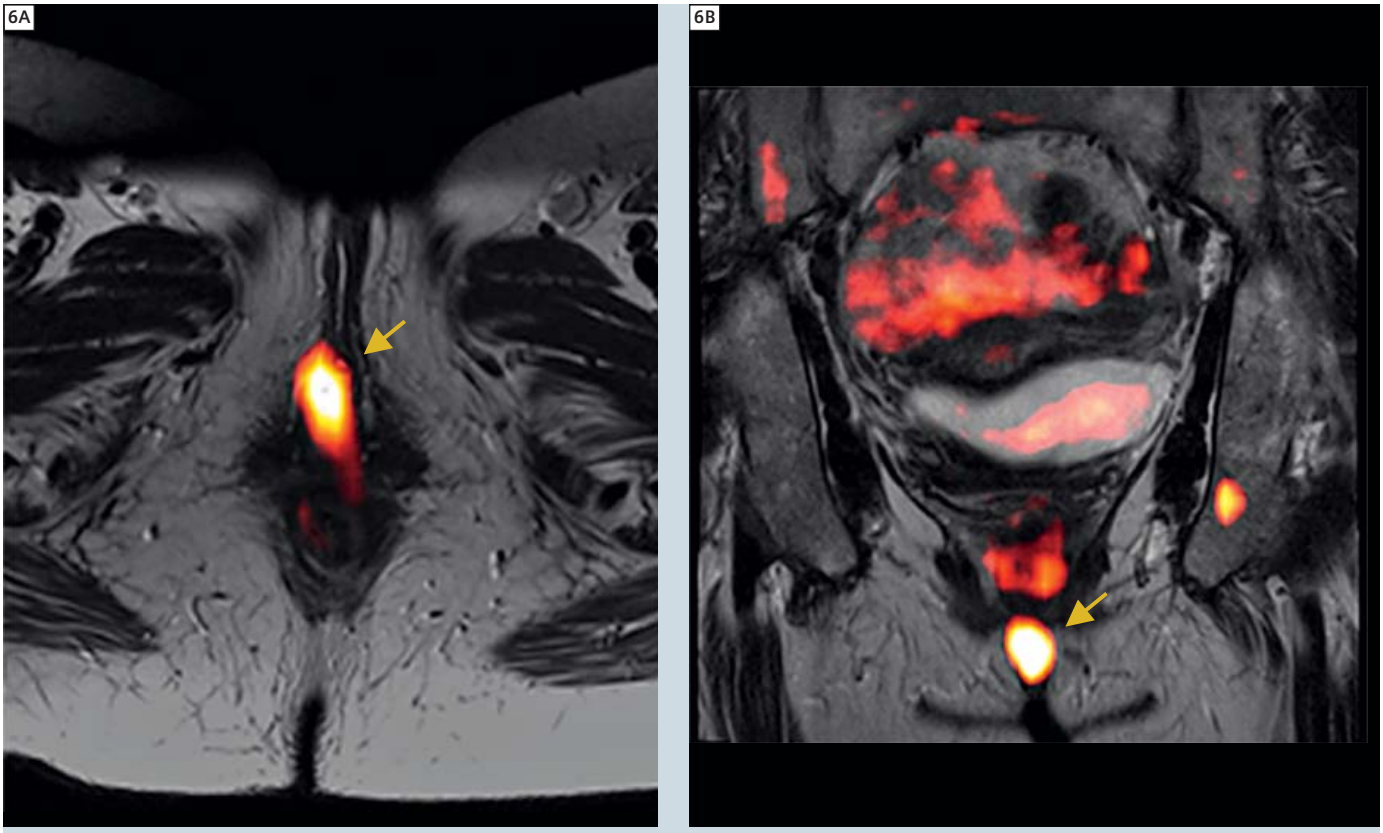

6 Patient with vulvar cancer; small focus of residual tumor within the pelvis could be missed on MR imaging alone. FDG PET overlay on transversal **(6A)** and coronal **(6B)** T2w TSE is shown.

location from urine activity. The combination of MR-PET; however, nicely demonstrates the metabolically active soft tissue lesion.

Discussion

MR-PET shows promise as a new oncologic imaging modality with inherent improved soft tissue contrast over CT, lower radiation dose, and potential for better correlation of PET findings to anatomy given the simultaneous acquisition. Several challenges are evident in developing optimal protocols, including optimal MR sequence parameters, motion correction, and validation of semiquantitative analysis using standardized uptake value (SUV) using MR attenuation correction. In some cases, the combination of PET SUV and MR ADC values may prove more specific in differentiating tumor from surrounding tissue than subjective assessment alone. Potential for benefit from simultaneous MR-PET acquisition also exists in receptor-targeted oncologic imaging, dementia assessment, and cardiac and atherosclerosis imaging.

Acknowledgement

Jennifer Frye, Glenn Foster, Linda Becker, Deb Hewing, Mike Harrod, Tim Street, Betsy Thomas

References

1 Pichler BJ, Judenhofer MS, Wehrl HF. Eur Radiol. 2008; 18:1077-86.
2 Antoch G, Bockisch A. Eur J Nucl Med Mol Imag. 2009; 36 Suppl 1:S113-20.
3 Wehrl HF, Sauter AW et al. Technol Cancer Res Treat. 2010;9:5-20.

Contact
Professor Pamela K. Woodard, M.D.
Washington University
Mallinckrodt Institute of Radiology
510 S. Kingshighway Blvd.
St. Louis, MO, 63110-1076
USA
Phone +1 314-362-7697
woodardp@mir.wustl.edu

Case Report: Combining [18F] PET with MR for Detection of Bone Metastases in One Simultaneous Examination

Markus Lentschig, M.D.; Christiane Franzius, M.D.

ZEMODI, Zentrum für Moderne Diagnostik, Bremen, Germany

Background

In nuclear medicine, bone scanning is based on the principle of scintigraphy using bone-seeking radiopharmaceuticals. [99mTc] (or [99Mo]) -labelled polyphosphonates are used as tracers for this purpose. They accumulate in sites of increased bone formation; metastases are detected either by increased uptake of the lesion itself (osteoplastic), as reaction of the surrounding healthy bone matrix or as defect (osteolytic).
Bone scintigraphy has found its way into several clinical guidelines over the last decades and is a standard procedure in the evaluation of bone metastases. However, degenerative changes of bones are challenging to diagnose accurately especially in elderly patients. The low sensitivity of scintigraphy for (small) osteolytic lesions often requires complimentary imaging, either X-ray, computed tomography (CT) or – especially in case of bone tumors and bone marrow involvement – magnetic resonance imaging (MRI). It has to be stated that bone scintigraphy is also associated with poor spatial resolution and as a consequence of the imaging mechanism itself this method has limited diagnostic specificity for lesion characterization and an insufficient sensitivity for bone marrow diseases.
Positron emission tomography (PET) using [18F]-fluoride has already demonstrated to be a clinically useful alternative to traditional bone scintigraphy. Interestingly, [18F] was initially replaced by [99mTc]-labelled polyphosphonates as osteotropic tracer. But with the development of modern PET/CT technology, the advantages over traditional bone scintigraphy are eminent; [18F] PET adds diagnostic information mainly by its superior resolution compared to scintigraphy and nowadays PET is routinely acquired as 3D data. In addition, CT used as input for attenuation correction helps to characterize suspicious bone modelling. Also it should be kept in mind that from a patient perspective, [18F] PET/CT is considered to be the more convenient procedure (with special focus on preparation time and scan duration). Independent of its diagnostic advantages, the importance of [18F] PET has increased recently because of its importance as a substitute for conventional skeletal scintigraphy in a time with limited availability of [99Mo]/[99mTc]. To ensure healthcare, [18F] PET has now become part of common outpatient care [1–5]. Within the last decade, MRI has also increasingly challenged the clinical value of bone scintigraphy with superior diagnostic performance. The potential to assess not only changes of the bone but especially of the bone marrow and soft

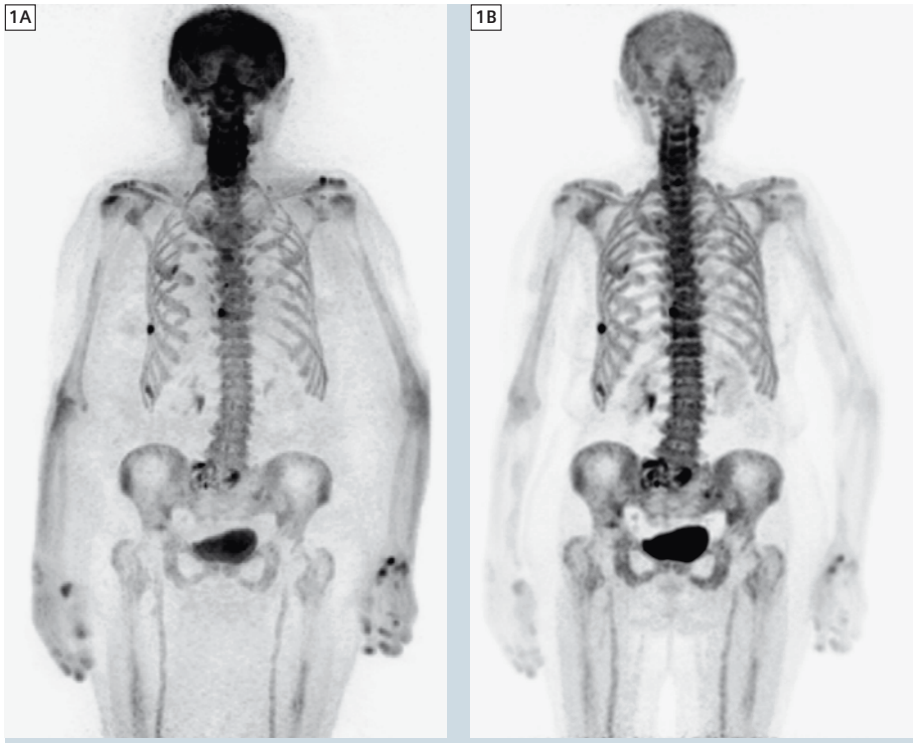

1 Maximum intensity projection (MIP) of the [18F] PET data **(1A)** uncorrected and **(1B)** after attenuation correction (MR based).

tissue in general at highest sensitivity can add important information and have a clear impact on patient care. This is already proven for dedicated patient cohorts. In combination with the advent of multi-regional MRI and further advances in MR technology, diffusion-weighted imaging (DWI) is used more and more routinely to add functional information to MRI. The images derived from such an exam show PET-like appearance; however, the underlying mechanism is restriction of water motion. How DWI will add further diagnostic accuracy in the detection of bone metastases and especially therapy follow-up is still subject of debate but its potential is more than evident [6–11].

Combining [^{18}F] PET and MRI for evaluation of bone processes is therefore appealing but was only available in a small number of very selected cases up to now. One practical reason is the associated effort for conducting, synchronizing (time and indication wise) and reading two complex exams (this is especially true for MRI, where a standard whole-body scan produces more than 1000 images which have to be read). In addition, fusion techniques, which are often used to assist in this task, are of limited value especially for scans covering a larger volume simply because of different positions of the bones between the two examinations. The limitation of two separate exams can only partially be overcome by positioning aids (with all their associated disadvantages). It can, however, be overcome by using hybrid MR/PET systems (with the advantage to perform only one scan). Much has been written about the need and the technology behind this new hybrid imaging modality (see also the most recent issues of MAGNETOM Flash). It should be pointed out that simultaneous MR and PET imaging also has advantages in clinical routine over a sequential approach – not only from a workflow aspect.

A very obvious aspect is that it clearly improves spatial registration between metabolic and morphological information by reducing the time gap between the acquisition of MR and PET. This is a clear advantage not only in imaging the pelvis, bowel, lung and liver, but also in patients with limited capability for holding still in one position over a longer time period. Also it should be mentioned that there are no limitations in the performance of the individual imaging methods of such a combined simultaneous MR/PET system. Hybrid MR/PET systems rely on segmentation algorithms for providing the input function of the attenuation correction. At this point in time, bone segmentation is available only for dedicated areas like the skull base and not yet integrated in whole-body scanning. Nevertheless, based on existing data and experience, the need for bone segmentation can be negated in a clinical setting especially when a qualitative reading of PET is performed. The need for quantification of PET is unquestioned for follow-up exams and, so far, the introduced error as compared to a standard PET/CT (which has also a certain level of confidence only) seems to be negligible even for longitudinal studies – if performed with an MR/PET system. Nevertheless, the advent of this technology has reminded us that the discussion about the accuracy of PET quantification is of high importance and far from concluded (which is also true for the comparability of results acquired with different PET/CT systems).

The diagnostic capabilities of MR and PET alone and in combination are of course dependent on the underlying pathology and the applied MR imaging methods and tracers. [12–15]

Case report

Patient history and sequence details

A 91-year-old female with severe sacral pain was referred to our institution for a bone scan with [^{18}F] as substitute to bone scintigraphy. The patient was diagnosed in 1986 with beast cancer and in 2004 a malignoma of the uterus was treated. Application of [^{18}F] was performed according to guidelines. MR/PET was conducted as a multi-step exam covering the whole body. During simultaneous PET acquisition, a coronal T1w TSE (512 matrix, 450 mm FOV, 5 mm SL) and T2w STIR (384 matrix, 450 FOV, 5 mm SL) was acquired. In addition, a transversal DWI was measured (b-values 50, 400, 800 s/mm^2, spectral fat saturation, 192 matrix, 5 mm SL; inline ADC calculation). All images shown were acquired using Biograph mMR (Siemens Healthcare, Erlangen, Germany) and a combination of the head/neck, spine and body coils.

Imaging findings

A large osteolytic lesion is shown within the sacral bone (massa lateralis). A clear mismatch between lesion size and corresponding bone formation is obvious. In addition, tumor-suspicious bone formation with corresponding lytic aspect in MRI is demonstrated for the 10th and 7th right rib. Based on DWI, these lesions are characterized by high signal on the original b-value images and restriction of water diffusion. In addition, multiple degenerative bone formations without corresponding oedema in MRI are visualized: spondylosis of the thoracic spine and coxarthrosis of the right hip are the most obvious ones. Focal uptake is also seen in the dorsal processus of the 6th and 7th cervical vertebra. Based on T2w STIR images at least for the bone formation of the 7th vertebra a corresponding hyperintense lesion with space occupying aspects at least on the coronal original orientation can be shown. Often reactive oedema can be seen also in degenerative findings, however, based on the space occupying appearance further manifestation of the bone metastases

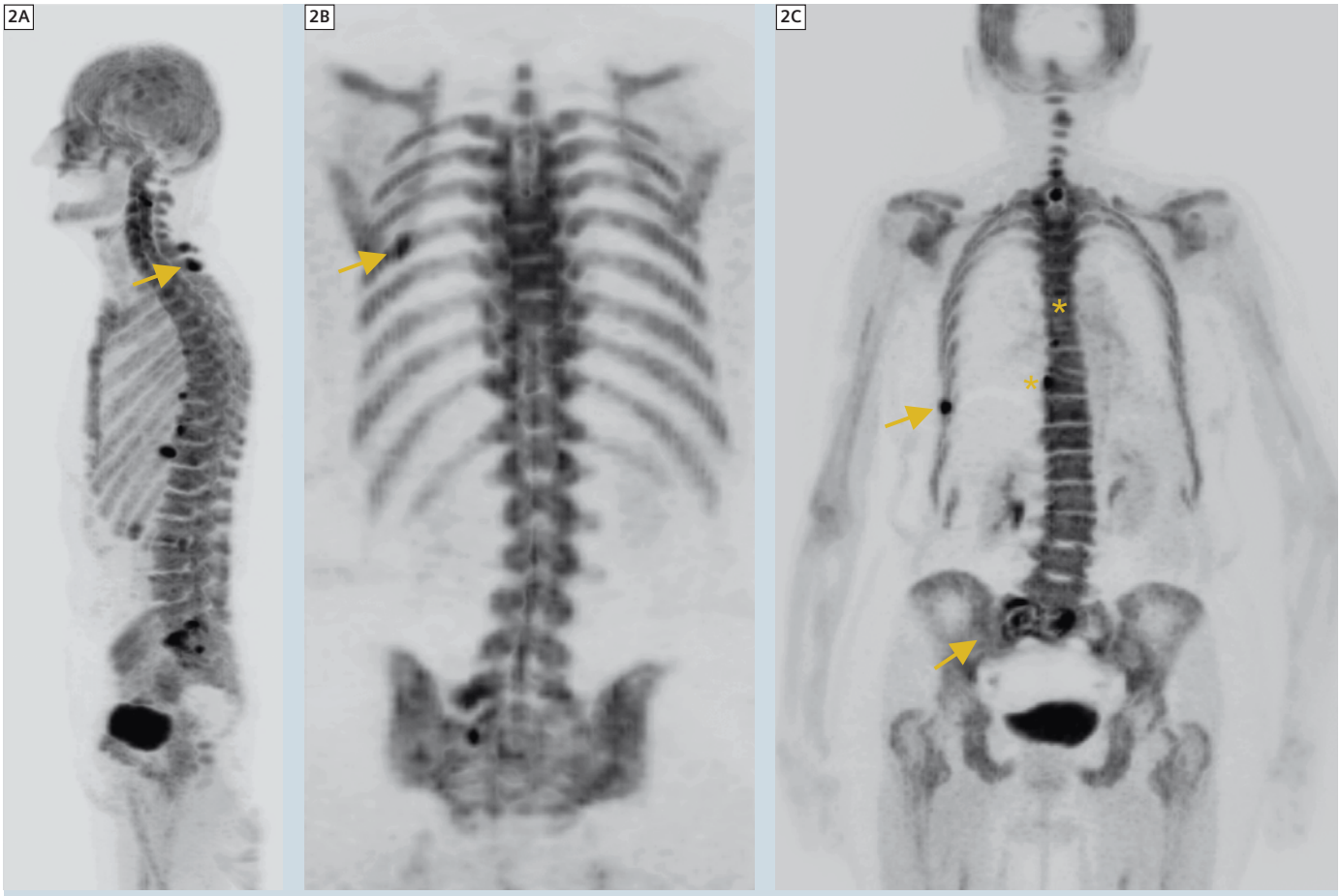

2 Sagittal MIP **(2A)**, coronal **(2B)**, thick-slice MIP **(2C)** showing pathologic bone formation within the os sacrum and the 10th and 7th right rib as well as the 7th / 6th cervical vertebra (dorsal processus) (arrows). In addition, multiple degenerative bone formation can be seen (e.g. spondylosis of the thoracic spine; asterisk).

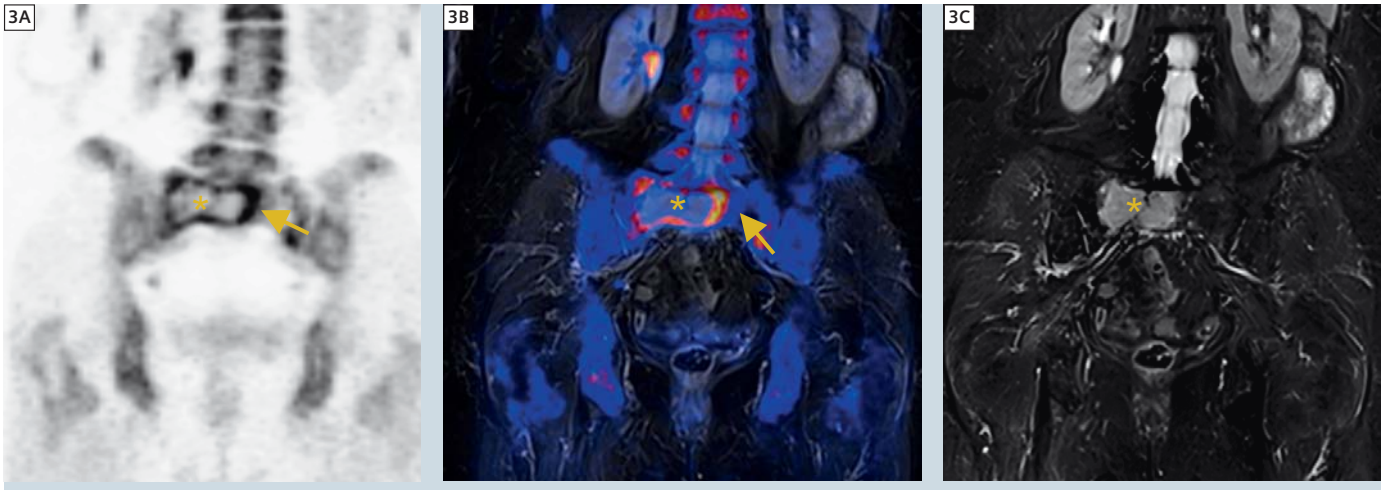

3 Clear mismatch between bone formation (arrows) and true extend of the metastasis (asterisk) in the massa lateralis of the os sacrum is shown. Coronal multiplanar reconstruction (MPR) of the [18F] PET **(3A)**, overlay of metabolic information on MRI **(3B)**, corresponding coronal T1w TIRM **(3C)**.

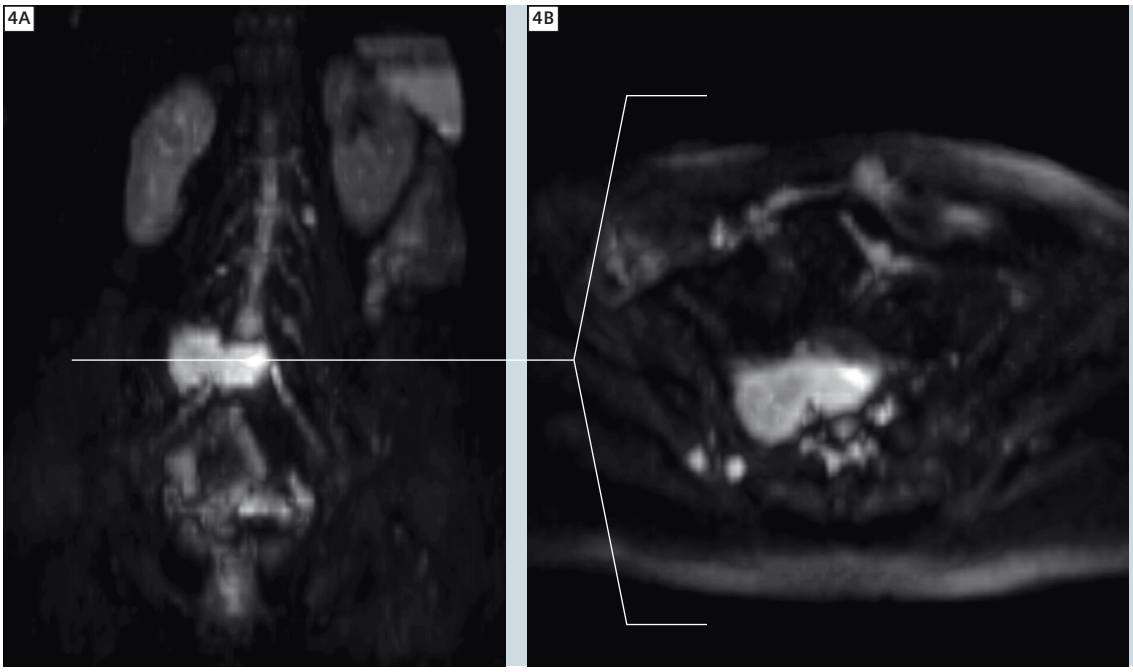

4 Thick-slice MPR based on the b = 800 s/mm² DWI images. By suppression of the background the tumor tissue is well delineated. ADC mapping (not shown) did proof restriction of water diffusion. Coronal **(4A)** and transversal **(4B)** reformation.

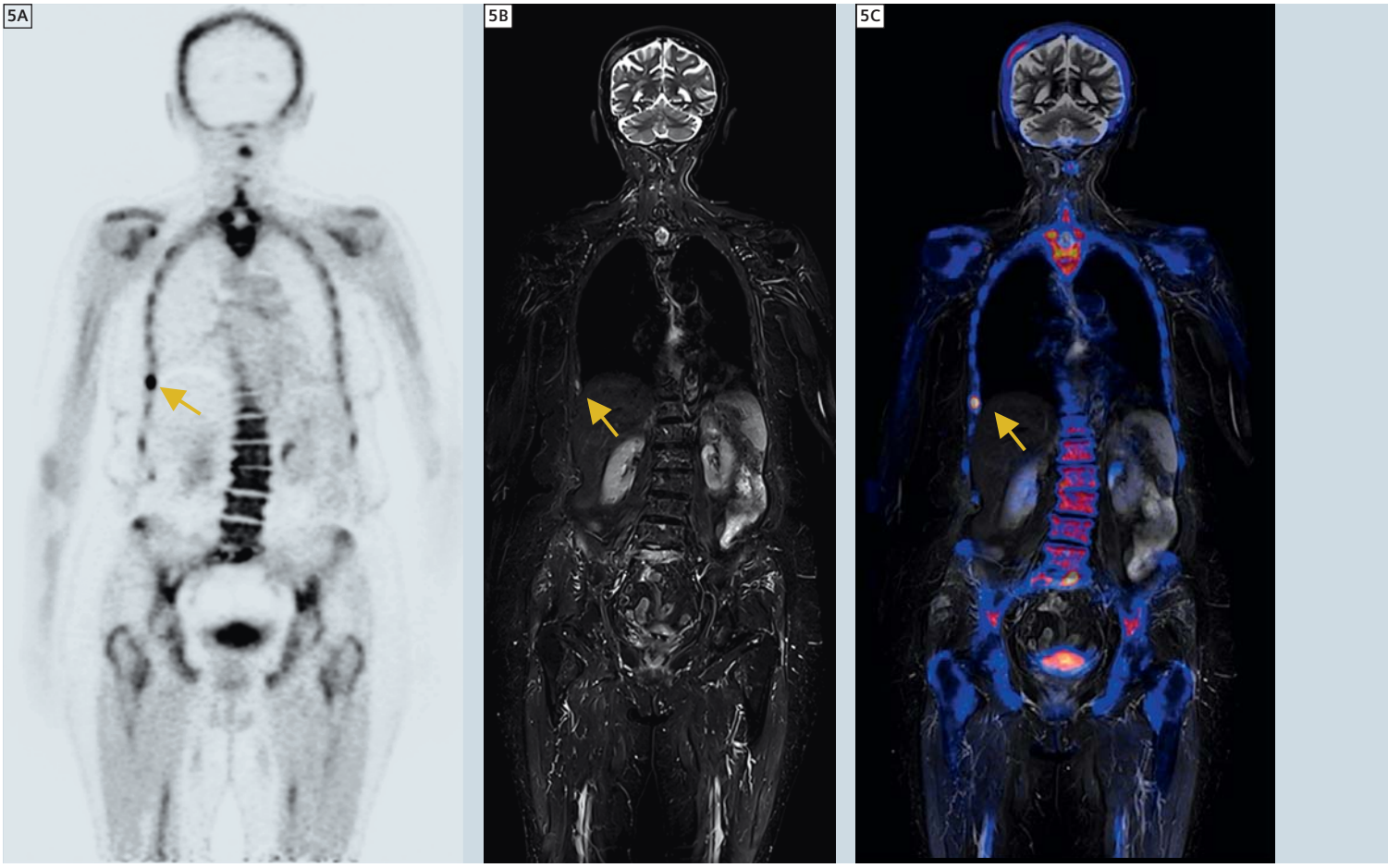

must be concluded. No evidence for further metastases within the long bones of the upper and lower (not shown) extremities, no fractures or soft tissue involvement, no spinal cord compression. The used protocol was mainly focused on the skeletal system, however, further tumor manifestations outside the bone (including lymph nodes) can be ruled out with sufficient diagnostic accuracy.

Diagnosis

Multifocal metastatic disease of the skeletal system has to be concluded. Based on imaging findings and patient history, a late metastatic manifestation of the mamma carcinoma seems to be the most plausible explanation. With increased numbers of successful treatment of the primary tumor and also in concordance with latest epidemiological data, tumor recurrence of mamma carcinoma after the 5-years follow-up interval has to be taken into account. However, a third tumor manifestation cannot be ruled out based only on imaging findings and missing presence of a potential primary tumor. Therefore the final conclusion of this exam has to be bone metastases of a cancer of unknown primary (CUP). Because of clinical presentation (severe pain), a therapy relevance is obvious but further diagnosis and therapy will be to be discussed in detail and based on a very individual decision as a consequence of the patients age and general condition.

Conclusion

Combining [^{18}F] PET and MRI in one simultaneous exam is appropriate when it comes to providing best patient care. Based on the knowledge with PET and MRI alone, it is more than justified in our opinion to state that this imaging method can be applied to a large cohort of patients. While the presented case may be a not so common clinical scenario for the future application of MR/PET, it clearly demonstrates the potential of this method as the most accurate method for evaluation of osseous and bone marrow processes. Especially in cases with suspicion of bone marrow involvement and for younger patients, simultaneous MR/PET will play an important role in the future. How far

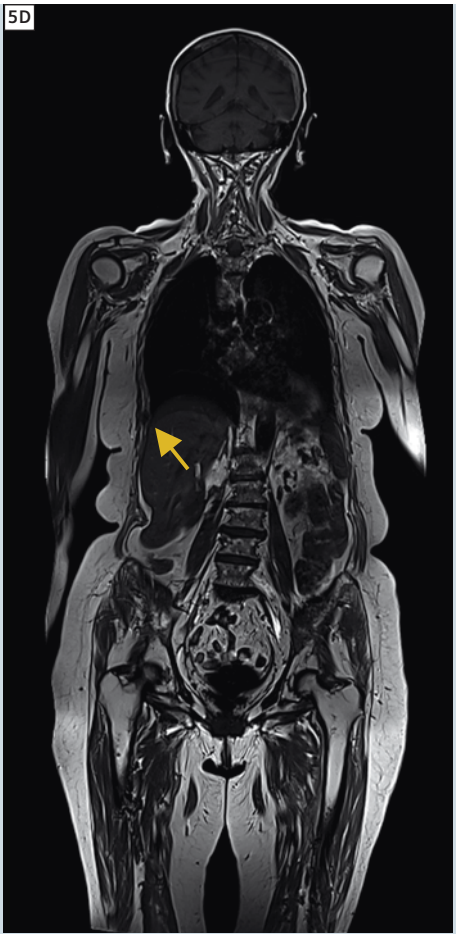

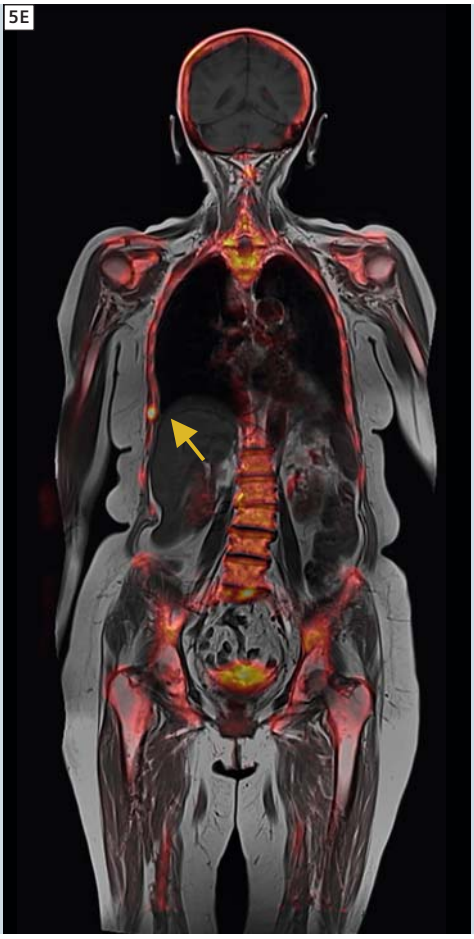

5 Excellent spatial registration between MRI and PET data is shown exemplary with the small osteolytic metastasis of the right lateral thoracic wall (10th rib). Coronal MPR of [^{18}F] PET **(5A)**, corresponding T2w TIMR **(5B)**, overlay of PET data on T2w TIRM **(5C)**, corresponding T1w TSE without **(5D)** and with **(5E)** overlay of PET information.

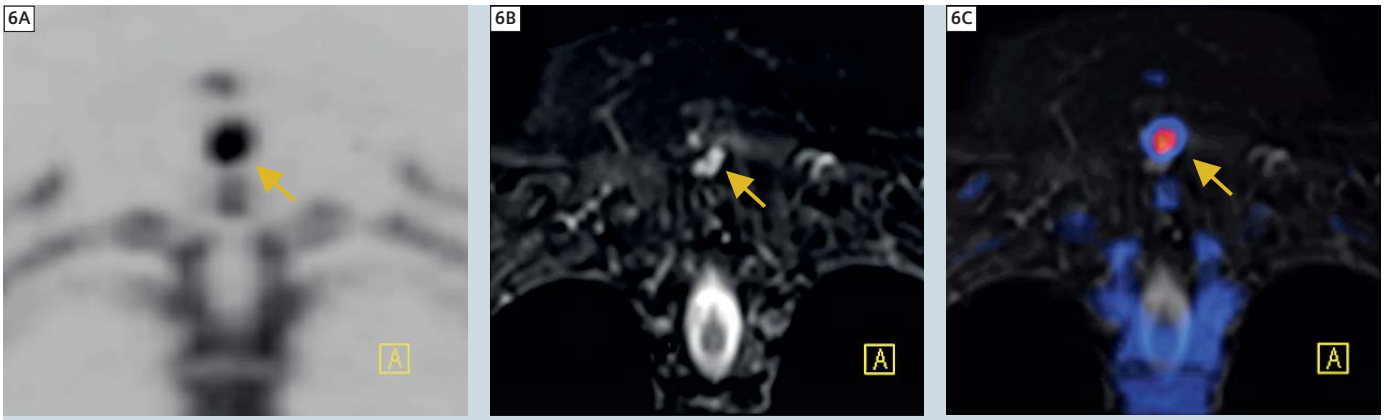

6 The pathologic bone formation of the 6th and especially 7th (coronal MPR of the PET is shown in **(6A)**) dorsal processus of the cervical vertebra has also to be rated as potentially metastastic. A space occupying lesion with similar imaging features as shown for the other metastases can be demonstrated on the coronal T2w TIRM MRI **(6B)**; the overly of the PET data **(6C)** shows a slight spatial mismatch of the two imaging modalities as a consequence of the different imaging mechanisms of [18F] PET (bone formation metabolism) and MRI (soft tissue characteristics).

this method will be added to, or will even replace, conventional imaging will of course be also a question of upcoming therapy options and tracers e.g. for evaluation of hormone receptor status. But certainly the presented combination of [18F] PET and MRI is already a further step towards a more accurate and patient-specific diagnoses and therapy selection – and all within one exam.

References

1 Cook GJ. PET and PET/CT imaging of skeletal metastases. Cancer Imaging. 2010 Jul 19;10:1-8.
2 Hellwig D, Krause BJ, Schirrmeister H, Freesmeyer M. [Bone scanning with sodium 18F-fluoride PET and PET/CT. German guideline Version 1.0.]. Nuklearmedizin. 2010;49(5):195-201. Epub 2010 Sep 13.
3 Hahn S, Heusner T, Kümmel S, Köninger A, Nagarajah J, Müller S, Boy C, Forsting M, Bockisch A, Antoch G, Stahl A. Comparison of FDG-PET/CT and bone scintigraphy for detection of bone metastases in breast cancer. Acta Radiol. 2011 Nov 1;52(9):1009-14. Epub 2011 Oct 3.
4 Withofs N, Grayet B, Tancredi T, Rorive A, Mella C, Giacomelli F, Mievis F, Aerts J, Waltregny D, Jerusalem G, Hustinx R. 18F-fluoride PET/CT for assessing bone involvement in prostate and breast cancers. Nucl Med Commun. 2011 Mar;32(3):168-76.
5 Yen RF, Chen CY, Cheng MF, Wu YW, Shiau YC, Wu K, Hong RL, Yu CJ, Wang KL, Yang RS. The diagnostic and prognostic effectiveness of F-18 sodium fluoride PET-CT in detecting bone metastases for hepatocellular carcinoma patients. Nucl Med Commun. 2010 Jul;31(7):637-45.
6 Pfannenberg C, Aschoff P, Schanz S, Eschmann SM, Plathow C, Eigentler TK, Garbe C, Brechtel K, Vonthein R, Bares R, Claussen CD, Schlemmer HP. Prospective comparison of 18F-fluorodeoxyglucose positron emission tomography/computed tomography and whole-body magnetic resonance imaging in staging of advanced malignant melanoma. Eur J Cancer. 2007 Feb;43(3):557-64. Epub 2007 Jan 16.
7 Müller-Horvat C, Radny P, Eigentler TK, Schäfer J, Pfannenberg C, Horger M, Khorchidi S, Nägele T, Garbe C, Claussen CD, Schlemmer HP. Prospective comparison of the impact on treatment decisions of whole-body magnetic resonance imaging and computed tomography in patients with metastatic malignant melanoma. Eur J Cancer. 2006 Feb;42(3):342-50. Epub 2005 Dec 20.
8 Schmidt GP, Reiser MF, Baur-Melnyk A. Whole-body MRI for the staging and follow-up of patients with metastasis. Eur J Radiol. 2009 Jun;70(3):393-400. Epub 2009 May 19. Review.
9 Ketelsen D, Röthke M, Aschoff P, Merseburger AS, Lichy MP, Reimold M, Claussen CD, Schlemmer HP. [Detection of bone metastasis of prostate cancer – comparison of whole-body MRI and bone scintigraphy]. Rofo. 2008 Aug;180(8):746-52. Epub 2008 May 29. German.
10 Wu LM, Gu HY, Zheng J, Xu X, Lin LH, Deng X, Zhang W, Xu JR. Diagnostic value of whole-body magnetic resonance imaging for bone metastases: a systematic review and meta-analysis. J Magn Reson Imaging. 2011 Jul;34(1):128-35. doi: 10.1002/jmri.22608. Epub 2011 May 25.
11 Padhani AR, Koh DM, Collins DJ. Whole-body diffusion-weighted MR imaging in cancer: current status and research directions. Radiology. 2011 Dec;261(3):700-18. Review.
12 Schlemmer HP, Pichler BJ, Krieg R, Heiss WD. An integrated MR/PET system: prospective applications. Abdom Imaging. 2009 Nov;34(6):668-74.
13 Schwenzer NF, Schmidt H, Claussen CD. Whole-body MR/PET: applications in abdominal imaging. Abdom Imaging. 2012 Feb;37(1):20-8.
14 Delso G, Martinez-Möller A, Bundschuh RA, Ladebeck R, Candidus Y, Faul D, Ziegler SI. Evaluation of the attenuation properties of MR equipment for its use in a whole-body PET/MR scanner. Phys Med Biol. 2010 Aug 7;55(15):4361-74. Epub 2010 Jul 20.
15 Delso G, Fürst S, Jakoby B, Ladebeck R, Ganter C, Nekolla SG, Schwaiger M, Ziegler SI. Performance measurements of the Siemens mMR integrated whole-body PET/MR scanner. J Nucl Med. 2011 Dec;52(12):1914-22. Epub 2011 Nov 11.

Contact
Markus G. Lentschig, M.D.
ZEMODI
Zentrum für Moderne Diagnostik
Schwachhauser Heerstr. 63a
28211 Bremen
Germany
Phone +49 421 69641-600
Fax +49 421 69641-649
www.zemodi.de

Relevant clinical information at your fingertips

From technology to clinical applications, you will find all the latest news on Siemens MR at

www.siemens.com/magnetom-world

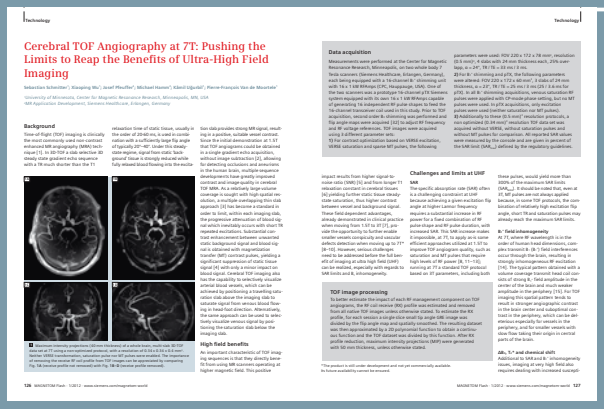

Cerebral TOF Angiography at 7T: Pushing the Limits to Reap the Benefits of Ultra-High Field Imaging

The centrepiece of the MAGNETOM World Internet platform consists of clinical results and articles on MR technology. Here you will find review articles, case reports and clinical methods.

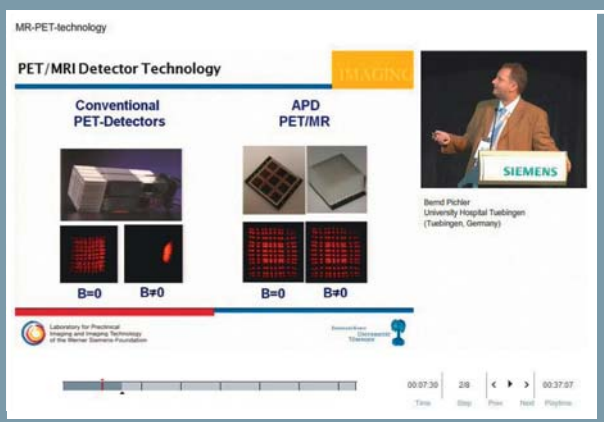

Don't miss the talks of international experts covering all aspects of MR imaging and development.

Brain Perfusion; How & Why

Just a mouse click away you will find application vidos and useful tips allowing you to optimize your daily MR examinations.

For the whole range of clinical MR and MR/PET information visit us at

www.siemens.com/magnetom-world

Multiparametric Imaging of Tumors – an Emerging Paradigm

Dr. Anwar Padhani MB BS, FRCP, FRCR

Paul Strickland Scanner Centre, Mount Vernon Cancer Centre, Northwood, Middlesex, UK

Introduction

To date, the main focus for innovations in imaging has been the achievement of excellence in anatomical resolution. In the field of cancer therapy response, morphological imaging is recognized to have significant limitations including the presence of tumors that cannot be measured, poor measurement reproducibility and mass lesions of unknown activity that persist following therapy. In neuro-oncology for example, the full extent of gliomas is poor depicted on contrast enhanced T1-images and by T2-FLAIR hyperintensity.
Anatomic imaging techniques may be insensitive to changes that inform on overall therapeutic success of cytostatic therapies, because the basic assumption that changes in tumor size reflect biological activity is violated. An example is pseudoresponse of glioblastomas treated with antiangiogenic therapy, where decreasing enhancement due to vascular normalization can be seen but with increasing mass effect and/or increasing tumor infiltration. The disconnection between anatomically determined progression free survival (PFS) and therapeutic efficacy (overall survival – OS) is recognized for a number of cytostatic therapies. The latter has recently resulted in a recommendation to withdraw the license to use the antiangiogenic drug bevacizumab for metastatic breast cancer by a committee of the US Food and Drug Administration (FDA), because improved PFS which was used for initial licensing did not ultimately result in improved OS. More sophisticated measurement methods such as tumor volume and CT density changes maybe unable to completely address these limitations.
Functional-molecular imaging methods made possible by the availability of MRI and PET scanners in particular have enabled many current clinical limitations to be addressed, as well as extending the applications of imaging in medicine. Thus, over the last decade we have seen the increasing use of functional-molecular imaging in the staging of patients with cancer and for monitoring their therapeutic response. Some of these functional-molecular imaging techniques are able to predict the success of therapy before conventional measurements of size are changed. Functional-molecular parameters are also being used as pharmacodynamic biomarkers in early phases of drug development (preclinical and clinical), in order to provide confidence to proceed to more expensive clinically studies of therapeutics with novel mechanisms of action. Advantages of functional-molecular imaging techniques include the fact that quantitative biomarkers obtained are spatially resolved, although resolution is in general less than corresponding anatomical images. Moreover functional-molecular imaging techniques are now beginning to identify the emergence of therapy resistance to a variety of treatments including novels drugs. An example of the latter is new internal enhancement on CT/MRI scans or ^{18}FDG-PET uptake in a size stable gastrointestinal tumor (GIST) treated with imatinib mesylate.
Examples of clinically deployed functional imaging MRI and PET techniques and the biological properties that they depict are given in tables 1 & 2. Reviews of the physical basis for MRI and PET and their differing sensitivity to depict biological processes, reveals that MRI is more suited to evaluating the structure and dynamic aspects of microenvironment of tissues (e.g., blood flow, vascular permeability, cell packing, necrosis and pH), some of which requires the administration of exogenous contrast agents or other methods of enhancing MRI sensitivity (e.g., by hyperpolarisation). On the other hand, because PET has a great sensitivity to compounds present at nanomolar or even picomolar concentrations but has a slower mode of acquisition, it more suited to evaluating cellular and molecular processes (depending largely on the radiotracers used). Until recently, these techniques were used mostly in isolation. However, there is now an increasing possibility to undertake multifunctional/multiplex imaging

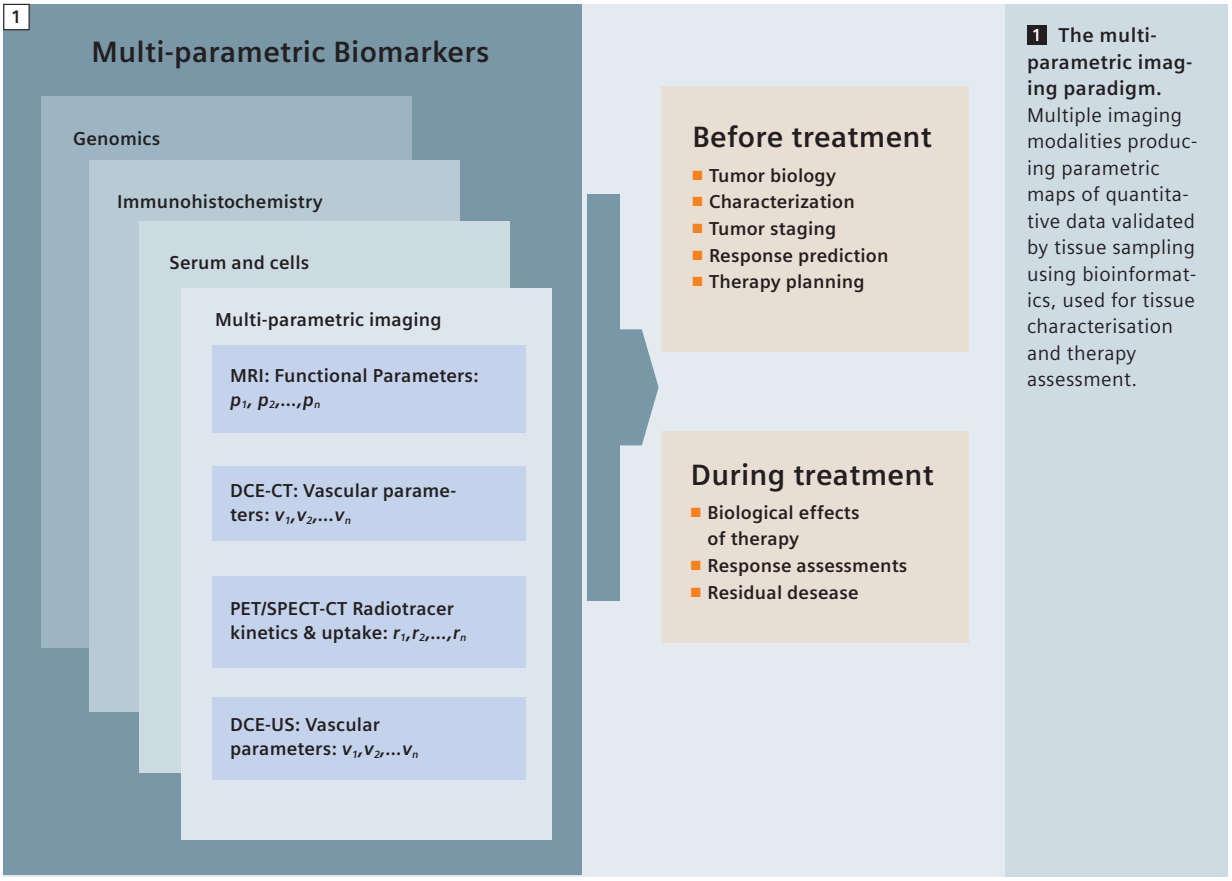

1 The multi-parametric imaging paradigm. Multiple imaging modalities producing parametric maps of quantitative data validated by tissue sampling using bioinformatics, used for tissue characterisation and therapy assessment.

(Kobayashi, Longmire et al. 2010) for biological investigations in animals but also clinically (Antoch and Bockisch 2009; Padhani and Miles 2010). Combined/multiplex approaches have been made possible by (a) the development of hybrid imaging technologies such as SPECT-CT and PET-CT and the soon to be available PET-MRI, (b) technological advancements within individual imaging modalities which enable multi-functional data acquisitions within short periods of time including the use of multiple PET isotopes with very short half lives, (c) advances in software enabling both fusion of imaging data between different imaging modalities and derivation of quantitative biologically relevant biomarker data that can be co-registered with anatomical images, and lastly (d) bioinformatics allowing integration of quantitative imaging parameters with other biological data such as serum cytokines, circulating cells and tissue genomic and protein expressions levels from targeted tissue biopsies (Figure 1). We have come to recognize that the multiparametric imaging approach is fast becoming an important means for biological investigation because of its multi-dimensional (multispectral, multispatial and temporally resolved) nature. In this article we do not discuss the technological advances that have made multiparametric imaging a reality. Instead we will appraise the current clinical roles of multiparametric imaging for characterizing tumors and in the therapy response setting indicating the added value imparted by this new approach. In so doing we can gain insights into the potential future areas where multiparametric approaches with combined PET-MRI maybe able to take us both scientifically and clinically.

Imaging depiction of altered tumor biology

Observations show us that cancers are complex, evolving, multiscale systems that are characterized by profound spatial and temporal heterogeneity in their biological characteristics. Most clinically manifested invasive epithelial cancers have typical, hallmark characteristics as a result of genetic changes and metabolic reprogramming that enables pre-cancer lesions to develop into virulent invasive tumors, by successfully

Table 1: Summary of commonly available functional MRI techniques, the quantitative parameters derived and their biological correlates.

Functional Imaging Technique	Biological property on which imaging is based	Commonly derived quantitative imaging parameters/ biomarkers	Pathophysiological correlates
Diffusion-weighted MRI (DW-MRI)	Diffusivity of water	■ Apparent diffusion coefficient (ADC) ■ Fractional anisotropy (FA) ■ Water diffusivity (D) ■ Perfusion fraction (F_p)	Cell density and distribution of cell sizes, extracellular space tortuosity, gland formation, cell membrane integrity, necrosis, fluid viscosity
Dynamic contrast-enhanced MRI (DCE-MRI)	Contrast medium uptake rate in tissues, which is influenced by: ■ Perfusion & transfer rates ■ Extra-cellular volume ■ Plasma volume fraction	■ Initial area under gadolinium curve (IAUGC) ■ Transfer and rate constants (K^{trans}, k_{ep}) ■ Leakage space fraction (v_e) ■ Fractional plasma volume (v_p)	Vessel density Vascular permeability Perfusion Tissue cell fraction Plasma volume
Dynamic susceptibility contrast MRI (DSC-MRI)	Blood volume and blood flow	■ relative blood volume/ flow (rBV/rBF) ■ Mean transit times (MTT) ■ Vessel size index	Vessel density Blood flow Tumor grade Vessel diameter
^{1}H-MR spectroscopic imaging (^{1}H-MRSI)	Cell membrane turnover/energetics and replacement of normal tissues	■ Quantified ratios of metabolites including choline, creatine, lipids, citrate, lactate and others depending on echo time and tissues evaluated	Tumor grade Proliferation index
Blood oxygenation level dependent (BOLD) or intrinsic susceptibility-weighted (ISW) MRI	Deoxyhaemoglobin shows higher relaxivity than oxyhaemoglobin. Measurement also reflect blood volume, perfusion and Intrinsic composition of tissues	■ Intrinsic tissue relaxation rate (R2* =1/T2*)	Tissue susceptibility properties including air and bone interfaces, ferromagnetic properties and blood oxygenation

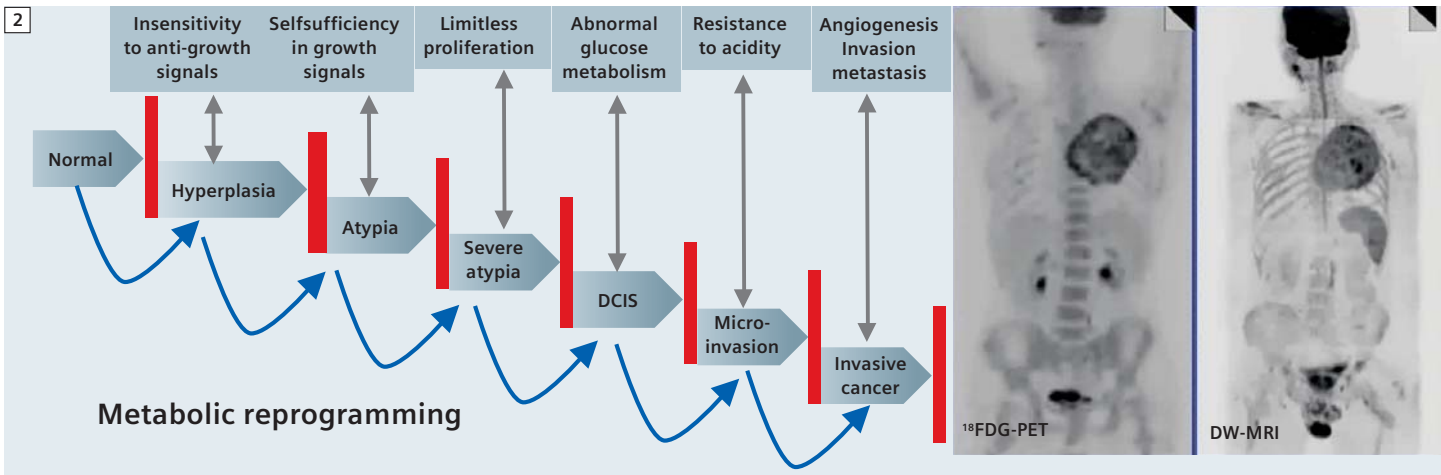

2 Carcinogenesis: hallmarks and metabolic reprogramming. In the transition from normal cells to clinically manifested invasive cancers, typically phenotypic characteristics become manifested (the hallmarks of cancers) resulting from metabolic reprogramming. Functional imaging techniques can depict these metabolic processes and cancer hallmarks at the tumor level, in peritumoral regions and at the organ/whole organism levels. The whole-body images on the right side of the image are of a patient with non-small cell lung cancer imaged with ^{18}FDG-PET and DW-MRI.

adapting or circumventing the body's natural microenvironmental barriers to uncontrolled proliferation (Figure 2). These hallmarks must be present in order to sustain tumor growth and for tumors to spread (Hanahan and Weinberg 2000). These genetic changes and metabolic reprogramming often occurs in a stepwise fashion as epithelial lesions develop from normal → hyperplasia → dysplasia → carcinoma-in-situ → local invasive cancers → metastatic cancers as described by Gatenby and Gillies (Gatenby and Gillies 2008). Imaging techniques can depict some of these molecular and functional aberrations (directly or by inference) within precancerous (e.g., polyps) and cancerous lesions, in peritumoral regions and at the organ/whole organism levels. Many key cancer hallmarks can be mapped including altered metabolism (including that of glucose, amino acids and nucleosides), tumor cell hyperproliferation and apoptosis, hypoxia, angiogenesis and aberrant neovascularity, local infiltration and distant metastases. Since there is a stepwise development of the biological aberrations in cancers so functional-molecular imaging tests maybe able to inform on the stage of development of lesions. By combining the information derived from a number of techniques, it becomes possible to build up a unique, multi-faceted phenotypic view of tumor evolution thus allowing improved characterizations (Figure 1). As many cancer hallmarks are also key anticancer targets, the role of functional-molecular imaging can be extended into the areas of drug development and for monitoring of the clinical effectiveness of therapeutics. The rationale for the latter being that decisions regarding continuation or discontinuation of a targeted therapy could rely on specific methods that image pathways being targeted. Resistance to conventional and novel therapies is highly dependent on the tumor microenvironment and on host-tumor interactions, so the potential exists for functional-molecular imaging to inform on which patients or lesions are more or less likely to continue to respond or to develop therapy resistance. This is made possible because functional-molecular imaging depictions including the displayed heterogeneity do reflect underlying gene-protein expressions in a number of cancer types.

Continued on page 70

Table 2: Examples of radionuclide imaging techniques used for assessing tumors:

Radiotracer	Biological property on which imaging is based	Commonly derived quantitative imaging parameters/ biomarkers	Comments
^{18}Fluorodeoxyglucose (FDG)	Glucose metabolism	■ Standardised uptake value (SUV) ■ Tumor to background uptake ratio ■ Metabolic rate of glucose	Up-regulation of GLUT-1 transporters and hexokinase II activity Some normal tissue have background activity – e.g., brain, liver
^{15}O-Water	Perfusion	■ Perfusion (ml/(g*min)) ■ Standardised uptake value ■ Tumor to background uptake ratio	Angiogenesis, vascularity, blood flow
^{18}Fluorothymidine (FLT)	Cellular proliferation	■ Standardised uptake value ■ Tumor to background uptake ratio	Activity of cytosolic thymidine kinase Incorporation into newly synthesized DNA Does not cross blood brain barrier
^{124}I Annexin-V	Apoptosis	■ Standardised uptake value ■ Tumor to background uptake ratio	Exposure of phospatidylserine in the cell membrane during programmed cell death
^{99}TCm Methoxyisobutyl-isonitrile (MIBI)	pGlycoprotein mediated multi-drug resistance	■ Tumor to background uptake ratio	Ejection of cytotoxic drugs from tumor cells
^{18}Fluoromisonidazole (MISO)	Hypoxia	■ Tumor to blood ratio	Tissue oxygenation Nitroreductase activity
Copper-diacetyl-bis (N4-methylthiosemicarbazone) (Cu-ATSM)	Hypoxia	■ Tumor to muscle ratio	Tissue oxygenation
^{11}C-choline and ^{18}F-choline	Cellular proliferation	■ Standardised uptake value ■ Tumor to background uptake ratio	Cell membrane synthesis and breakdown
^{18}F-FET and ^{11}C-methionine	Amino acid metabolism	■ Standardised uptake value	Indicates proliferative activity Useful for brain tumor recurrence

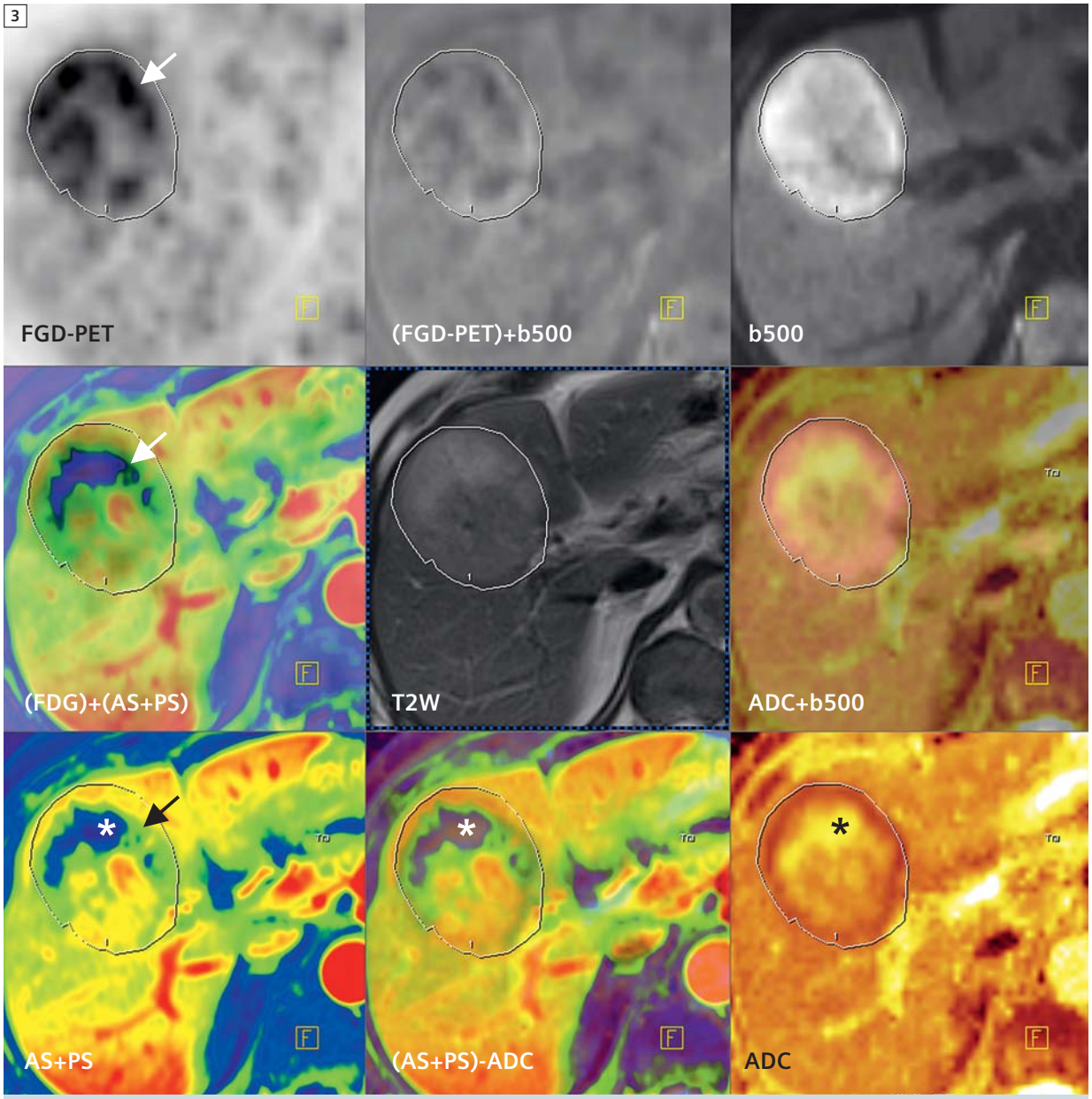

3 Fusion imaging of MRI and FDG-PET.
56-year-old male with metastatic colorectal cancer to the liver. Morphological T2-weighted, DW-MRI (b500 and ADC), DCE-MRI (arterial slope (AS) and portal slope (PS) added to yield total flow) and ^{18}FDG-PET scans were combined using fusion software. Region of interest around the tumor outline on the b500 images was copied onto all images to aid cross correlations. The area of non-enhancement (*) on the (AS+PS) image has the highest ADC values indicating necrosis. Around the area of necrosis, perfusion is decreased (green color) compared to adjacent normal liver (yellows and reds). Note that FDG uptake is greatest at the edge of necrosis in the low vascularity area (arrows) possibility related to upregulated glucose transporters (Glut-1) secondary to hypoxic stress. Higher cellular density (low ADC values) coincides with well vascular tissues where FDG uptake is relative similar to that of the liver.

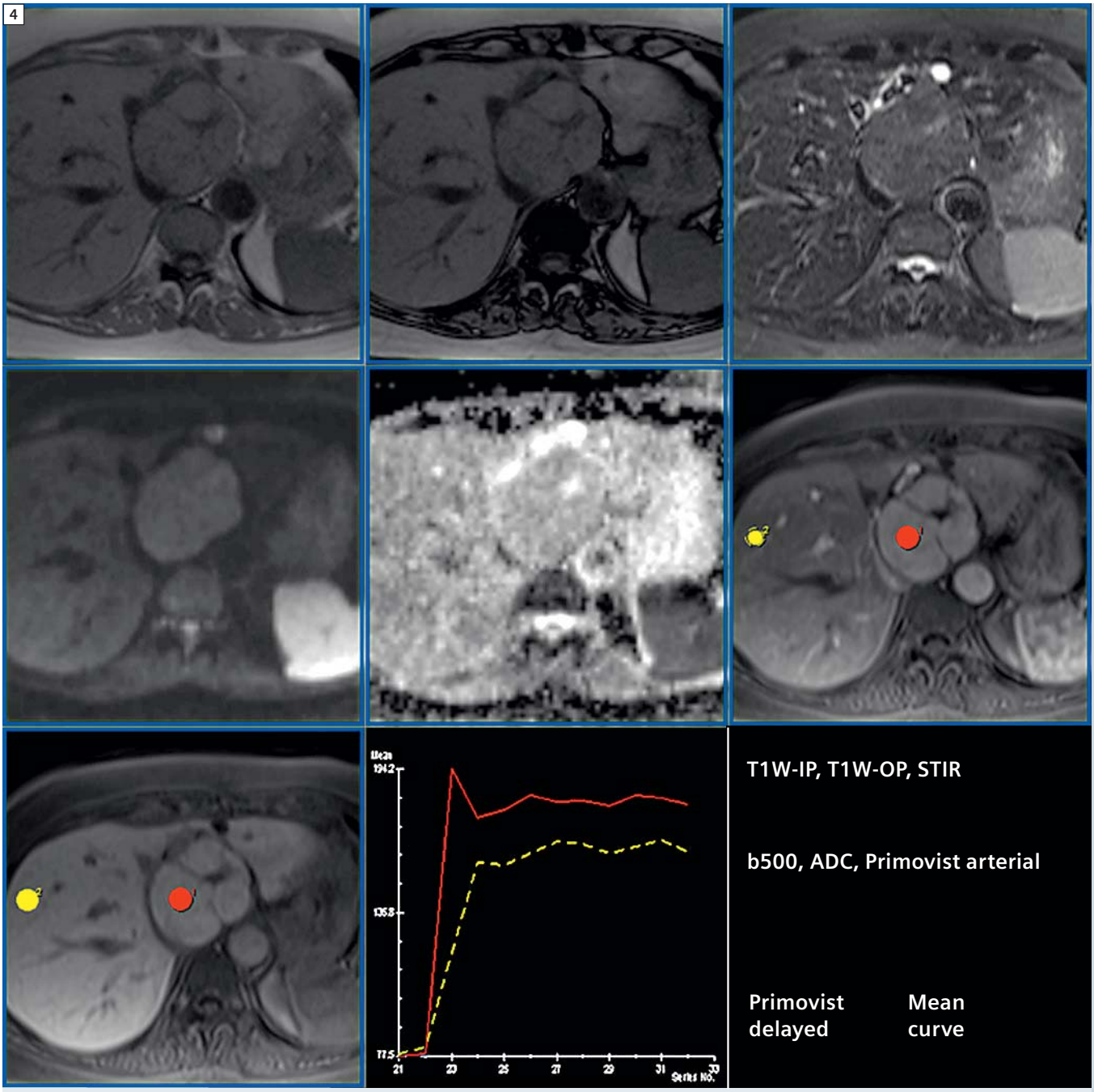

Fibro Nodular Hyperplasia (FNH)

4 Multiparametric MRI for liver lesion characterization. Two benign liver lesions (Fibronodular hyperplasia (FNH) and adenoma) evaluated by multifunctional MRI. Each lesion is depicted using T1w sequences (in-phase and opposed-phase), STIR sequences, DW-MRI (b500 and ADC) and DCE-MRI using a liver specific contrast agent Gadoxetic acid (Eovist in the USA and Primovist outside

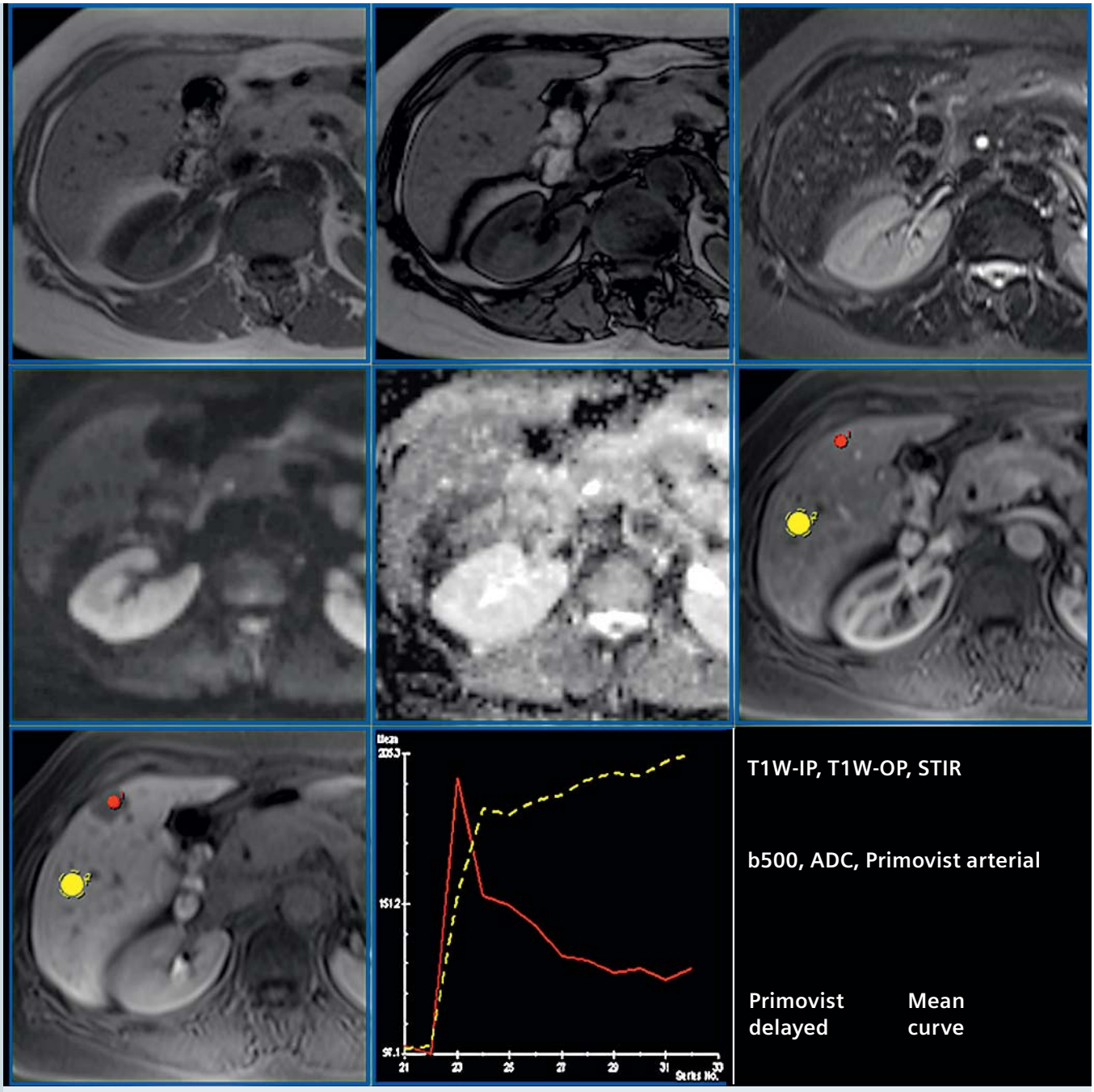

Liver adenoma

the USA). The different curve shapes on DCE-MRI reflect the relationship between histological structure (atretic canaliculi in FNH and no biliary canaliculi in adenomas) and functionality of contrast media transporters present on the portal and biliary sides of hepatocytes. Such structural-functional relationships can be used to more confidentially characterize liver lesions.

Continued from page 65

Roles of multiparametric imaging

A review of the current literature shows that the multiparametric approach is used in a number of clinical areas:

(1) For the improved depiction of biological features

Multifunctional evaluations make it possible to correlate observations between imaging biomarkers at the tumor or voxel levels. Such cross correlations can be used to:

- refine the interpretation of imaging observations made by one technique using corresponding data from another. An example is the improved depiction of tissue oxygenation using BOLD-MRI by using blood volume distribution from DSC-MRI (Padhani, Krohn et al. 2007).
- To validate an emerging biomarker against an accepted standard (by ascertaining the strength of relationships between them and by exploring the circumstances under which the strength of relationships may be changed). For example, transfer constant from DCE-MRI can serve as a biomarker of tumor blood flow before therapy (because of a high first pass extraction of low molecular weight constant agents in tumors). However, in the brain (because of an intact blood brain barrier) or when tumors are successfully treated, transfer constant becomes a biomarker of vascular permeability.
- To clarify the spatial relationships between depicted biological functions at the voxel level, so as to gain insights into the consequences of tumor metabolic reprogramming (Figure 3). For example, correlating tissue oxygenation and perfusion or perfusion and glucose metabolism has been shown to be useful for tissue characterization and for predicting therapy response as discussed below.

(2) For clinical characterisation of known disease

Functional-molecular imaging is often used to clarify the nature of abnormalities seen on morphological tests such as a CT or ultrasound scan. Multifunctional evaluations are a natural extension of this approach which has found roles in the characterization of lesions at a variety of anatomical sites including the brain, salivary glands, liver and prostate gland. So if an indeterminate liver lesion is found using anatomic CT/US imaging, then a multifunctional MRI scan maybe performed (including chemical shift imaging, diffusion MRI and dynamic contrast enhancement with a non-specific or liver specific contrast agent) (Figure 4). An unhelpful MRI scan may result in the use of a further imaging test such as an ^{18}FDG-PET for further clarification. When multifunctional assessments are used for disease detection and characterisation, it maybe found that individual modalities are discordant at the regional or tumor level. Discordance can occur because of tumor biology (see below) or for technical reasons including the fact that individually techniques have areas of strength and weakness, which can be overcome by combining imaging modalities together. An example is the improved staging of lymphoma by the combined use of ^{18}FDG-PET and diffusion-weighted MRI (DW-MRI). ^{18}FDG-PET is not sensitive enough for the detection of bone marrow infiltration which can be partially overcome by using DW-MRI. On the other hand DW-MRI is not sensitive enough to detect splenic disease which can be detected by ^{18}FDG-PET (Figure 5).

Discordant results can also be biologically meaningful often provoking new lines of investigations into tumor structural-functional relationships. For example, a number of studies have evaluated the relationship between glucose metabolism (^{18}FDG-PET) and tissue perfusion (which can be done with ^{15}O-water-PET, perfusion-CT and dynamic susceptibility contrast MRI (DSC-MRI). The recently introduced capability to perform perfusion-CT/^{18}FDG-PET has broadened the availability of this multiparametric approach. Although tightly coupled in most normal tissues, many studies have shown that the relationships between blood flow and glucose metabolism is not well matched in all tumors. Flow-metabolism mismatches have been shown in many tumor types depending on spatial location within tumors, on tumor type and grade, size and stage (Miles and Williams 2008). Miles and Williams suggested that low vascularity with high glucose uptake represents appropriate metabolic tumor adaptation to hypoxic stress whereas low vascularity with low glucose uptake represents a failure of tumor adaptation (Figures 6). Importantly the adaptive response (i.e., high glucose metabolism relative to blood flow) has been shown to be associated with poorer patient outcomes in breast and pancreatic cancers (Mankoff, Dunnwald et al. 2009). In the future, we can expect multifunctional-molecular imaging with PET-MRI systems to enable similar correlations between other biological processes to be undertaken, so as to gain greater insights into structural-functional relationships in health and disease and how these are altered in response to therapy.

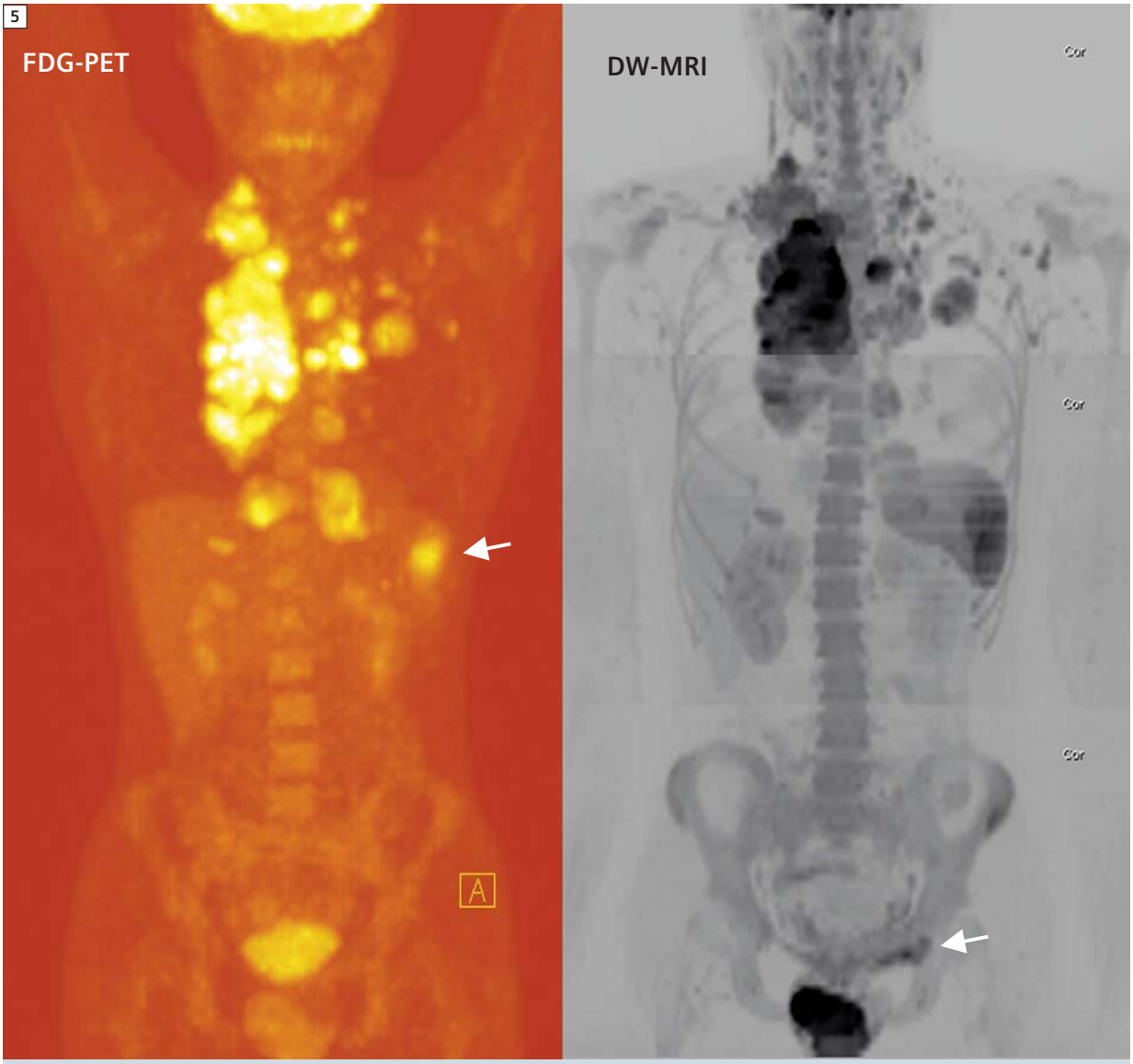

5 Improved lymphoma staging with whole-body ^{18}FDG-PET and DW-MRI. 23-year-old male with Hodgkin's lymphoma. Nodal distribution of disease between whole-body ^{18}FDG-PET and DW-MRI is very similar. The ^{18}FDG-PET scan shows a splenic deposit (arrow on the PET scan) which is not visible on the DW-MRI (where only normal increased signal intensity is seen). On the other hand the bone marrow abnormality seen in the left superior pubic ramus on the DW-MRI (arrow) is not appreciated on the PET scan. Both lesions were unproven histologically because their presence does not affect the therapy to be given. There is some variation in the signal intensity of the top station of the DW-MRI compared to the middle and lower stations.

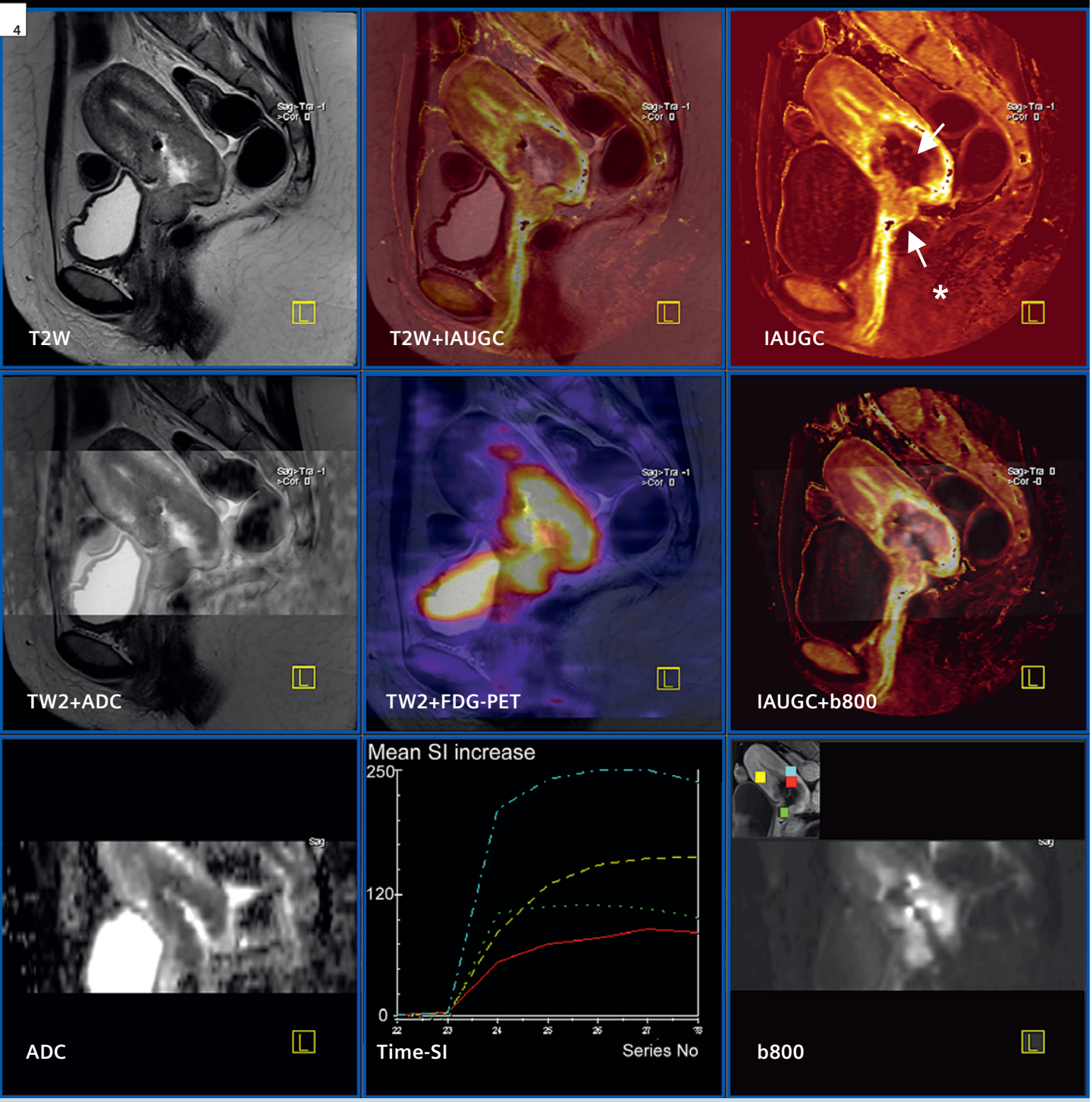

6 Fusion imaging of morphology MRI with DW-MRI, DCE-MRI and ^{18}FDG-PET 30-year-old female with non-metastatic poorly differentiated squamous carcinoma of the cervix. T2-weighted and DCE-MRI (initial area under gadolinium curve – IAUGC) was performed in the sagittal plane. DW-MRI (b800 s/mm^2 and ADC maps) and ^{18}FDG-PET scans were acquired in the axial plane and reconstructed into the sagittal plane. Top row images (left to right): T2-weighted (T2w), T2w image fused with initial area under gadolinium curve (IAUGC) and IAUGC maps. Middle row (left to right): fused T2w with ADC, T2w image fused with FDG-PET scan and IAUGC fused with b800 image. Bottom row (left to right) ADC map, time signal-intensity curves for regions of interest indicted in small insert on top of the b800 diffusion-weighted image. Note that the entire tumor depicted on T2w image is hypercellular (high signal intensity on b800 image and low on ADC map), hypermetabolic on the PET scan but the degree of vascularity is not uniformly distributed. The large hypovascular region (down arrow; red curve on the time-SI curves) has high glucose metabolism (adaptive response) which is likely to be more hypoxic than the anterior lip of the cervix (upward arrow with *) which is more vascular (green line). It is in adaptive areas (low flow with high glucose metabolism) where more aggressive tumor cell clones have been noted to emerge.

(3) Improved understanding of the biological effects of therapies

Monitoring changes during therapy with multifunctional imaging can provide invaluable information on the *in-vivo* mechanisms of action of therapeutics and of likely patients' outcomes. A number of studies have reported on the multiparametric approach for monitoring the effects of conventional therapies and for drugs with novel mechanisms of action. With respect to the latter, large numbers of new therapeutics are being developed as a result of the improved understanding of the molecular and genetic pathways controlling cellular function. Targeted molecular approaches typically seek to inhibit specific characteristics that are specific to cancers. As the pharmaceutical industry moves towards increasingly complex multi-targeted therapies, the anticipated effects on tumor tissues *de-novo* has become more difficult to predict. There is a growing recognition that biomarkers (including those derived from functional-molecular imaging) will play increasingly important roles in the drug development process (Figure 1). Imaging biomarkers can be used to confirm mechanisms of action of drugs *in-vivo* in early phase pre-clinical and clinical studies. Such pharmacodynamic (PD) data can then be potentially be harnessed for making "go-no-go" decisions at early stages of drug development; an important aim of which is to reduce the risk of failure of higher cost pivotal trials.

It is increasing being recognized that multiple tumor microenvironmental characteristics such as oxygenation levels, perfusion, extracellular pH, glucose metabolism and interstitial pressure as well as host-tumor interactions are important determinants of response to therapy, also determining the subsequent development of therapy resistance. For example, Batchelor et al. recently evaluated the antiangiogenic drug cediranib, given as monotherapy to patients with recurrent glioblastomas (Batchelor, Sorensen et al. 2007). Multiparametric MRI assessments showed rapid reductions in transfer constant, extracellular leakage space, and water diffusivity following treatment as the blood brain barrier became normalized. These effects were seen only in the enhancing volume of the tumor indicating that microenvironmental factors are determinants of therapy response. Interestingly, the enhancing tumor which had initially decreased in volume began to expand despite persistent decreases in microvessel permeability (pseudoresponse) suggesting that therapy resistance had developed (Figure 7). The mechanisms for the development of therapy resistance to antiangiogenics and other novel therapies are still being evaluated and will certainly include microenvironmental factors and host-tumor interactions. The ability to image the development of adverse characteristics leading to therapy resistance might enable us to develop strategies to circumvent such tumor adaptations, for the benefit of patients.

(4) Radiation therapy planning

Advances in imaging hardware related to radiation delivery have led to improvements in the physical conformality of radiation planning, treatment and delivery to tumors and organ boundaries using conformal and intensity-modulated techniques. The additional ability to combine image-depicted biology with image-guided radiotherapy has opened the way for further refinements of target definition and dose delivery, such that it is now possible to shape-dose volume distributions not only to the geometry of targets but also to differences in the radiobiology across tumors. Imaging-depicted radiobiologically relevant characteristics include tumor grade, hypoxia, acidosis or cellular proliferation.

Multiparametric imaging can potentially bring real benefits for radiation therapy planning in patients with brain gliomas where tumor delineation and gauging the aggressiveness of cancers by conventional contrast enhanced MRI/CT is severely limited (Dhermain, Hau et al. 2010). Uncoupling between tumor cell distribution and tumor grade makes it difficult to define effective, yet safe, margins for radiotherapy using conventional imaging. Uniform margins will either cover too much uninvolved brain (potentially exposing eloquent brain regions to unnecessary high radiation doses) or leave areas of tumor infiltration outside the treatment volume. This conundrum can potentially be overcome by multiparametric imaging; for example by combining ^{11}C-methonine PET with morphological MRI for tumor delineation and tumor grade mapping with perfusion MRI or ^{1}H-MR Spectroscopy (MRSI). This means that PET-MRI-planning CT scans ultimately need to be mapped onto the same frame reference for the purpose of brain radiation planning. In this regard, a combined MRI-PET scanner has obvious advantages minimizing the number of steps that use image co-registration software for data fusion and to correct geometrical distortions. Proof of concept studies, mostly retrospective, have shown that such multiparametric approaches can influence the placement of radiation treatment fields for glioma patients with the potential to improve treatment outcome (Dhermain, Hau et al. 2010), because the additional functional information is expected to increase the accuracy of target and normal tissue delineations. Validation of the efficacy of this new imaging-treatment approach will be needed, if this new paradigm is to become standard of clinical care.

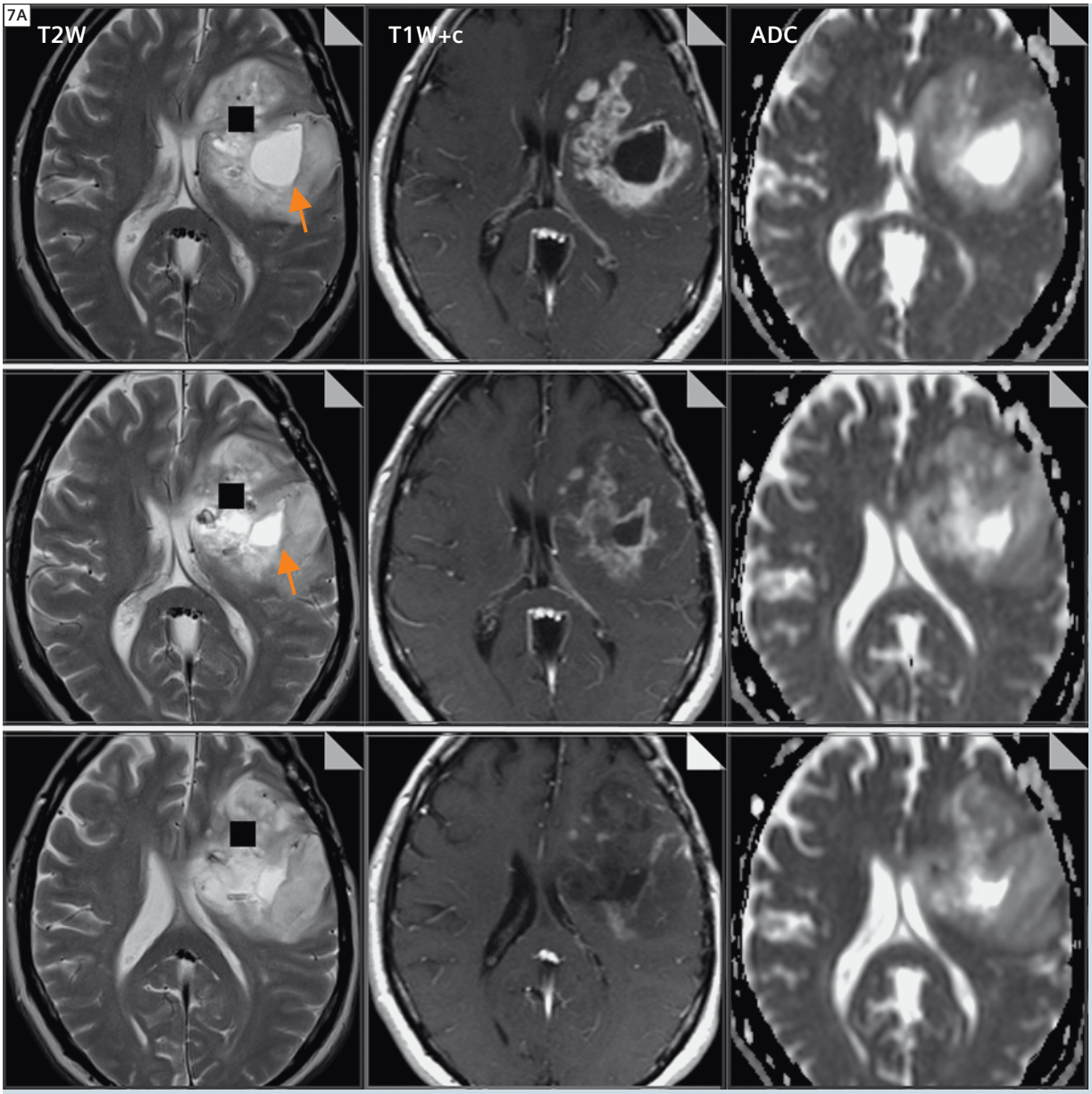

7 Multiparametric MR imaging of anti-VEGF antibody therapy. 40-year-old man with a high grade glioma before and during anti-VEGF antibody therapy. Rows: serial images obtained before, after 14 days and after 12 weeks of bevacizumab therapy. Figure 7A shows serial changes in morphology (T2w), contrast enhancement (T1w+c) and diffusion MRI (ADC). Figure 7B shows serial changes in MR spectroscopy (TE = 135 ms) and relative blood volume (rBV) and flow (rBF).
Row 1: pre-bevacizumab. The T2w image shows a large tumor with necrotic region (arrow). The T1 post-contrast image shows areas within the tumor where the blood-brain-barrier has broken down and other areas where no enhancement is seen. The ADC map shows areas of low ADC (similar to brain) and very high ADC regions indicating necrosis. The MR spectrum taken from the region of the black box region on the T2w image, demonstrates a large choline (Cho) peak which correlates with hypercellularity, a reduced N-acetylaspartate (NAA) peak showing that neurons have been destroyed or displaced, and an inverted lactate acid (Lac) peak indicating anaerobic glycolysis.

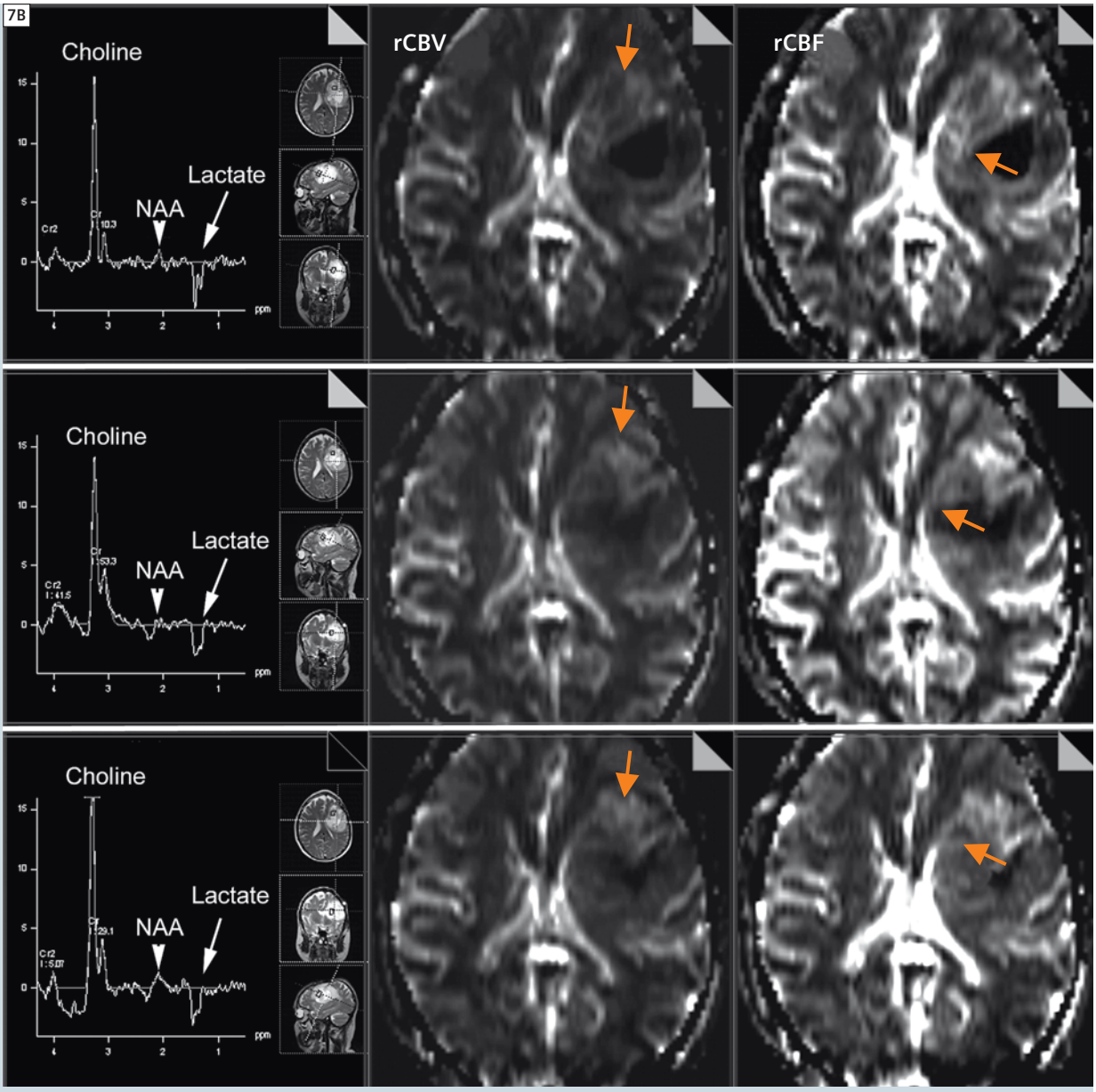

Row 2: 14 days post-bevacizumab. Some reduction in the size of the mass is seen particularly of the necrotic component on the T2w image. A marked reduction in contrast enhancement indicates that capillary permeability has been reduced but the MRSI has remained unchanged indicating that there has been no cell death. Note that there has been some reduction in relative cerebral blood flow (upward pointing arrow) in a small region of the tumor.
Row 3: 12 weeks post-bevacizumab. The tumor has increased in size and thickness by growing into the area of necrosis. Again there is a reduction in enhancement indicating an on-going anti-permeability effect of bevacizumab. MRSI has not changed indicating the absence of tumor cell kill confirmed by the lack of change in the tumor ADC map. Increasing relative blood volume and flow (down pointing arrow) is consistent tumor progression also.

Challenges for implementation

Multifunctional imaging observations reinforce the underlying message of this review, that it is only by combining biomarker data from a number of imaging techniques that one may begin to truly understand how tumors interact with the host and how therapies affect tumor cells and tissue microenvironments. Such observations can also provide unique insights into the mechanism of drug action *in-vivo* and useful pharmacodynamic information. However, if functional-molecular imaging is to take up its unique position of enhancing decision-making at critical milestones in drug development, or in personalized medicine where therapy is adapted according to tumor-host phenotype or in novel radiation therapy planning, then procedural rigor and validation will be needed to establish biomarker-combinations for such roles.

It is possible to acquire spatially-matched multiparametric imaging data in potentially every patient at a given time point. Currently, integration of multidimensional imaging datasets represents a major challenge. If multiparametric data is acquired several times during a treatment, then there is an added level of complexity brought on by changing morphological features and patient repositioning. Sophisticated, user-friendly software workspaces need to be developed urgently, in order to be able to integrate/cross correlate data analysis procedures so as to follow changes in response to therapy. Computer platforms need to incorporate bioinformatics approaches, so that imaging biomarkers can be correlated with findings from immunohistochemistry, gene expression profiles, and tissue and clinical biomarker data. Ultimately, multispectral imaging analyses should be able to generate probability biomaps of important biological characteristics or to infer underlying molecular gene expression patterns. Composite biomaps incorporating functional imaging would be invaluable in lesion characterisation, therapy planning and for assessing the effects of therapies.

Conclusions

When considering the potential opportunities for multiparametric imaging to influence patients' management, it should be remembered that the perceived advantages of such approaches are currently without a sound evidence base regarding selection of patients who would benefit from these more complex approaches, and whether improved patient outcomes will ultimately be seen. Furthermore, functional-molecular imaging techniques are at different stages of development with incomplete validation or acceptance of standards for data acquisition and analysis. Frameworks for the validation of functional-molecular imaging to support clinical decision making are only now beginning to emerge. Additionally, there are practical challenges for incorporating both anatomical-functional-molecular into therapy paradigms including image-guided radiotherapy systems, which will need to be overcome. However, we can state with some confidence that there are extraordinary opportunities for multiparametric imaging approaches to evolve into qualified biomarkers that are useful clinically, for pharmaceutical drug development, radiation therapy planning and for predicting therapeutic efficacy. Multidisciplinary efforts will be required to bring this vision into fruition.

References

1 Antoch, G. and A. Bockisch (2009). "Combined PET/MRI: a new dimension in whole-body oncology imaging?" Eur J Nucl Med Mol Imaging 36 Suppl 1: S113-20.

2 Batchelor, T. T., A. G. Sorensen, et al. (2007). "AZD2171, a pan-VEGF receptor tyrosine kinase inhibitor, normalizes tumor vasculature and alleviates edema in glioblastoma patients." Cancer Cell 11(1): 83-95.

3 Dhermain, F. G., P. Hau, et al. (2010). "Advanced MRI and PET imaging for assessment of treatment response in patients with gliomas." Lancet Neurol 9(9): 906-920.

4 Gatenby, R. A. and R. J. Gillies (2008). "A microenvironmental model of carcinogenesis." Nat Rev Cancer 8(1): 56-61. Hanahan, D. and R. A. Weinberg (2000). "The hallmarks of cancer." Cell 100(1): 57-70.

5 Kobayashi, H., M. R. Longmire, et al. (2010). "Multiplexed imaging in cancer diagnosis: applications and future advances." Lancet Oncol 11(6): 589-95.

6 Mankoff, D. A., L. K. Dunnwald, et al. (2009). "Blood flow-metabolism mismatch: good for the tumor, bad for the patient." Clin Cancer Res 15(17): 5294-6.

7 Miles, K. A. and R. E. Williams (2008). "Warburg revisited: imaging tumour blood flow and metabolism." Cancer Imaging 8: 81-6.

8 Padhani, A. R., K. A. Krohn, et al. (2007). "Imaging oxygenation of human tumours." Eur Radiol 17(4): 861-72.

9 Padhani, A. R. and K. A. Miles (2010). "Multiparametric imaging of tumor response to therapy." Radiology 256(2): 348-64.

Contact
Dr Anwar Padhani MB BS, FRCP, FRCR
Consultant Radiologist and Head of Imaging Research
Paul Strickland Scanner Centre
Mount Vernon Cancer Centre
Rickmansworth Road
Northwood, Middlesex
HA6 2RN
United Kingdom
Tel: ++44-(0) 1923-844751
Fax: ++44-(0) 1923-844600
anwar.padhani@stricklandscanner.org.uk

Benefit from the outstanding presentations that we have captured during the 8. MAGNETOM World Summit

Bruce Rosen
Athinoula A. Martinos Center for Biomedical Imaging
Charlestown, MA, USA

MR and PET: Clinical update and the future

Markus Lentschig
CEMODI - Center for modern diagnostic MRT and MR/PET
Bremen, Germany

Simultaneous MR/PET in daily practice – where do we stand?

Nina Schwenzer
University Hospital Tübingen
Tübingen, Germany

Integrating MR and PET information – how to do this?

Tzu-Chen Yen
Chang Gung Memorial Hospital
Linkou, Taiwan

Molecular MR – clinical update on simultaneous MR/PET

Check out these and many more talks on the clinical and technological aspects of MR/PET at

www.siemens.com/magnetom-world

T_1-weighted DCE Imaging Concepts: Modelling, Acquisition and Analysis

Paul S. Tofts, PhD

Brighton and Sussex Medical School, Falmer, Sussex, United Kingdom

1. Introduction

There are increasing opportunities to use Dynamic Contrast-Enhanced (DCE) T_1-weighted imaging to characterize tumor biology and treatment response, using the modern fast sequences that can provide good temporal and spatial resolution combined with good organ coverage [1]. Quantification in MRI is recognized as an important approach to characterize tissue biology. This article provides an introduction to the physics concepts of mathematical modelling, image acquisition and image analysis needed to measure aspects of tumor biology using DCE imaging, in a way that should be accessible for a research-minded clinician.

Quantification in MRI represents a paradigm shift, a new way of thinking about imaging [2]. In qualitative studies, the scanner is a highly sophisticated camera, collecting images that are viewed by an experienced radiologist. In quantitative studies, the scanner is used as a sophisticated measuring device, a scientific instrument able to measure many properties of each tissue voxel (e.g. T_1, T_2, diffusion tensor, magnetisation transfer, metabolite concentration, K^{trans}). An everyday example of quantification would be the bathroom scales, used to measure our weight. We expect that the machine output shown on the dial, in kg, will be accurate (i.e. close to the true value), reproducible (i.e. if we make repeated measurements over a short time they will not vary), reliable (the scales always work) and biologically relevant (the quantity of weight does indeed relate to our health). An example of a clinical measurement would be a blood test; we expect it to work reliably every time. This is the aspiration for quantitative MRI: that it should deliver a high quality measurement that relates only to the patient biology (and not the state of the scanner at the time of measurement).

The transfer constant K^{trans} (see below) characterizes the diffusive transport of low-molecular weight Gd chelates across the capillary endothelium [3]. It can be measured using DCE MRI, and has been widely used in imaging studies to characterize tumor biology and treatment response. The fractional volume v_e of the extravascular extracellular space (EES; i.e. the interstitial space), can also be measured. A consensus recommendation [4] proposed that in assessing anti-angiogenic and anti-vascular therapies, K^{trans} should be a primary endpoint. Secondary endpoints should include v_e, the rate constant k_{ep} ($k_{ep}=K^{trans}/v_e$) and the plasma volume v_p (if available). The traditional clinical evaluation of tumor treatment is the RECIST criterion, based on tumor diameter; however a tumor could die but not shrink, and K^{trans} and v_e may often be more sensitive markers of tumor metabolism. There are also applications of DCE-MRI in tissues other than tumors, e.g. renal and myocardial function; this article focuses on tumor applications, with one example of renal function.

2. MRI modelling

Before any pharmacokinetic analysis can take place, the Gd contrast agent (CA) concentration has to be found from the MRI signal enhancement. This requires an MRI model, which has two components. First, T_1 is reduced by the presence of CA (eqn. 1 see appendix). The relaxivity r_1, (i.e. the constant of proportionality between Gd concentration and increase in relaxation rate $R_1=1/T_1$) is usually assumed to be equal to the in-vitro value (measured in aqueous phantoms), although it can alter in-vivo. The native T_1 of the tumor (i.e. the value before injection of CA, T_{10}) must also be known. Second, the way in which the T_1 reduction increases the signal is modelled (eqn. 3); this is specific to each sequence type, and also requires accurate knowledge of the flip angle FA. The most common sequence is the simple gradient echo (FLASH), on account of its speed; the sequence must be truly spoilt (i.e. there is no build up of steady state transverse magnetisation). Provided

these 3 parameters (r_1, T_{10}, FA) are known then there is a clear relationship between signal and Gd concentration.
Some studies attempt to find Gd concentration from signal by using a phantom calibration curve; however these approaches are usually flawed, since the signal is also proportional to proton density (which is greater in an aqueous solution than in tissue), and the FA may be different when imaging the phantom (caused for example by different coil loading or B_1 inhomogeneity).
The plasma concentration (required for the pharmacokinetic modelling – see below) may be measured from the blood signal. In this case, blood concentration is first found from the blood signal (using eqn. 3).
The plasma concentration is about 70% higher, once haematocrit is taken account of (eqn. 4).

3. Pharmacokinetic modelling

Given the Gd concentration as a function of time, pharmacokinetic analysis can now be undertaken to model how the CA distributes in the body, and how this depends on characteristics of the tumor biology
This is independent of the imaging conditions (MRI field strength etc.), and in principle even independent of imaging modality (CT or MRI). Most modelling uses the concept of a compartment; this is like a bucket: the Gd tracer inside is dissolved in water and at the same concentration everywhere, and the flow into or out of the bucket is small enough to allow the contents to remain well mixed.
The simplest compartmental model has one tissue compartment in addition to a vascular compartment; the so called 'Tofts model' [5] (mathematically equivalent to that proposed by Kety [6] in a non-MRI context), used to measure K^{trans} and v_e (see fig. 1). The bolus injection of Gd gives a time-varying blood plasma concentration $C_p(t)$, which can be measured in each subject, or else a population average can be used. Since the commonly used contrast agents are small (<≈ 1000 Daltons) then the leakage from the capillaries into the EES is diffusive and hence reversible; it is therefore proportional to the difference in concentrations, and K^{trans} is the constant of proportionality (eqn. 5).
The total Gd concentration in a voxel or ROI (eq 6) is the sum of the EES contribution (which usually dominates, since v_e ≈ 10–60%) and the intravascular contribution (the 'vp term') which is often small and ignored (v_p ≈ 1–10%) [7].
This model was able to explain signal enhancement in multiple sclerosis lesions [5] (fig. 2), and gave values of K^{trans} and v_e consistent with the known biology of acute and chronic lesions.

1

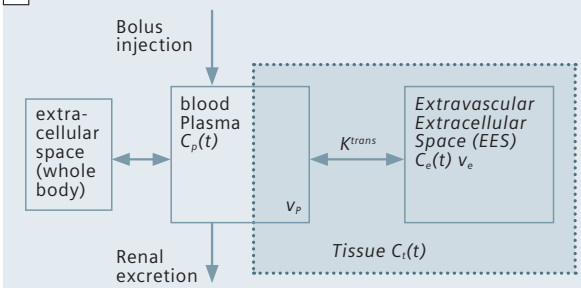

1 Simple compartmental model.

2

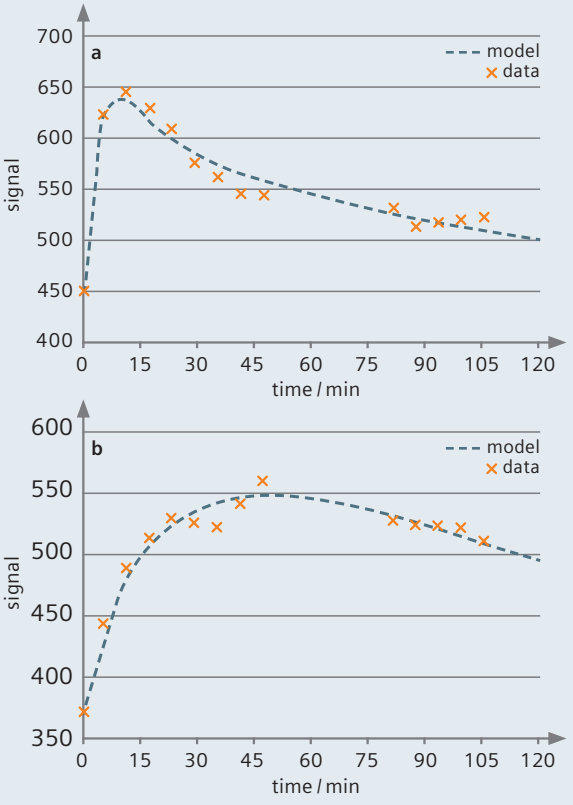

2 First case of DCE-MRI to measure capillary leakage, published in 1991 by Tofts and Kermode [5]. The upper plot shows enhancement in an acute multiple sclerosis lesion. The signal peaks at about 12 min, model fitting gave K^{trans} = 0.050 min^{-1}, v_e = 21%. The lower plot shows a chronic lesion with a less permeable blood-brain barrier (K^{trans} = 0.013 min^{-1}), and an enlarged EES (v_e=49%), with signal peaking later (at about 50 min). These data were collected in 1989 using a multislice spin echo sequence; note the poor temporal resolution by modern standards, and the missing data when the patients took a break. *(Reproduced from Magn Reson Med 1991).*

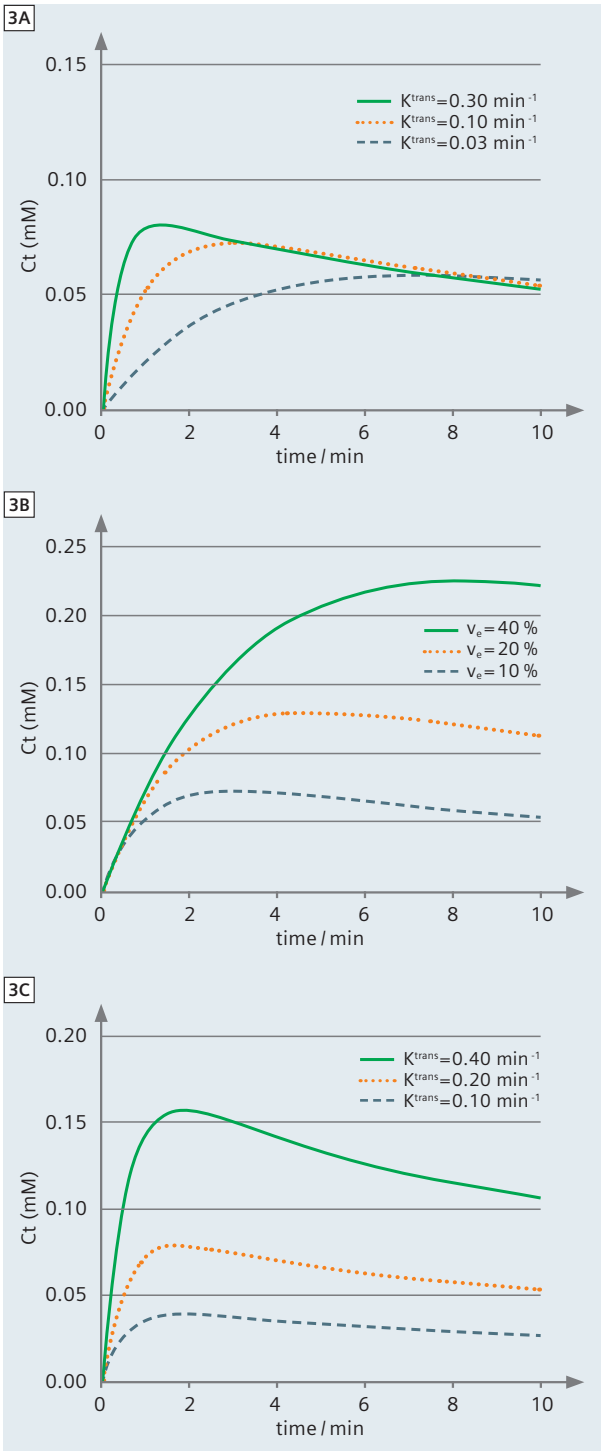

3 Simulations of tissue concentration after bolus injection of 0.1 mmole/kg of Gd, for a range of K^{trans} and v_e values, ignoring any IV contribution.
(A) Increasing K^{trans}, with fixed v_e = 10%.
(B) Increasing v_e, with fixed K^{trans} = 0.1 min^{-1}.
(C) Constant k_{ep} = 2 min^{-1}, increasing K^{trans}.

The differences in enhancement curve shape, and the time of peak enhancement, both apparent in fig. 2, are important. A model simulation [5] using typical K^{trans} values for tumors shows that the initial slope depends on K^{trans} (fig. 3A), and is independent of v_e (fig. 3B). The final peak value depends on v_e, and larger v_e tumors take longer to reach their peak (fig. 3B). The shape of the curve is determined by k_{ep}, and if K^{trans} is increased whilst keeping k_{ep} fixed, the curve increases in amplitude but retains the same shape (fig. 3C) as is expected from equation 6.

In the original formulation of the model (applied to multiple sclerosis), trans-endothelial leakage was low enough that there would not be significant local depletion of Gd concentration in the capillary. Perfusion F was sufficient to maintain the capillary concentration at the arterial value. In this case, K^{trans} is just the permeability surface area product (PS), and DCE could reasonably be called permeability imaging'. This 'permeability-limited' case is defined by F≪PS. In tumors, the endothelium can be much more leaky, there may be local depletion, and K^{trans} will represent a combination of permeability and perfusion [3]. In the limiting case of very high permeability, then K^{trans} will equal perfusion, and DCE could reasonably be called 'perfusion imaging'. This is the 'flow-limited case', defined by F≪PS.

The modelling of the capillary vasculature shown in figure 1 is naive, and not surprisingly at high temporal resolution it fails. Modern sequences can sometimes provide a temporal resolution of ~1 s (depending on the organ and the coverage required), and in these cases the initial rise in signal gives information about perfusion, as Gd arrives in the capillary bed over a few seconds. More sophisticated models are then able to extract pure perfusion information [8, 9], and potentially pure permeability information as well. In DCE kidney imaging, the perfusion peak in tissue is clearly delayed (by about 4 s) with respect to the arterial peak (see fig. 5).

4. Image acquisition

In DCE imaging, repeated T_1-weighted images are collected for several frames before Gd is injected, and then for several minutes afterwards. This is often preceded by a T_1 measurement. A good bolus injection can be achieved by using a power injector, with a saline flush after the Gd. The receiver gain must be controlled for the whole series of DCE images.

Quality assurance [2] can be used to ensure the scanner is stable for the DCE acquisition period. Either a phantom can be repeatedly imaged (this can also be used to check T_1 accuracy), or a volunteer can be repeatedly scanned (without Gd).

The sequence parameters will involve compromise between coverage, temporal resolution and spatial resolution. Newer scanners have faster gradients (allowing shorter TR's), and multi-array receive coils give higher SNR at short TR's. The optimal sequence will depend on the organ being measured; often frame times of 2–20 s can be achieved. 3D (volume) sequences are preferred, since they have better FA accuracy than 2D (slice selective) sequences. Body coil transmission gives better FA accuracy than combined transmit/receive coils. In the abdomen, a coronal-sagittal oblique slice orientation (instead of transverse) has two advantages: the aorta can be sampled along its length, removing wash-in effects, and breathing movement is mostly in-plane and therefore more easily corrected.

The blood curve may be measured, in order to provide an AIF for the modelling. In this case a temporal resolution of ~3 s or less is desirable, and it is usually the aorta that is imaged. Wash-in effects are reduced by ensuring that the blood is fully saturated (i.e. has experienced several RF pulses) by the time it reaches the location of the region of interest (ROI).

The DCE sequence should ideally be run long enough to sample the enhancement plateau. If not, then v_e cannot be reliably measured, since it does not affect the rising part of the curve, only the plateau value (see fig. 3B).

An example of rapid DCE is shown in figure 4. Imaging of the kidney and aorta at a temporal resolution of 2.5 s, using half standard dose of Gd, allows the perfusion phase of the tissue signal to be seen, and it has a clear delay with respect to the aortic peak. In this organ the blood volume is large (about 30%), and can be estimated because the perfusion peak is so distinct. A modified model fits the data well (fig. 5); in this model of the uptake phase (up to 90 s), the vascular delay and dispersion are accounted for, and there is no efflux from the parenchymal ROI. Renal filtration occurs mostly after bolus passage, and can be well estimated. GFR estimates in controls are in good agreement with normal values (reference 10 and manuscript in preparation).

There is scope to optimise the FA. A small FA gives more signal at low concentration, but has limited dynamic range (see fig. 6 FA = 5°); increasing the FA gives increased sensitivity to Gd (fig. 6 FA = 10°); further increases (fig. 6 FA = 20° or 30°) give a wider dynamic range (at the expense of reduced sensitivity) and are needed if measuring the AIF (peak blood concentration 6mM [11] and see fig. 7 below) as well as tissue enhancement. Nonlinearity is not a concern as it is properly dealt with in the MRI model.

Breathing causes serious artifacts in body imaging. There are several approaches to minimising its effect:

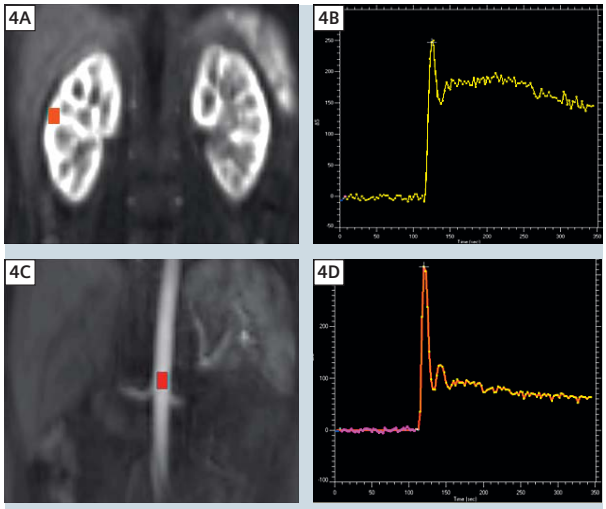

4 Signal enhancement in kidney and aorta. A cortical ROI **(A)** is used to define the time of peak enhancement **(B)** and hence the arterial ROI **(C)** giving the blood curve **(D)**.

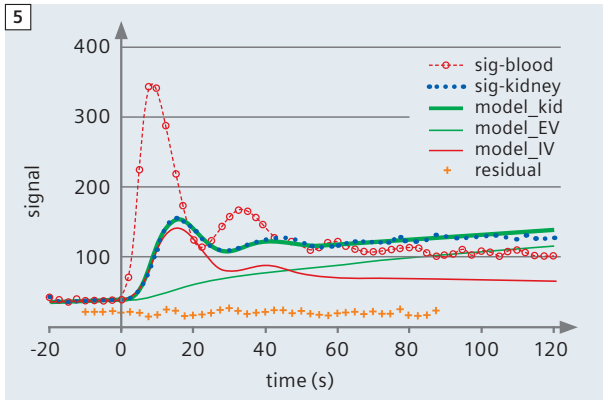

5 Model analysis of renal enhancement. The kidney signal (sig-kidney) is clearly delayed (by about 2 time points) from the blood signal (sig-blood). The model fit (model-kid) shows separately the extravascular filtered Gd (model-EV, from which GFR is found) and the intravascular Gd (model-IV, from which blood volume and perfusion are estimated).

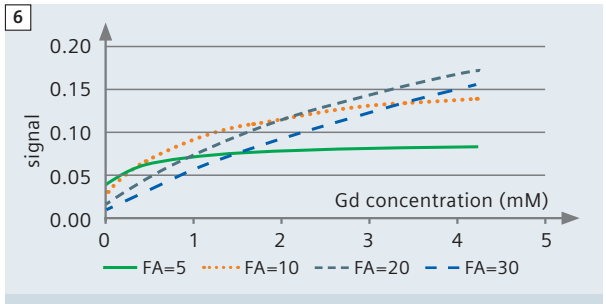

6 Performance of gradient echo sequence with various FA values. Eqns 2 and 3 were used, with TR = 3 ms; T_1 = 1 s.

i) Allow free breathing and minimise diaphragm movement by having hands above the head. This can be uncomfortable; having a single hand above the head is easier and nearly as effective.
ii) Breath-hold for first pass (~20 s) then allow breathing (although this can result in a large movement as breathing resumes).
iii) Free breathe and discard data at the extremes of position (using the images or respiratory monitoring to detect the extrema).
iii) Guided free breathing (instructions from the imaging radiographer).

Whether breathing should be controlled or not is currently unclear (this may depend on the kind of patient, and the availability of registration – see below), and is the subject of ongoing research.

Flip angle accuracy is often poor yet crucial in determining the accuracy of the K^{trans} value. It affects the calculation of concentration from enhancement (eq. 3), the estimation of the AIF, and the measurement of T_{10}.

B_1 nonuniformity (heterogeneity), if present, means that the FA distribution is also nonuniform. There are two primary causes of such nonuniformity. Firstly, dielectric resonance produces standing waves in the subject, which are more pronounced at higher fields (≥3T), and in larger objects (the effect is greater in the body than in the head). Secondly, smaller transmit coils are less uniform, and therefore the body transmit coil is to be preferred (not a smaller combined transmit/receive coil).

During the FA setup procedure, a good technique will optimise the FA over just the volume to be imaged (not the whole slice), and an accurate FA may then be obtained in spite of more global FA nonuniformity.

An additional source of FA error is in 2D multislice imaging, where the slice profile is often poor, and a distribution of FA values exists across the slice. Therefore 3D (volume) acquisitions are preferred.

B_1 maps can be measured quite quickly [12] (<2 min) and these may enable corrections to be made in the presence of FA inaccuracy and inhomogeneity. Phased transmit array technology is in development (essential for imaging >3T). This gives impressive control over B_1 at each location in the subject, and such 'RF shimming' is expected to give uniform and accurate FA values.

The tissue T_1 value (T_{10}) can be measured, or else a standard value from the literature used. An accurate measurement is preferred for each individual subject, since in disease this can alter; this can often be carried out in < 5 minutes. The most common method is the variable flip angle method, where gradient echo sequences with several FA values are used. These include a mostly PD-weighted sequence (low FA) and one or more T_1-weighted sequence (higher FA). Clearly the T_{10} accuracy is crucially dependent on the FA accuracy. Inversion recovery methods (with variable TI, fixed FA) are more robust, but usually slower.

The measured K^{trans} value is very sensitive to the accuracy of the T_{10} value. An example from breast cancer shows that [13] for a range of feasible T_{10} values, the fits are equally good, K^{trans} can vary by at least a factor of 2, and v_e can reach impossible values (v_e>100%); see table 1. k_{ep} is relatively robust. An increase of 1% in T_{10} gives a resulting decrease of 1% in K^{trans}, such that the product remains approximately constant.

Any low molecular weight contrast agent can in principle be used for DCE methodology. The initial work [5] was carried out with Gd-DTPA, size 570D, and then with Magnevist (938D). Clearly larger molecules will have lower permeability and hence K^{trans} values, and the AIF may alter a little with viscosity. In view of the con-

Table 1: Sensitivity of tissue parameters to T_{10} value. ***(Adapted from Tofts 1995 [13])***

Tissue	T_{10} (s)	K^{trans} (min^{-1})	v_e (%)	residual in fit	k_{ep} (min^{-1})	K^{trans} T_{10}
Normal low risk fatty portion	0.46	0.88	143	0.091	0.62	0.41
Tumor – low T_1	0.60	0.63	96	0.092	0.65	0.38
Normal high risk diffuse density portion	0.71	0.51	76	0.093	0.67	0.36
Tumor – high T_1	1.3	0.26	36	0.095	0.72	0.34

cerns about NSF, there will be value in gaining experience using the newer cyclic compounds. Potentially suitable candidate compounds are as follows. Dotarem (754D), Eovist (725D), Gadovist (605D), Magnevist (938D), Multihance (1058D), Omniscan (574D), Optimark (662D), Primovist (685D), Prohance (559D) and Teslascan (757D) (see http://www.rxlist.com).

5. Image analysis

Analysis can be carried out on individual ROI's, or on a pixel-by-pixel basis to produce a map for the whole organ. The reduction of motion artefact using spatial registration, if available, is likely to improve the quality of the fit (depending on the tissue location). Because the motion is non-rigid, effective removal is much harder than in the brain, and a topic of ongoing research. In-plane movement is relatively easy to reduce.

The pharmacokinetic model requires knowledge of the arterial plasma concentration $C_p(t)$; this arterial input function (AIF) can be calculated from the blood signal (which confusingly can also be called the AIF!). It can be measured for each subject, and thus within- and between-subject variation can be taken into account, although if the technique is not implemented well it can introduce extra variation which contaminates the final measurements of tissue physiology.

Alternatively a population average AIF can be used. Some of these are described analytically (i.e. using mathematical equations, rather than just a list of numbers), which makes them more convenient to use. In particular they are available at any temporal resolution. The most popular are the original biexponential Weinmann plasma curve [5], derived from low temporal resolution arterial blood samples, and the more complex Parker blood function [11], derived from high temporal resolution MRI data. In the Parker function, bolus first pass and recirculation are represented. After bolus passage and recirculation, the MRI measurement (Parker C_p(1 min) = 1.53 mM assuming Hct = 42%) is 86% higher than the direct measurement (Weinmann C_p(1 min) = 0.82 mM). The possible reasons for this discrepancy include a population difference and wash-in effects in the MRI method. The numerical AIF's of Fritz-Hansen [14] showed excellent agreement between an inversion recovery MRI method and direct blood measurements; their values (average over 6 subjects C_p(1 min) = 1.09 mM) are closer to the Weinmann value. The choice of AIF will depend on the tissue being studied and the sequences available.

When it comes to the modelling, several versions can be considered. The primary free parameters are K^{trans} and either k_{ep} or v_e (since k_{ep} and v_e are related). It is worth including v_p to see if the fit improves. The onset time of the bolus t_onset will be needed if a population average AIF is used (since the timing of bolus arrival with respect to the start of tissue enhancement is unknown). The appropriate approach will again depend on the organ and the temporal resolution.

The mathematical process of fitting the model to the data works as follows. The model signal can be calculated for many combinations of the free parameters (K^{trans} etc. see table 2 below). For each of these combinations, the differences between the model signal value (at each time point) and the measured data are found. These differences are squared and summed across each time point to provide a 'total difference'. The free parameters are adjusted until this total difference is minimised. The model has then been 'fitted' to the data. This is called the 'least squares solution'. The differences between the data and the fitted model are called 'residuals' (see e.g. fig. 5). From these can be found the 'root-mean-square residual', which is a kind of average difference between the model and the data, and which gives an indication of the quality of the model and of the fit. If the residuals appear random in character then these probably derive from a random effect such as image noise or movement; if there seems to be a systematic pattern to the residuals then the model can often be improved.

'Fit failures' can occur, particularly if the data are noisy (e.g. deriving from single pixels instead of a ROI); no

7

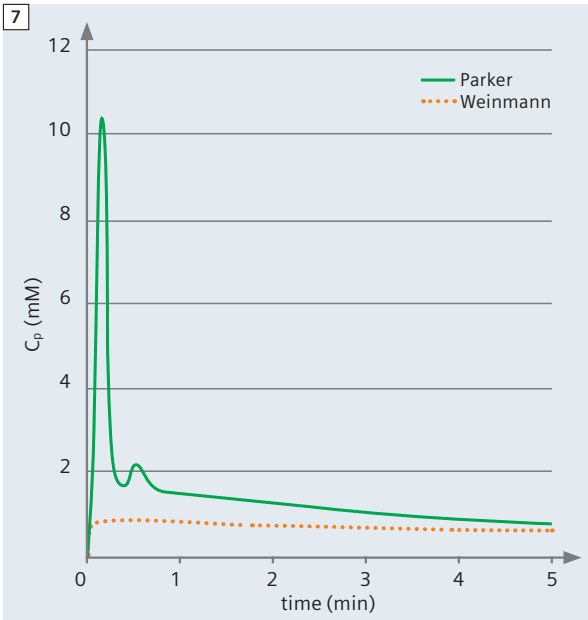

7 Population average AIF's (dose = 0.1 mmole/kg).

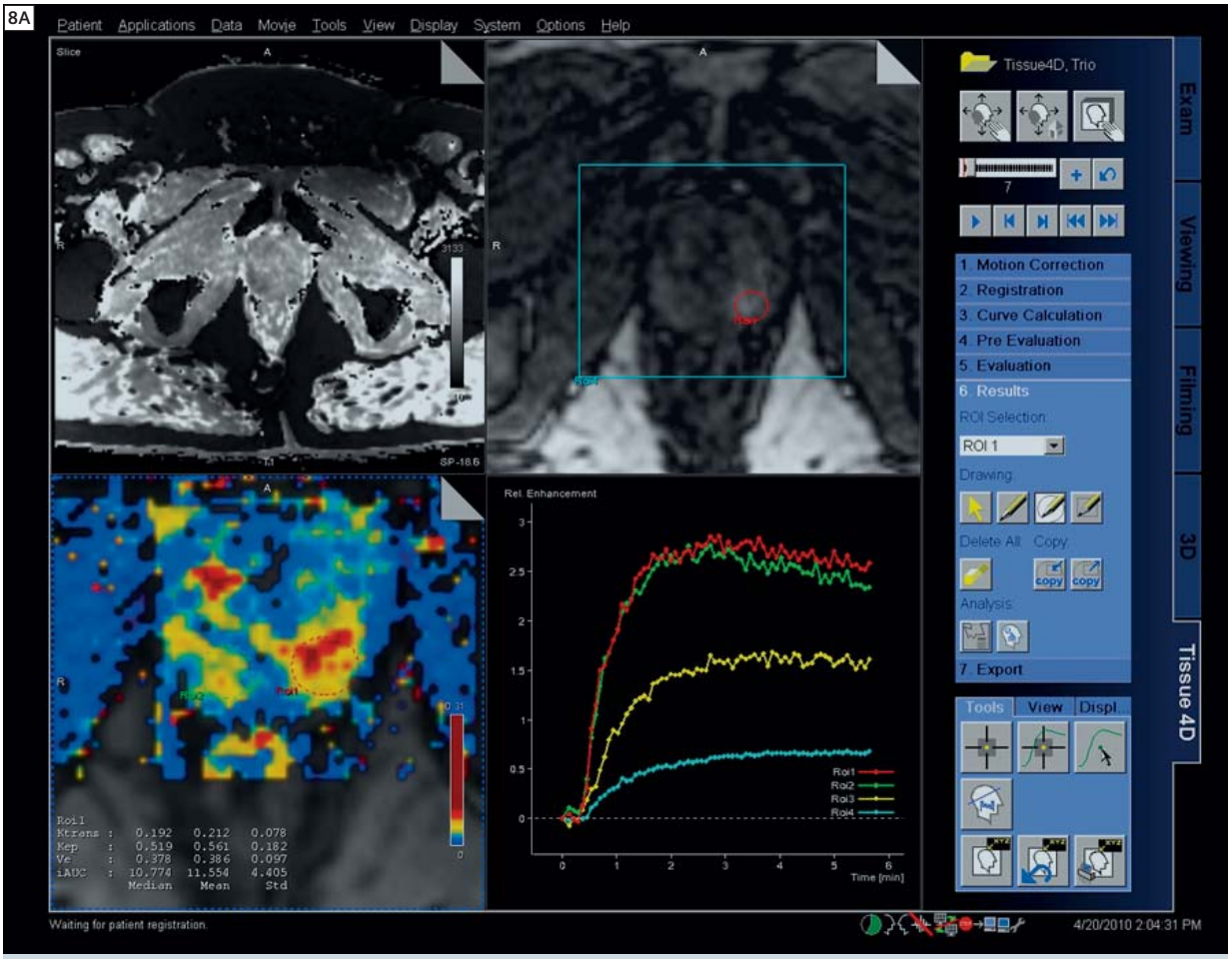

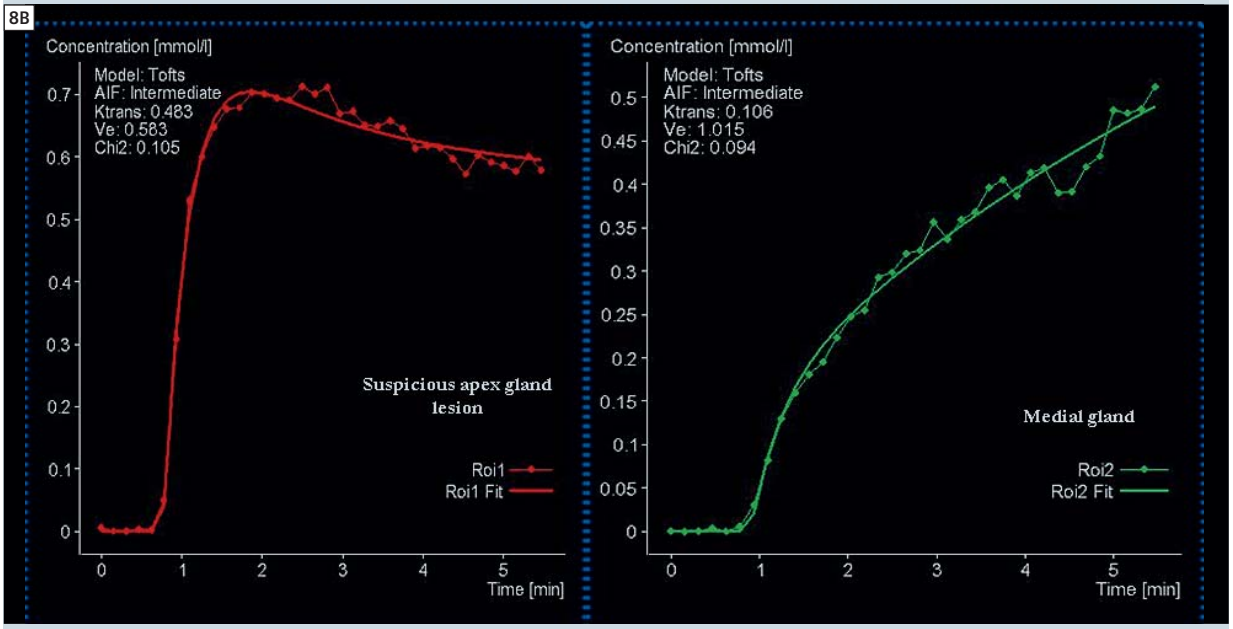

8 **(A)** Tissue4D output. The workflow includes motion correction and registration. **(B)** Fit to data from prostate ROI's.

valid parameter values are produced for that dataset. In the fitting process it is important to identify and flag these failures, so that the output (i.e. invalid parameter values) does not contaminate any subsequent analysis. Values of v_e>100% may occur if an incorrect value of T_{10} has been used (see table 1), or if the enhancement peak has not been reached (see fig. 3B).

Fitting can be implemented in two ways. The simplest way is to use ROI data (which are inherently low noise) and put these into a spreadsheet (e.g. Microsoft Excel running on a PC). The mathematics can be set up using inbuilt formula functions, and the 'solver' function can carry out the minimisation process. This does of course require some mathematical and computer ability. The more complex way is to set up pixel-by-pixel mapping, either using a standard environment (e.g. matlab) or by obtaining this from a supplier. Pixel mapping almost certainly needs spatial registration of the images to reduce the effect of motion; the operation is much more computer-intensive, and the single-pixel data are inherently noisy, so care must be taken to identify fit failures. The benefits of pixel mapping include the abilities to interrogate all the tissue without bias, and to generate histograms.

Histograms can show the distribution of parameter values, in a Region- or Volume-of-Interest. By taking care of histogram generation and architecture, histograms become more useful and comparisons are more easily made [15]. The y-values can be calculated such that the area under the histogram curve is either the total volume under interrogation (in mL), or 100%. By taking account of bin width, the histogram amplitude becomes virtually independent of bin width, and in a multicenter brain MTR study the intercenter difference was completely eliminated [16]. Features such as peak location and height can be extracted from histograms. Characterising the distribution tails can have predictive value [17, 18], and principle component analysis of the histogram shape can be powerful [19].

An example of a quite comprehensive software package to carry out pixel-by-pixel analysis is Tissue4D (fig. 8). The various functions needed are provided in a single workflow scheme, and ROI analysis is also available (this is useful to evaluate the quality of the modelling).

An example of using a spreadsheet to implement modelling of ROI data is shown in figure 9. The prostate data have quite low temporal resolution (34 s), T_{10} had to be assumed (1.5 s), and a Parker AIF was used. Including the v_p term did not improve the fitting (and in fact it became rather unstable). In several ROI's from the same subject, fitted onset time agreed within 2 s, suggesting that it can be found quite reliably.

9A

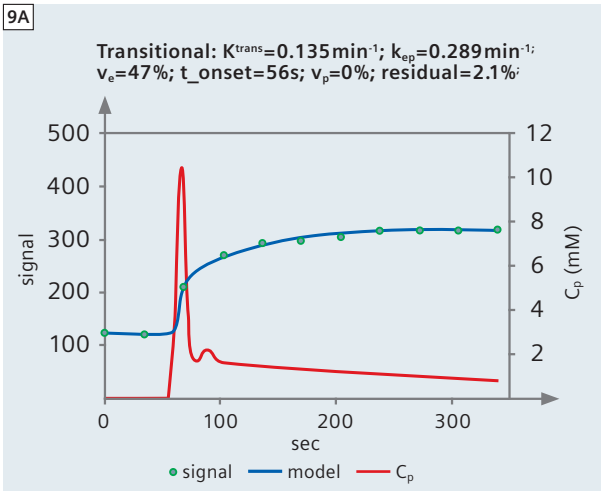

9B

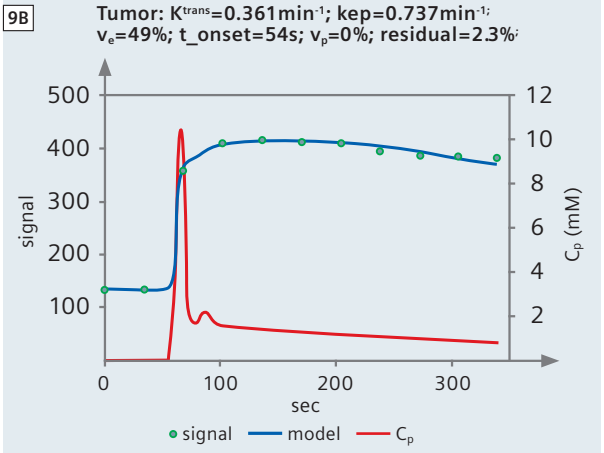

9 Modelling of prostate cancer DCE data. The Parker AIF was used (fig. 7), with v_p=0. Although data were only acquired every 34 s, the model was calculated with a temporal resolution of 1 s. Spreadsheet output is shown for transitional tissue **(A)** and tumor **(B)** ROI's. *(Data from University of Miami.)*

6. Conclusions

The principle physiological parameters that can be measured with DCE-MRI are the transfer coefficient K^{trans} (related to capillary permeability, surface area and perfusion) and v_e the size extravascular extracellular space. To do this needs good control of flip angle and an accurate measurement of tissue T_1 before injection of Gd. If T_1 is not available, then it may be possible to use a standard value; in any case the rate constant k_{ep} can still be measured, which is probably useful. The possible and optimum acquisition protocols and models will depend on which tissue is being imaged. Spread sheet analysis can provide quick access to modelling.

Acknowledgements

David Collins, Martin Leach and David Buckley contributed valuable insight into DCE imaging. Isky Gordon (University College London) and Iosif Mendichovszky provided data for figure 5. Peter Gall (Siemens Healthcare) contributed figure 8 and the list of CA's. Radka Stoyanova (University of Miami) provided data for figure 9.

Appendix

MRI model

T_1 is reduced from its native value T_{10} by the presence of a concentration C of Gd:

$$\frac{1}{T_1} = \frac{1}{T_{10}} + r_1 C \qquad \text{Equation 1}$$

r_1 is the relaxivity, and usually an in-vitro value of 4.5 s^{-1} mM^{-1} is used. Often it is more convenient to use the relaxation rate:

$$R_1 = R_{10} + r_1 C \qquad \text{Equation 2}$$

Note that to apply eqns 1 and 2 to total tissue Gd concentration implicitly assumes fast exchange i.e. that all the Gd in a voxel is available to relax all of the water. The signal S from a spoilt gradient echo sequence (i.e. FLASH) is:

$$S = S_0 \frac{(1-e^{-TR/T_1})\sin\theta}{1-e^{-TR/T_1}\cos\theta} \qquad \text{Equation 3}$$

where S_0 is the relaxed signal ($TR \gg T_1$, θ=90°), and θ is the FA. S_0 can be found from the measured pre-Gd signal (before injection of CA).

To find the plasma concentration (if required), firstly the blood concentration $C_b(t)$ is found from the blood signal, using eqns 1 and 3. Blood T_{10} is about 1.4 s [20]. The plasma concentration $C_p(t)$ is higher, by a factor related to the haematocrit Hct (typically 42%):

$$C_p = \frac{C_b}{1-Hct} \qquad \text{Equation 4}$$

Pharmacokinetic model

The flow of Gd across the endothelium into the EES is

$$v_e \frac{dC_e(t)}{dt} = K^{trans}(C_p(t) - C_e(t)) \qquad \text{Equation 5}$$

The solution to this is [7] a convolution of C_p with the impulse response function $K^{trans}\exp(-k_{ep}t)$; when the IV Gd is taken into account, the total tissue concentration is:

$$C_t(t) = v_p C_p(t) + K^{trans}\int_0^t C_p(\tau)e^{-k_{ep}(t-\tau)}d\tau \qquad \text{Equation 6}$$

Model parameters

There are several kinds of parameters used in the model. *Fixed* parameters (*FA TR Hct* T_{10} T_{10}^{blood} r_1) have preset values which are required before fitting can start. *Free* parameters (K^{trans} v_e k_{ep} and maybe v_p and t_onset) are varied and then estimated as part of the fitting process. Other parameters (C_p etc) are used temporarily as part of the process of modelling the signal. The fixed and free parameters are summarised in table 2.

References

1 Jackson A, Buckley DL, Parker GJ. Dynamic Contrast-Enhanced Magnetic Resonance Imaging in Oncology. Springer, 2004.

2 Tofts PS. Quantitative MRI of the brain: measuring changes caused by disease. John Wiley, 2003.

3 Tofts PS, Brix G, Buckley DL, Evelhoch JL, Henderson E, Knopp MV, Larsson HB, Lee TY, Mayr NA, Parker GJ, Port RE, Taylor J, Weisskoff RM. Estimating kinetic parameters from dynamic contrast-enhanced T(1)-weighted MRI of a diffusable tracer: standardized quantities and symbols. J Magn Reson Imaging 1999;10:223-232.

4 Leach MO, Brindle KM, Evelhoch JL, Griffiths JR, Horsman MR, Jackson A, Jayson GC, Judson IR, Knopp MV, Maxwell RJ, McIntyre D, Padhani AR, Price P, Rathbone R, Rustin GJ, Tofts PS, Tozer GM, Vennart W, Waterton JC, Williams SR, Workman P. The assessment of antiangiogenic and antivascular therapies in early-stage clinical trials using magnetic resonance imaging: issues and recommendations. Br J Cancer 2005;92:1599-1610.

5 Tofts PS, Kermode AG. Measurement of the blood-brain barrier permeability and leakage space using dynamic MR imaging. 1. Fundamental concepts. Magn Reson Med 1991;17:357-367.

Table 2: Fixed and free parameters in DCE modelling.

Quantity	symbol	units	type
flip angle[a]	*FA*	degrees	fixed
haematocrit	*Hct*	%	fixed (42%)
onset time	*t_onset*	s	free
rate constant[b]	k_{ep}	min^{-1}	free
transfer constant	K^{trans}	min^{-1}	free
T_1 relaxivity	r_1	$s^{-1}\ mM^{-1}$	fixed ($4.5\ s^{-1}\ mM^{-1}$)
T_1 of blood	T_{10}^{blood}	s	fixed (1.4 s)
T_1 of tissue	T_{10}	s	fixed
TR	*TR*	s	fixed
fractional volume of EES[c]	v_e	$0<v_e<100\%$	free
fractional volume of blood plasma in tissue	v_p	$0<v_p<100\%$	free

[a] θ is the flip angle in radians, [b] $k_{ep} = K^{trans}/v_e$, [c] Extravascular Extracellular Space

6 Kety SS. The theory and applications of the exchange of inert gas at the lungs and tissues. Pharmacol Rev 1951;3:1-41.

7 Tofts PS. Modeling tracer kinetics in dynamic Gd-DTPA MR imaging. J Magn Reson Imaging 1997;7:91-101.

8 St Lawrence KS, Lee TY. An adiabatic approximation to the tissue homogeneity model for water exchange in the brain: I. Theoretical derivation. J Cereb Blood Flow Metab 1998;18:1365-1377.

9 Donaldson SB, West CM, Davidson SE, Carrington BM, Hutchison G, Jones AP, Sourbron SP, Buckley DL. A comparison of tracer kinetic models for T1-weighted dynamic contrast-enhanced MRI: application in carcinoma of the cervix. Magn Reson Med 2010;63:691-700.

10 Tofts PS, Cutajar M, Mendichovszky IA, Gordon I. Accurate and precise measurement of renal filtration and vascular parameters using DCE-MRI and a 3-compartment model. Proc Intl Soc Mag Reson Med, 18th annual meeting, Stockholm.2010; 326.

11 Parker GJ, Roberts C, Macdonald A, Buonaccorsi GA, Cheung S, Buckley DL, Jackson A, Watson Y, Davies K, Jayson GC. Experimentally-derived functional form for a population-averaged high-temporal-resolution arterial input function for dynamic contrast-enhanced MRI. Magn Reson Med 2006;56:993-1000.

12 Dowell NG, Tofts PS. Fast, accurate, and precise mapping of the RF field in vivo using the 180 degrees signal null. Magn Reson Med 2007;58:622-630.

13 Tofts PS, Berkowitz B, Schnall MD. Quantitative analysis of dynamic Gd-DTPA enhancement in breast tumors using a permeability model. Magn Reson Med 1995;33:564-568.

14 Fritz-Hansen T, Rostrup E, Larsson HB, Sondergaard L, Ring P, Henriksen O. Measurement of the arterial concentration of Gd-DTPA using MRI: a step toward quantitative perfusion imaging. Magn Reson Med 1996;36:225-231.

15 Tofts PS, Davies GR, Dehmeshki J. Histograms: measuring subtle diffuse disease (chapter 18). In: Paul Tofts, editor. Quantitative MRI of the brain: measuring changes caused by disease. Chichester: John Wiley, 2003: 581-610.

16 Tofts PS, Steens SC, Cercignani M, Admiraal-Behloul F, Hofman PA, van Osch MJ, Teeuwisse WM, Tozer DJ, van Waesberghe JH, Yeung R, Barker GJ, van Buchem MA. Sources of variation in multi-centre brain MTR histogram studies: body-coil transmission eliminates inter-centre differences. Magn Reson Mater Phy 2006;19:209-222.

17 Tofts PS, Benton CE, Weil RS, Tozer DJ, Altmann DR, Jager HR, Waldman AD, Rees JH. Quantitative analysis of whole-tumor Gd enhancement histograms predicts malignant transformation in low-grade gliomas. J Magn Reson Imaging 2007;25:208-214.

18 Donaldson SB, Buckley DL, O'Connor JP, Davidson SE, Carrington BM, Jones AP, West CM. Enhancing fraction measured using dynamic contrast-enhanced MRI predicts disease-free survival in patients with carcinoma of the cervix. Br J Cancer 2010;102:23-26.

19 Dehmeshki J, Ruto AC, Arridge S, Silver NC, Miller DH, Tofts PS. Analysis of MTR histograms in multiple sclerosis using principal components and multiple discriminant analysis. Magn Reson Med 2001;46:600-609.

20 Spees WM, Yablonskiy DA, Oswood MC, Ackerman JJ. Water proton MR properties of human blood at 1.5 Tesla: magnetic susceptibility, T(1), T(2), T*(2), and non-Lorentzian signal behavior. Magn Reson Med 2001;45:533-542.

Contact
Professor Paul Tofts
Clinical Imaging Sciences Centre
Brighton and Sussex Medical School
University of Sussex
Brighton
BN1 9PX
United Kingdom
Website: www.paul-tofts-phd.org.uk
dce@paul-tofts.org.uk

Global Siemens Headquarters

Siemens AG
Wittelsbacherplatz 2
80333 Muenchen
Germany

Global Siemens Healthcare Headquarters

Siemens AG
Healthcare Sector
Henkestrasse 127
91052 Erlangen
Germany
Phone: +49 9131 84-0
www.siemens.com/healthcare

www.siemens.com/healthcare-magazine

Order No. A91MR-1100-58C-7600 | Printed in Germany | CC 439 09120.5 | © 09.12, Siemens AG

Global Business Unit

Siemens AG
Medical Solutions
Magnetic Resonance
Henkestr. 127
DE-91052 Erlangen
Germany
Phone: +49 9131 84-0
www.siemens.com/healthcare

Local Contact Information

Asia
Siemens Pte Ltd
The Siemens Center
60 MacPherson Road
Singapore 348615
Phone: +65 6490-8096

Canada
Siemens Canada Limited
Medical Solutions
2185 Derry Road West
Mississauga ON L5N 7A6
Canada
Phone: +1 905 819-5800

Europe/Africa/Middle East
Siemens AG
Medical Solutions
Henkestr. 127
91052 Erlangen
Germany
Phone: +49 9131 84-0

Latin America
Siemens S.A.
Medical Solutions
Avenida de Pte. Julio A. Roca No 516,
Piso 7
C1067ABN Buenos Aires
Argentina
Phone: +54 11 4340-8400

USA
Siemens Medical Solutions U.S.A., Inc.
51 Valley Stream Parkway
Malvern, PA 19355-1406
USA
Phone: +1-888-826-9702